SHEAR MODULUS OF HEAVY OILS, RHEOMETER MEASUREMENTS:

CONFINEMENT EFFECT AND AMPLITUDE DEPENDENCE

by

Patricia Evelyn Rodrigues

A thesis submitted to the Faculty and the Board of Trustees of the Colorado School of Mines in partial fulfillment of the requirements for the degree of Doctor of Philosophy (Geophysics).

Golden, Colorado

Date _____

Signed: _____
Patricia Evelyn Rodrigues

Signed: _____
Dr. Michael L. Batzle
Thesis Advisor

Golden, Colorado

Date _____

Signed: _____
Dr. Terence K. Young
Professor and Head
Department of Geophysics

ABSTRACT

The success of seismic and other acoustic monitoring techniques is based on the ability of geophysicists to accurately model acoustic waves propagation. True “fluids” are not capable of supporting shear stress; however, heavy oils are viscoelastic and allow the transmission of shear waves. The shear modulus of heavy oils is highly dependent on frequency which adds a major difficulty since the data we study are obtained at different frequencies. Measuring elastic properties at high frequencies has been done for many years and it is much simpler than low frequencies measurements; specifically in bulk heavy oils. The equipment deforms the sample at frequencies from 3 to 3000 Hz and it works well for solid-like samples but cannot be used for liquid-like samples. An alternative method to measure the shear modulus of heavy oils at low frequencies is the rheometer which measures the shear modulus at frequencies from 0.01 to 100 Hz with strains amplitudes in the order of 10^{-4}, two or three orders of magnitude larger than tension/compression. Linear viscoelasticity theory indicates that measurements done in the linear viscoelastic regime should be consistent between techniques as elastic properties are independent of amplitude. My research is focused on understanding rheometer measurements, and validating them against the tension/compression technique. However, in this work I identified two aspects of the rheometer that make their measurements not consistent with tension/compression results. The first is the presence of the two solid-liquid interfaces provided by the parallel plates; and the second is the increased strains amplitudes in the rheometer. The solid-liquid interfaces cause reorientation of the surface active components of the heavy oils, increasing the shear modulus near the interface in a scale that can be measured by the rheometer. This was evidenced by an increased of the shear modulus when reducing the gap between the rheometer plates. On the other hand, the increased amplitudes on the rheometer cause decrease in the shear modulus with respect to what is measured in seismic techniques. Heavy oils are aggregates that at rest or under low shear, behave as a solid due to weak bonds between the aggregate particles. As strain amplitude is increased the weaker bonds are broken and the heavy oil behaves liquid-like. This was seen by the increased values measured by the tension/compression results at low amplitudes in comparison to the much lower values measured by the rheometer at higher amplitudes. This indicates that two linear viscoelastic regimes can be present in the heavy oil at different amplitudes. The main two implications of this work are the fact that under confinement heavy oils properties change and the shear modulus and viscosity increases affecting not only the measurements but also the flow in porous media where heavy oils are confined between grains. On the other hand, the use of the rheometer for seismic or acoustic applications is limited as the higher strain of the rheometer can measure values that are lower than those measures with seismic techniques.

LIST OF CONTENTS

LIST OF FIGURES

LIST OF TABLES

ACKNOWLEDGEMENTS

I would like to thank the Chemical Engineering Department at Colorado School of Mines for allowing us to use their laboratories for the rheology and water content analysis. In particular I would like to thank Prof. Matthew Liberatore for the long discussions about rheometer results. I also would like to thank Prof. John Dorgan for very helpful discussions about slip phenomena in rheometer measurements. I would like to thank Dr. Ala Batzyleva for training me rheometer measurements and especially for the good discussions. I also would like to thanks Manika Prasad for her difficult questions and interesting suggestions that provided me with guidance to look beyond the expected. I cannot pass this opportunity to thank my fellows in the Center for Rock Abuse for their dedicated help in the laboratory and long conversations in the office, my thanks go greatly in special to Matthias Pohl and Azar Hasinov. Thanks to the DHI/Fluids Consortium at Colorado School of Mines for financial support.

Lastly, I want to thank Mike Batzle for making me understand and feel the difference between just doing a good job and deeply understanding what is happening.

To Reinaldo and all the blessing that came with him

To my children and step-children

To my parents

To God

1. INTRODUCTION

Even though heavy oils constitute the largest contributor of oils reserves in the world they still remain one of the least understood fluids in the reservoir by geophysicists. Many heavy oil reservoirs are characterized using seismic data, in particular, time-lapse (4D) seismic methods have been introduced to facilitate the monitoring of Enhanced Oil Recovery (EOR) methods which are often, if not always, required in these reservoirs. The success of seismic and other acoustic monitoring techniques is based on the ability of geophysicists to accurately model the P-wave and S-wave propagation through real and potential rock-fluid scenarios that will be encountered during EOR operations. It is essential therefore, to translate these scenarios into changes in the elastic properties that govern wave propagation (bulk modulus, shear modulus, and density), this is the goal of rock physics models. Rock physics models estimate the elastic properties of the rock-fluid system from its components, usually divided in two parts: rock and pore fluids. The grains comprising the rock are either treated as a whole, for example sandstone or limestone; or they can be treated as a combination of minerals like quartz, calcite, dolomite, and so forth. On the other hand, fluids are usually divided into gases (i.e. methane and CO2) and liquids (water and crude oil). Regardless of how the rock physics models divide its components, all are based on the assumption that the properties of the individual components are well known. This last statement is far from the truth in the case of heavy oils.

True “fluids” are not capable of supporting shear stress; however, heavy oils, and all their heavier relatives (API <10), behave acoustically different than the rest of the fluids in the reservoir allowing the transmission of shear waves below a certain temperature or above a certain frequency. Geophysicists working with the analysis of seismic data in heavy oil reservoirs must face this fact and consider the shear modulus of the heavy oil in their analysis. Authors such as Ke et al. (2010), Ciz & Shapiro (2007), Makarynska et al. (2010) and Gurevich et al. (2008) have developed rock physics models to include the viscoelastic behavior of heavy oils in their estimation of the elastic properties. Nonetheless, a large weakness in those models is the uncertainty in the magnitude of the shear modulus of heavy oil and moreover, how we can measure it. Wolf et al. (2008) raised that concern, emphasizing the authors limitation to model the shear wave due to the lack of appropriate rock physics models, and moreover the lack of experimental data to calibrate them. This constitutes a definite gap in rock physics models that estimate the elastic properties of heavy oils.

It has been demonstrated (Batzle, et al. 2004; Hasan 2010) that the shear modulus of heavy oils is highly dependent on temperature, composition, and frequency. Frequency dependency adds a major difficulty to the problem since the data we study are obtained at different frequencies. Laboratory acoustic experiments are usually done at ultrasonic frequencies (in the order of MHz) while seismic data

are collected in the range of 10-100 Hz, Vertical Seismic Profiles (VSP) at ~30-120 Hz and sonic logs at 10-30 kHz. To provide a complete picture of the shear modulus of heavy oils, we need to account for the properties at different frequencies.

Frequency dependency of the shear modulus of heavy oils, also called frequency dispersion, has been measured (Batzle, 2006a), but lacks extensive characterization due to the difficulty of measuring shear properties at different frequencies. Measuring elastic properties at high frequencies has been done for many years and it is much simpler than measuring the same properties at low frequencies. In particular, low frequency measurements of bulk heavy oils bring many complications. One technique used at Colorado School of Mines consists of a tension/compression system that deforms or compresses the sample at a frequency range from 3 to 3000 Hz. The equipment works well for solid or solid-like samples but cannot be used for liquid-like samples. An alternative method used to measure the shear modulus of heavy oils at low frequencies is the rheometer. Rheometer measurements constitute a convenient way of measuring shear modulus of oil samples as the equipment is widely available and much data has been published. The rheometer can measure the shear modulus in a frequency range of 0.01 to 100 Hz, providing insight into the low end of the frequency range were seismic data are found. Several authors such as Hinkle et al. (2008), Rojas et al. (2008), Hasan (2010), Bazyleva et al. (2010), and Behura et al. (2007) have measured the shear modulus of heavy oils with the rheometer, but no one has investigated how comparable these measurements are to what has been measured at ultrasonic frequencies and with tension/compression techniques at seismic applications frequencies. The lack of verification of the rheometer as an adequate technique to measure the shear modulus of heavy oils at low frequencies has created hesitation and reluctance in its use.

The objective of my research is to understand in depth the rheometer measurements, compare them to the tension/compression results and determine if the two techniques measure the same shear phenomena. Ensuring that the two techniques are measuring the same properties is crucial before the rheometer can be widely used for geophysical applications.

One major question in the use of the rheometer for geophysical applications is related to the strain amplitudes used. The minimum strains measured by the rheometer are in the order of 10^{-4} while strain amplitudes of geophysical acoustic measurements, including laboratory measurements, are in the order of 10^{-6}-10^{-7}. The linear viscoelasticity theory indicates that if measurements are done in the linear viscoelastic regime (LVR) the three techniques should be consistent as the elastic properties should be independent of the amplitude. As far as I know, the work I present here constitutes the first effort to compare the two low frequency techniques (rheometer and tension/compression) and ultrasonic techniques simultaneously and to demonstrate how the measurements relate over the broad frequency range. Comparisons between rheometer and ultrasonic measurements were done by Rojas (2010) but due to the large gap in frequencies between the two techniques, a clear validation is not provided. As a result of the different strains used in the rheometer and tension/compression techniques, I included in my

analysis a comprehensive inquiry on how the strain amplitude affects the structure of heavy oils and consequently the shear modulus. I will provide theories and evidence of the structural changes occurring in the heavy oil that affects the shear modulus when measured in the rheometer, when measured at different amplitudes and when measured in the presence of solid-liquid interfaces (rheometer). The insights I provide in this work are new to geophysics and have important implications on how we measure and interpret the shear behavior of heavy oils. In order to understand and explain the results of this work, I incorporated concepts and references from different sciences (i.e. road construction and chemical engineering) that have worked with either similar materials or techniques but in a completely different context.

Two additional aspects that I will mention but not develop in detail in my work are the temperature and composition dependency of the shear modulus of heavy oils. Temperature changes cause large changes in shear properties of heavy oils. The research here was restricted to the working temperatures for each sample to ensure they are in the viscoelastic regime and behave solid-like during the tests. On the other hand, compositional dependency has a major influence on properties and I will not thoroughly developed in my work but I will provide evidence and theory of the connection between elastic properties and composition of heavy oils. I will also propose an alternative composition technique that is related to the elastic properties of heavy oils and can eventually be used to quantitatively predict them.

My experimental work consists of measuring three heavy oil samples that are solid or solid-like at room temperature. This facilitates reaching temperatures at which the samples behave solid-like enabling the work in the tension/compression equipment. I measured heavy oils in rheometer, the tension/compression and the ultrasonic set-ups at the same temperatures, and compared the results using the Cole-Cole dispersion model to estimate the shear modulus at different frequencies. In addition, physical and chemical analysis were performed, including SARA fractionation, which consists of separating the oil into its Saturates, Aromatics, Resins and Asphaltenes fractions, pyrolysis, API gravity and water content.

My research will directly benefit geophysicists using rock physics models that require the shear modulus of heavy oils as an input and have struggled for long in how to measure it at low frequencies. The knowledge of the properties of heavy oils at low frequencies has a direct impact in the prediction of shear velocity of heavy oils from seismic which has a direct connection to viscosity and therefore the efficiency of EOR methods could be evaluated. Another important application of my research is the ability to directly compare and tie the acoustic properties of heavy oils at well log and seismic scale which are measured at different frequencies.

The report is divided in four main chapters: background, methodologies, results and discussions, and conclusions and implications. In the background chapter, I explain the theory of viscoelasticity and concepts of structured fluids, I also summarize the characteristics of heavy oil and introduce some

concepts widely used in chemical engineering but not as common in geophysics; finally I suggest some potential applications of my work. In the methodologies chapter, I focus in the two shear methodologies used in my work which are the rheometer and the tension/compression techniques. I will not give specific details on how to make the measurements, as these have been widely used and reported in other documents. I do however, focus on the aspects that were different or I developed during my research. Next, I separated the results chapter in three sections, in the first section I analyzed the quantitative correlations obtained between two heavy oil characterization techniques. In the second, I explain the effect that the solid-liquid interface has over the heavy oil rheometer results; and in the last section, I will compare the results from the rheometer with the tension/compression technique and develop a theory about the effects of the amplitudes in the structure of heavy oils. I analyze and explained all the results based in theories and evidence from different sciences. Finally, in the last chapter, I will summarize the conclusions and present important implications of my work.

2. BACKGROUND: FROM THEORY OF VISCOELASTICITY AND STRUCTURED LIQUIDS CONCEPTS TO RESEARCH APPLICATIONS

In this chapter, I provide background information with the purpose to aid in the understanding of my research project. In the first and second sections, I explain the theory of viscoelasticity and give the definition of some structured fluids which are important to understand heavy oils. With these concepts, I explain what heavy oils are and their characteristics (section 2.3). To finalize the background chapter, I briefly explain (section 2.4) additional concepts that are needed to better understand the results and close the chapter with potential applications of my research.

2.1. Theory of viscoelasticity

Viscoelastic materials exhibit characteristics of both elastic solids and viscous fluids. An elastic solid is defined as a material that responds to Hooke's law (Lakes 2009), this means stress is proportional to strain. In contrast, a viscous fluid under shear stress responds linearly to the rate of strain and the constant of proportionality is the viscosity.

All materials that behave between elastic and viscous regimes are considered viscoelastic, and there is a distinction between viscoelastic-solids and viscoelastic-fluids. After subjected to a constant rate of strain, the strain in a viscoelastic-solid eventually recovers to zero, in the case of a viscoelastic-fluid there is a residual strain. Figure 2.1 shows a creep experiment that exemplifies this behavior. A constant stress is applied for a period of time and then released; the strain response will depend on the material. An elastic material (solid) will show a step strain which is proportional to the stress (dotted line). A purely viscous (or liquid) material will keep deforming during the duration of the applied stress and it will remain deformed after releasing the stress (dashed line). A viscoelastic material will deform slowly during the duration of the stress and, after releasing the stress, the material will slowly try to go back to its original configuration. If the material achieves the original configuration then is called viscoelastic-solid, if a residual deformation remains then is called viscoelastic-fluid. The theory of linear viscoelasticity indicates that materials have a linear viscoelastic regime (LVR) in which the properties are independent of amplitude.

Lakes (2009) summarizes an elastic solid as a material that supports both shear stress and hydrostatic stress and its properties are independent of time or frequency. Viscous fluids support static hydrostatic stress and generate shear stress only if the strain is changing with time. Viscoelastic materials exhibit time or frequency dependence and require a function to describe its behavior. Heavy oils are viscoelastic materials.

The behavior described above is for the materials under constant load. However, of particular interest in the oil industry is the study of materials under sinusoidal load. Sinusoidal load are the basis of many geophysical acoustic methods like seismic, vertical seismic profiles (VSP), cross-well tomography, sonic logs, among others and it is the center of my research. During sinusoidal load, the stress varies sinusoidally with time, as equation 2.1:

$$\sigma(t) = \sigma_0 \sin(2\pi\omega t) \tag{2.1}$$

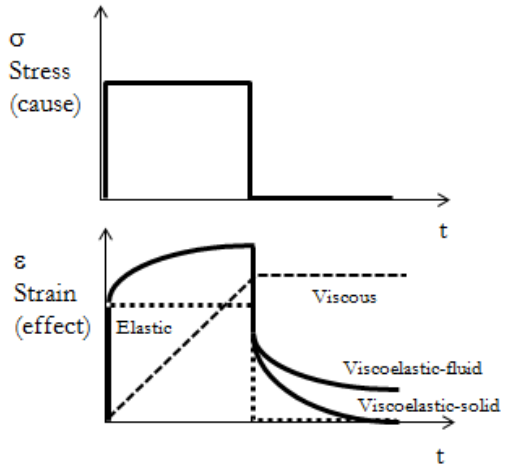

Figure 2.1. Creep and recovery, stress and strain vs. time. Modified from (Lakes 2009).

Where t is time, $\sigma(t)$ is the variable magnitude of stress with time, σ_0 is the initial stress magnitude and ω is the frequency (Hz). The time response of the strain ($\varepsilon(t)$) of a linear viscoelastic material is also sinusoidal in time, but the response will lag the stress by a phase angle δ, where ε_0 is the initial strain response.

$$\varepsilon(t) = \varepsilon_0 \sin(2\pi\omega t - \delta) \tag{2.2}$$

As a result of the phase lag between stress and strain, the modulus (M) can be treated as a complex number (Lakes 2009).

$$M^* = M' + iM'' \tag{2.3}$$

$$M' = \frac{\sigma}{\varepsilon_0}\cos\delta \tag{2.4}$$

$$M'' = \frac{\sigma}{\varepsilon_0}\sin\delta \tag{2.5}$$

The modulus typically is either Young's modulus (E) or shear modulus (G) depending on the type of loading, compressional or shear. The real part (G') of the shear modulus is also called the storage modulus while the imaginary part (G'') is called the loss modulus as it is related to the loss of energy in

the form of heat. In terms of molecular deformation when a material is subject to force, part of the energy is stored and it returns by deforming the material to the initial configuration when the force is released. In contrast, the loss component of the energy is consumed in an irreversible manner.

One definition of attenuation (1/Q) can be derived from the above definitions and equations. A material with large attenuation will have a large loss modulus (large phase lag), which is closer to pure liquid behavior. An elastic solid will have a large storage modulus (no phase lag) and no attenuation. In this way the attenuation of materials can be defined as tangent of the phase lag or the loss modulus over the storage modulus.

$$\frac{1}{Q} = \tan\delta = \frac{G''}{G'} \qquad (2.6)$$

Thus, the phase lag, also called phase angle, is a measure of how liquid-like or solid-like a material is. In the limits of Equations 2.4 and 2.5, a phase of zero degrees is achieved for an elastic-solid, while 90 degrees is achieved for viscous-fluids. For phases greater than zero and less than 90 the material is considered viscoelastic.

A graphic representation of the sinusoidal load showing the strain lagging the stress can be seen in Figure 2.2

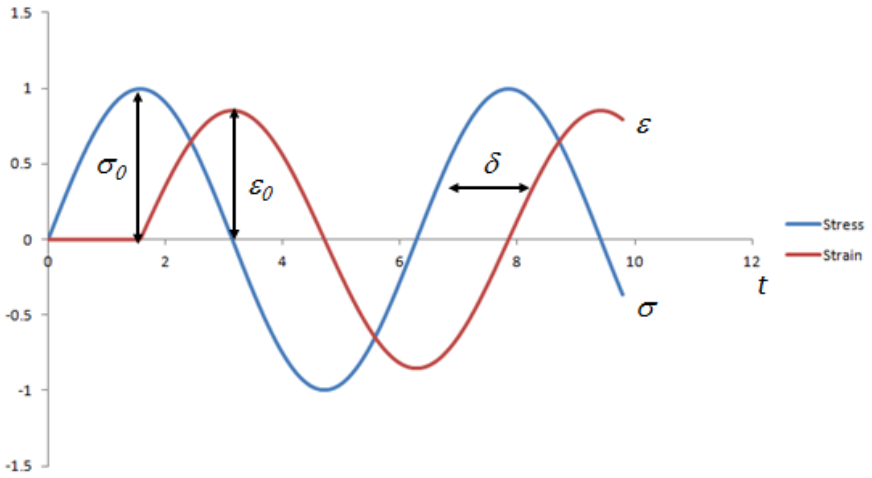

Figure 2.2. Sinusoidal load modified from (Lakes 2009). Strain ε (red) lags the stress σ (blue) by a phase angle δ in viscoelastic materials.

Viscosity and shear modulus are related through frequency and in this work I will refer to both terms often. The relationship between them is described by the following equations from (Ferry 1980):

$$\eta^* = \frac{G^*}{i\omega} \qquad (2.8)$$

Where η^* is the complex viscosity defined as:

$$\eta^* = \eta' - i\eta'' \quad (2.9)$$

$$\eta' = \frac{G''}{\omega} \quad (2.10)$$

$$\eta'' = \frac{G'}{\omega} \quad (2.11)$$

2.1.1. Kramers-Kronig Relations

The real and imaginary parts of the dynamic properties of a linear material are not independent (Lakes, 2009) and are related through the Kramers-Kronig relations. The storage and loss components are intimately related. It is also understood that the presence of loss at one frequency is linked to dispersion over the all frequency range. These relations can be used to connect the real and imaginary parts and they enable one to calculate one dynamic property from the knowledge of the other property (Pritz L., 1999). Even though the application of Kramers-Kronig could be beneficial there practical applications are limited due to calculation difficulties. However, there are approximations to these relations that could be used (Pritz, L., 1999).

2.2. Structured liquids

Literature published on heavy oils often refer to the terms, colloids, surfactants, aggregates and association which are terms used in the definition of structured fluids. In this section, I explain these terms based on the definitions by Witten & Pincus (2004). Structured fluids are liquids that contained large molecules connected to each other which form structures much larger than an atom but much smaller than a macroscopic body.

2.2.1. Colloids

Colloids are fluids containing particles suspended in a liquid solvent. Colloids are important as they change the physical properties of the fluid that contains them. They can be concentrated to the point that gives the suspension a solid-like consistency. The interaction between colloidal particles is affected by the solvent surrounding them.

2.2.2. Aggregates

The interaction between colloidal particles makes it possible for the molecules to self-organize and create structures not seen in simple liquids. When several of these particles merge they form an aggregate, also referred to as a colloidal aggregate. The process of aggregation is commonly referred to as flocculation. The attraction between molecules is so strong in these aggregates that they bond together permanently. Aggregates are therefore effective in increasing viscosity and tend to be rigid structures, not flexible like polymers of large chains. Figure 2.3 from Hiemenz & Rajagopalan (1997) shows examples of aggregates from gold colloids at different scales. Other example of particular interest

for this work are the asphaltenes aggregates shown in Figure 2.4 (Branco et al. 2001), in which the shape of the aggregate depends on the steric (required space) arrangement of the molecules. More examples of aggregates will be shown in section 2.3.

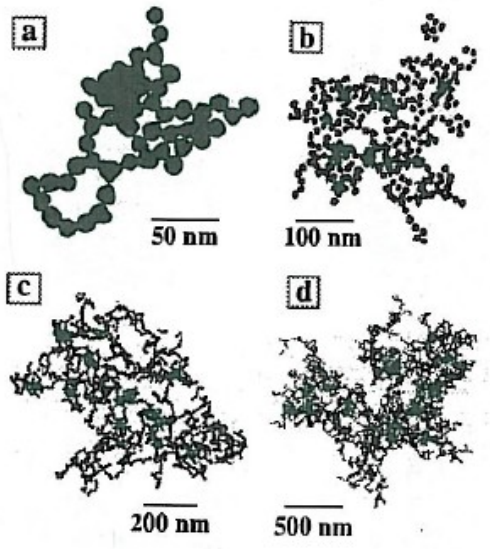

Figure 2.3 Aggregates of gold particles measured by transmission electron microscope (TEM) (Hiemenz & Rajagopalan 1997).

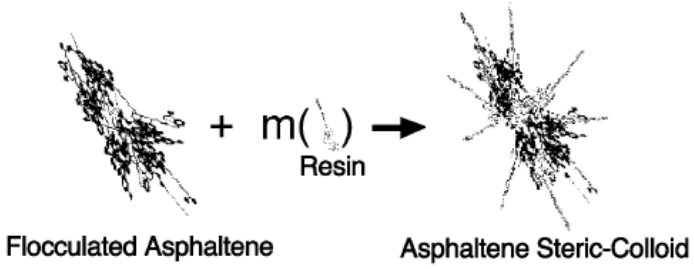

Figure 2.4. Asphaltene and resins aggregates formation in the presence of excess amounts of paraffin hydrocarbons (from Branco et al. 2001)

2.2.3. Surfactants and surfactant micelles

Surfactants or "surface-active" materials are molecules with strong hydrophobic and hydrophilic components. Hydrophobic or hydrophilic are terms that refer to opposite behavior regarding to attraction to the surrounding phase or an interface. The term "hydro" refers to the interaction with water but it is usually used generically to refer to the interaction with other materials. When these types of molecules are found in the presence of an interface they migrate and adsorb to the interface (Drew & Myers 1999). The orientation of the molecules will depend on the nature of the surface and the solvent were the surfactant is found. Figure 2.5 (Drew & Myers 1999) shows oriented molecules at the interface and the random orientation seen in solution.

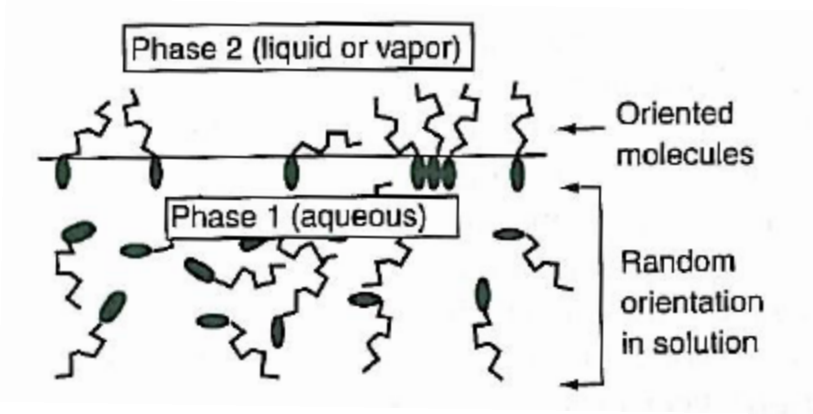

Figure 2.5. Adsorption of molecules at the interface. Molecules have a preferred orientation (Drew & Myers 1999).

Due to their dual behavior, individual surfactant molecules will not reside within a single fluid except in very small concentrations. If interfaces are not available, surfactants assemble themselves in micelles in which the immiscible parts of the molecules stick together at the center and the miscible parts are exposed to the liquid. Micelles are considered to be colloids as they act as "particles" suspended in a liquid. Asphaltenes present in heavy oils are known for having surface active behavior. In Figure 2.6 from Da Silva et al. (2001) they show the reduction in surface tension when increasing asphaltenes concentration in toluene. The reduction of surface tension with concentration is an indication that asphaltenes have surface active characteristics and molecules migrate to the interface. It is important to clarify that the term surface and interface are somehow interchangeable, but surface is used when one of the materials is a gas (i.e. air).

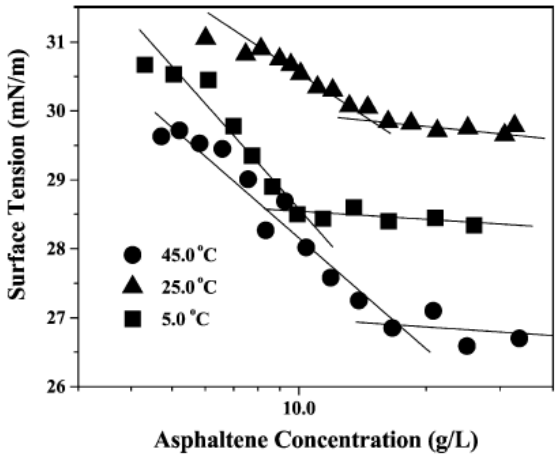

Figure 2.6. Surface tension vs. asphaltene concentration from Da Silva et al. (2001). A decrease in surface tension when increasing asphaltene concentration is an indication that asphaltenes molecules have surface active characteristics and migrate to the surface.

2.2.4. Association

Association is a term used to describe the secondary interaction between large structures like colloidal aggregates and micelles described above. Association is referred to a weaker or temporary interaction between structures. These are physical short range inter-particle interactions (Chougnet et al. 2007) not chemically bonded (Putz & Burghelea, 2009). Structures that are joined can transmit forces and alter the mechanical forces of the material. These associations are weak enough that they can break, for example, during the duration of an experiment and they can be altered in response of the local stress, flow or temperature (Witten & Pincus 2004). At rest, aggregates form a network that immobilizes the fluid (or solvent), and the system behaves as an elastic solid under low stress. As the force applied to the material is increased, a yield point is reached and the molecular network breaks apart and the system begins to flow and the viscosity of the material decreases (Hiemenz & Rajagopalan 1997).

2.3. Heavy Oil

Heavy oil is usually defined based on its density (Dawe 2000) and a common way to express the oil density is the API number (equation 2.12), where ρ is the specific gravity of the oil:

$$API = \frac{141.5}{\rho} - 131.5 \qquad (2.12)$$

The World Energy Council defined heavy oils as hydrocarbons with an API < 22.3° and they make a distinction for hydrocarbons with API < 10°, which are often called bitumen or extra-heavy oil. There are descriptive terms to refer to certain ranges of API gravity like tar, pyrobitumen and asphalts among others, but in my work I will use the term “heavy oil” to refer to all hydrocarbons with API < 20°.

Heavy oils have high molecular weight with composition so complex that individual components are difficult to identify. Heavy oils are often described in terms of solubility through SARA fractions. SARA (Saturates, Aromatics, Resins and Asphaltenes) fractionation is the technique used to separate the heavy oil in fractions soluble to different solvents (details of the analysis can be found on section 4.1.7). Examples of proposed molecular structures are shown in Figure 2.7. SARA fractions separate the heavy oil in terms of the polarity which is the tendency of molecules to interact with surrounding molecules due to an imbalance of the electric charge. Polarity increases from saturates to asphaltenes. Asphaltenes being the most polar fraction. Evidence of the increased polarity of asphaltenes and resins with respect to aromatics and saturates can be presented in terms of dipole moment, dielectric constant or conductivity as shown by several authors (Chow et al., 2004; Evdokimov & Losev 2010; Goual & Firoozabadi, 2002). Figure 2.8 from Chow et al. (2004) shows how the dielectric constant of toluene increased with the addition of asphaltene and resins. Goual & Firoozabadi (2002) reported the dipole moment of asphaltenes to be twice as much as the dipole moment of resins, and four times the dipole moment of the

maltenes (saturates plus aromatics). There is also an increased molecular weight from saturates to asphaltenes but there can be significant overlap in this property as shown in Figure 2.9.

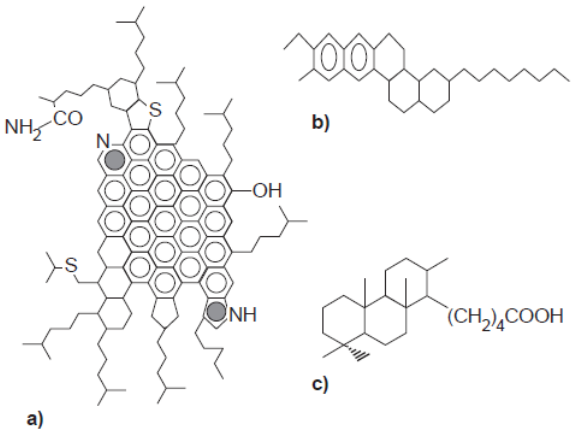

Figure 2.7. Proposed molecular structures of (a) asphaltene, (b) resin and (c) naphtenic acid from (Langevin et al. 2004)

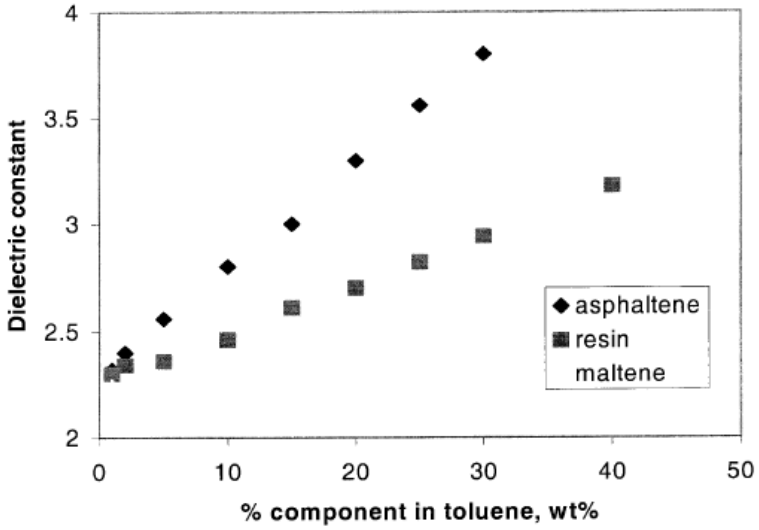

Figure 2.8. Measured dielectric constant of asphaltenes and resins from Athabasca bitumen as function of concentration in toluene (Chow et al. 2004).

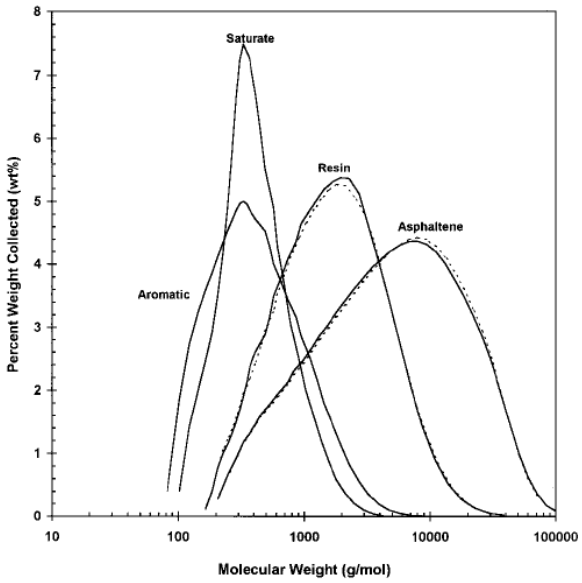

Figure 2.9. Distribution of molecular weight by SARA fraction. Significant overlap is seen between resins and asphaltenes, and between aromatics and saturates. Asphaltenes and resins have higher molecular weight than the lighter fractions (Peramanu et al. 1999).

Resins and asphaltenes are the fractions with the highest polarity and tend to interact and form aggregates or macromolecules (Figure 2.10 and Figure 2.11). These asphaltene aggregates are often called asphaltene colloids or micelles in the literature.

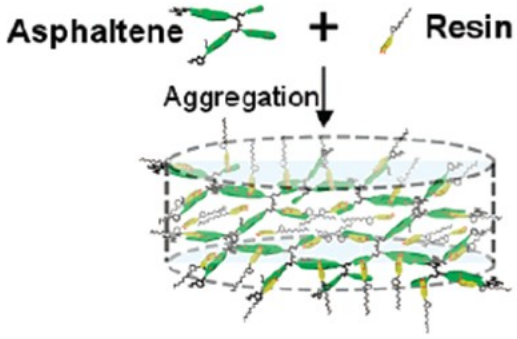

Figure 2.10. Asphaltenes and resins forming aggregates or macromolecules (modified from Yang,et al. (2007)).

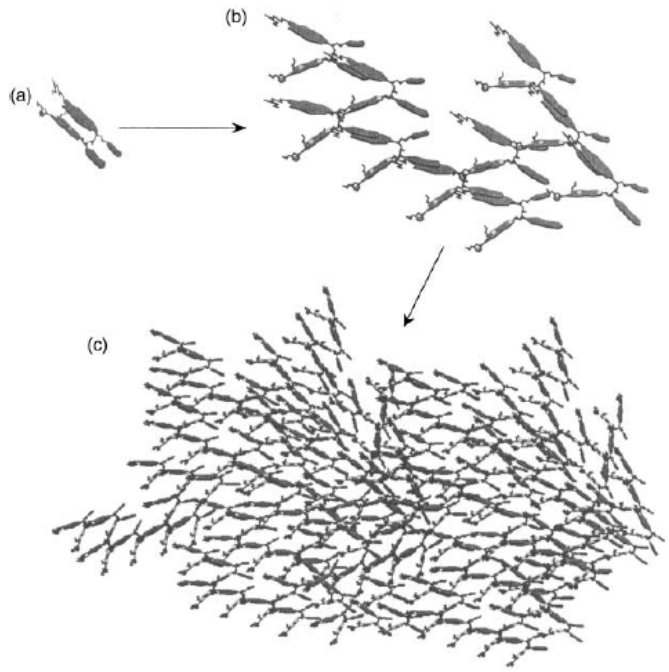

Figure 2.11. Schematic illustration depicting (a) an asphaltene monomer; (b) an asphaltene aggregate of small size and (c) an asphaltene aggregate with larger size (Gawrys and Kilpatrick 2004).

2.3.1. Asphaltene aggregate size and molecular weight

Asphaltene aggregates size varies significantly depending on the molecular weight, asphaltenes concentration, nature of the solvent and temperature. Studies such as the ones by Espinat et al. (2004) and Sheu & Acevedo (2001) indicate that asphaltenes have a high tendency to self-associate and form extended aggregates. The size of the aggregates is affected by the nature of the asphaltene, as for example, Pacheco-Sanchez et al. (2003) concluded that more aromatic asphaltenes have a higher tendency to produce graphite-like structures. The size of asphaltene molecules or aggregates has been reported to be in the range of several angstroms to several micrometers. The wide range of molecular weights and sizes reported are due to the controversy if scientists have been measuring the size or molecular weight of an individual asphaltene molecule or asphaltene aggregates. An example of these is shown in Figure 2.12 from Nielsen et al. (1994), were the average asphaltene particle is found to vary between 300 and 450 microns (figure is plotted in logarithmic scale) while authors such as Fenistein & Barre (2001) report radii of gyrations between 33 to 253 angstroms. Another example of asphaltene aggregate particle size is provided by Barre et al. (1997) in Figure 2.13, with particle size in the range of several microns. Fenistein & Barre (2001) also reported asphaltenes with molecular weights ranging from 24,000 to 1,560,000 g/mol while Espinat et al. (2004) and Vasquez & Mansoori (2000) show values as low as 100 g/mol (Figure 2.9 and Figure 2.14). The molecular weight of the asphaltenes, which is an indication of its size, has been reported to increase with asphaltene concentration (Espinat et al. 2004). However, due to the difficulties of measuring asphaltenes particle inside a crude oil sample, tests to

measure the size of asphaltene aggregates are usually carried out in diluted samples, therefore a good insight on the size of the asphaltenes molecules or structures inside the oil sample with high asphaltene and resins content as the ones I used in my work was not found in the literature.

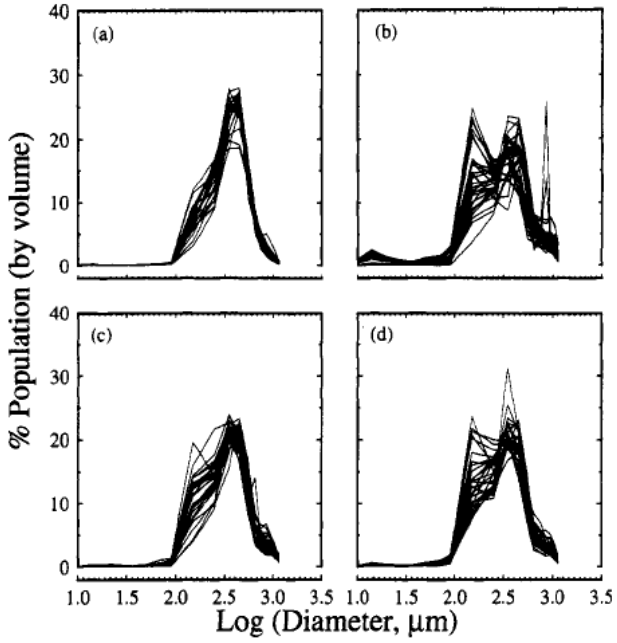

Figure 2.12. Asphaltenes particle size at 0 degrees C for four different heavy oils with varying asphaltenes content (a) Border condensate (0.6% asphaltenes), (b) Countess oil (5.7%), (c) Lindberg heavy oil (17.6%) and Cold Lake bitumen (21.8%). Particle size for samples (c) and (d) were obtained after dilution in toluene (from Nielsen et al. (1994)).

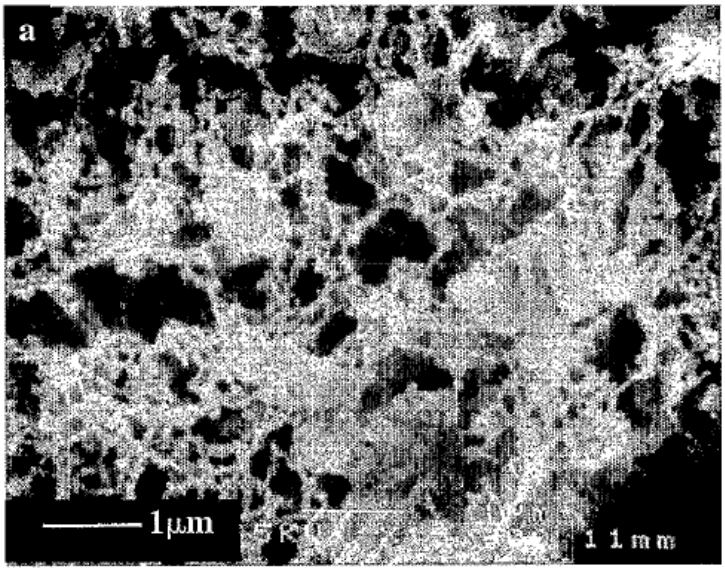

Figure 2.13. Vacuum residue asphaltene in toluene with n-heptane solution. Dimensions of the structures are in the several microns range (Barre et al. 1997).

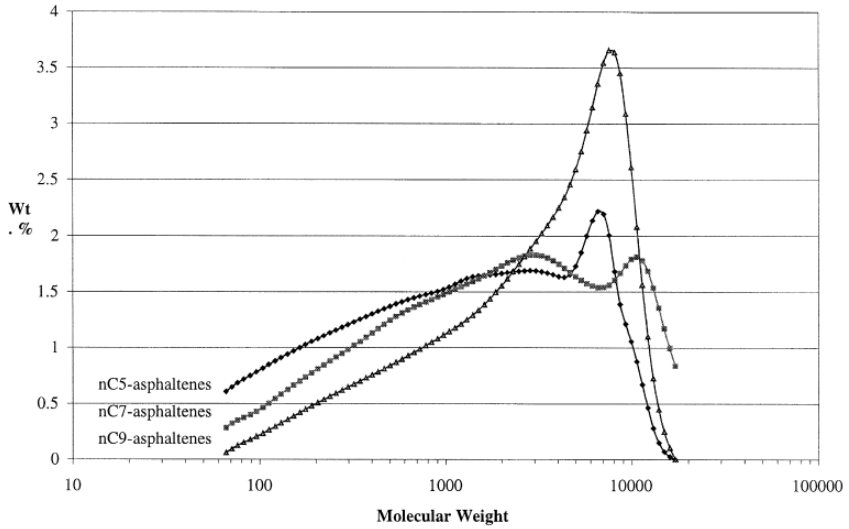

Figure 2.14. Molecular weight distribution of asphaltenes obtained by Gel Permeation Chromatography (GPC) studies from five different crude oils using different solvents for precipitation (nC5, nC7 and nC9) (Vasquez & Mansoori 2000). Molecular weight varies from ~100 to ~20,000 g/mol.

2.3.2. Effect of temperature in aggregates size

One important factor controlling the size of the asphaltenes aggregates is temperature. Espinat et al. (2004) measured a progressive increase in aggregate molecular weight when decreasing temperature. They calculated the radii of gyration of the asphaltenes in toluene with temperature and saw an important increase as they lowered the temperature. They described that when reducing temperature, first the asphaltenes follow a fractal-like type of association followed by flocculation (Figure 2.15). During cooling of the asphaltenes solution they were able to see very large aggregates with their bare eyes. In their work they compare the effects of lowering the temperature to those of adding a light hydrocarbon (i.e. n-heptane) to induce flocculation. A similar trend was seen by Sheu & Acevedo (2001) also for asphaltenes in toluene Figure 2.16.

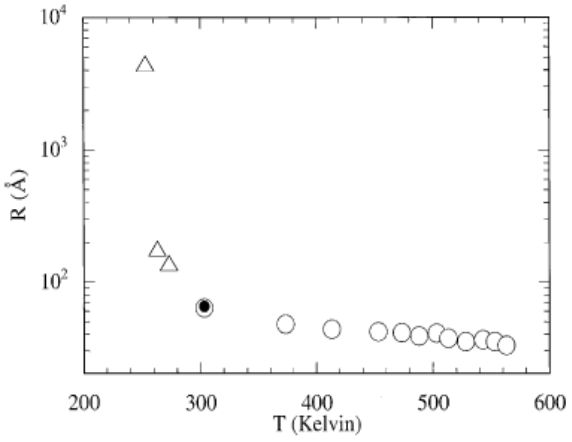

Figure 2.15. Radii of gyration vs. temperature for asphaltenes in toluene measured by three techniques represented by the different symbols (Espinat et al. 2004)

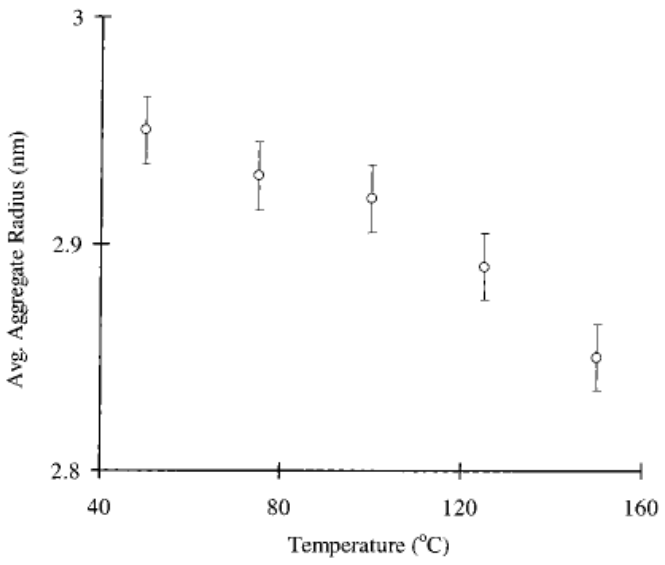

Figure 2.16. Average radius or gyration of asphaltene particles in toluene vs. temperature (Sheu & Acevedo 2001)

2.3.3. Viscosity and shear modulus of heavy oils

A key characteristic of heavy oils is the large viscosity and shear modulus it presents at room temperature. Viscosity of heavy oils is highly dependent on temperature and it shows a loose relation with API gravity as portrayed in Figure 2.17 and Figure 2.18a. Note the orders of magnitude variability in viscosity for any given API. These figures show that density alone cannot explain the rheological behavior of heavy oils. Hinkle et al. (2008) found that composition in terms of SARA fractions was a better predictor of viscosity bringing a direct connection between polarity of the sample and the shear properties. Figure 2.18 shows the viscosity prediction for seven heavy oils versus API gravity (a) and versus the asphaltenes plus resins fractions (b). The SARA fractions with highest polarity (resins and asphaltenes), shows an excellent correlation with viscosity.

The relation between composition and viscosity is a key finding since viscosity is the major attribute controlling production and recovery of heavy oil reservoirs. Production and thermal recovery methods are designed around viscosity reduction for its extreme dependence on temperature as viscosity values can change orders of magnitude with relative small changes in temperature.

Another important characteristic of heavy oils, in which I will be focusing my work, is its acoustic and mechanical behavior. The acoustic behavior of heavy oils differs from the rest of the reservoir fluids (gas, water and lights oils) as it can propagate shear waves while all other fluids cannot. The capacity of heavy oils to propagate shear waves is due to its viscoelasticity, which means it simultaneously exhibit properties of both elastic solids and viscous fluids as it was explained in section 2.1.

As it was mentioned in the introduction, my research is focused on the measurements and understanding of the shear behavior of heavy oils, therefore in the next subsections I will explain what it was known until now about the dependence of heavy oils on temperature, composition, frequency and amplitude.

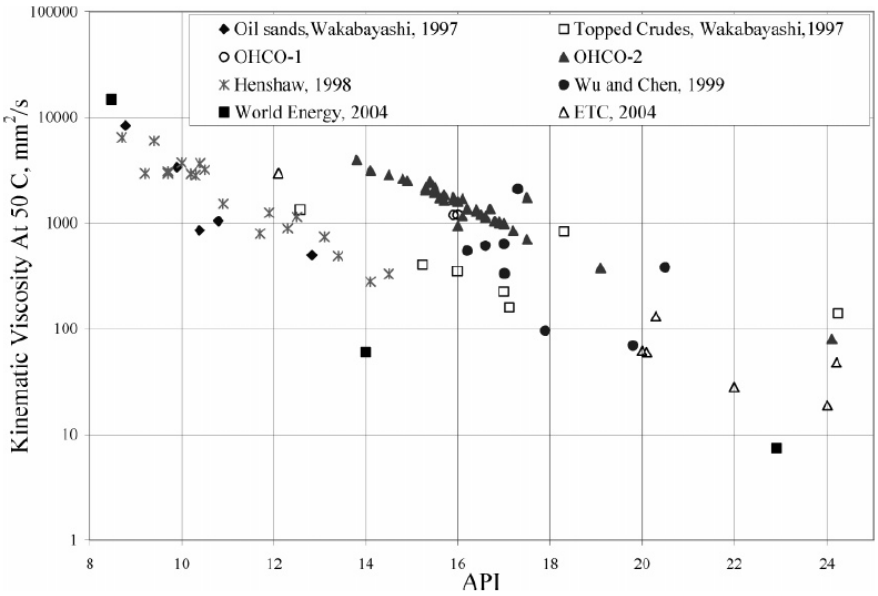

Figure 2.17. Viscosity vs. API gravity at 50 C from Al-Maamari, et al. (2006)

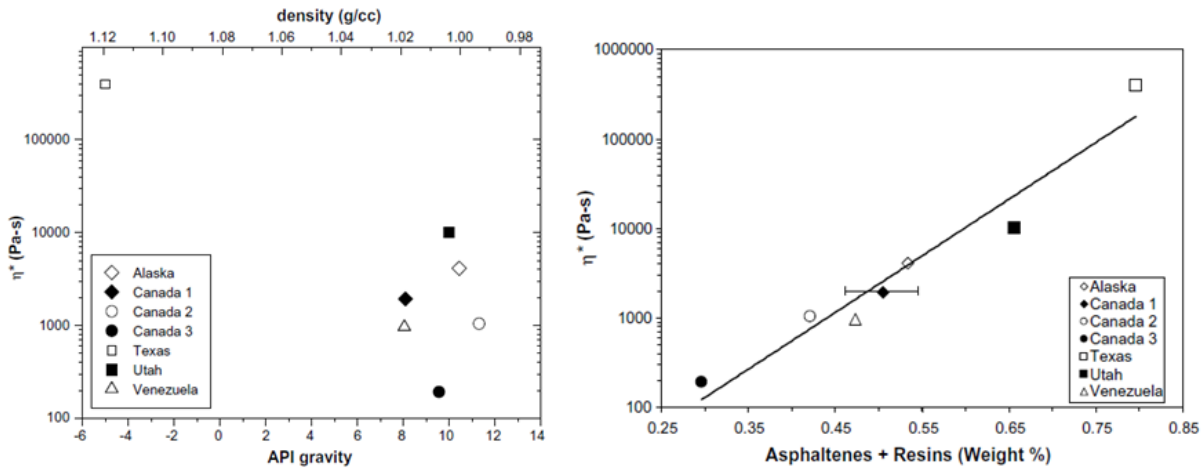

Figure 2.18. (a) Viscosity vs. API gravity, (b) Viscosity vs. Asphaltene + Resins fractions from Hinkle et al. (2008).

2.3.4. Shear modulus dependence on temperature

The dependence of the shear modulus of heavy oils with temperature has been recognized for long time. Eastwood (1993) observed a large change of P-wave velocity of Cold Lake bitumen fluid sample with temperature. Within that variation he observed a departure from a linear relation for temperatures less than 60C (Figure 2.19). Even though not recognized at that time, this departure constituted evidence of the presence of the "liquid point" in heavy oils when a transition from liquid to solid behavior begins to occur.

Heavy oil behavior with temperature presents two definite points where its properties change systematically, the glass and liquid points. There are several ways to define the glass and liquid points; for example in terms of differential scanning calorimetry (DSC) where phase changes can be identified based on discontinuities in the heat flow (Abivin et al. 2011). These discontinuities represent changes in the molecular configuration when passing from solid to quasi-solid (or viscoelastic) and from quasi-solid to liquid state. Acoustically, the liquid point can be defined as the temperature below at which a fluid sample begins to transmit shear waves and there is a non-linear change of P-wave velocity with temperature. On the other hand, the glass point is the transition from non-linear to linear velocity variations of both P and shear wave velocities with temperature (Figure 2.20). At temperatures above the liquid point, heavy oils behave like viscous-liquids and below the glass point they behave like elastic-solids. Between the liquid and glass points the heavy oil behaves like a viscoelastic material.

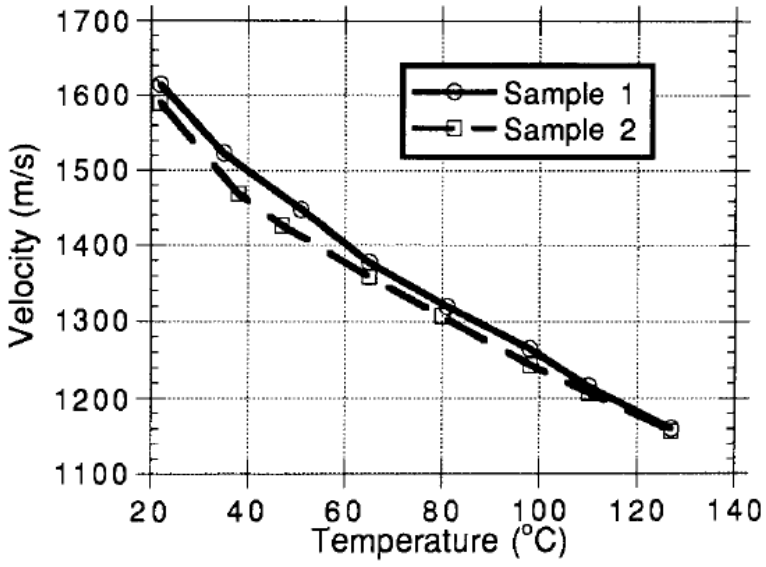

Figure 2.19. Measured compressional velocities of bitumen samples as a function of temperature. A departure from the linear behavior at 60 C is an indication of the onset of the viscoelastic behavior of the heavy oil (Eastwood 1993).

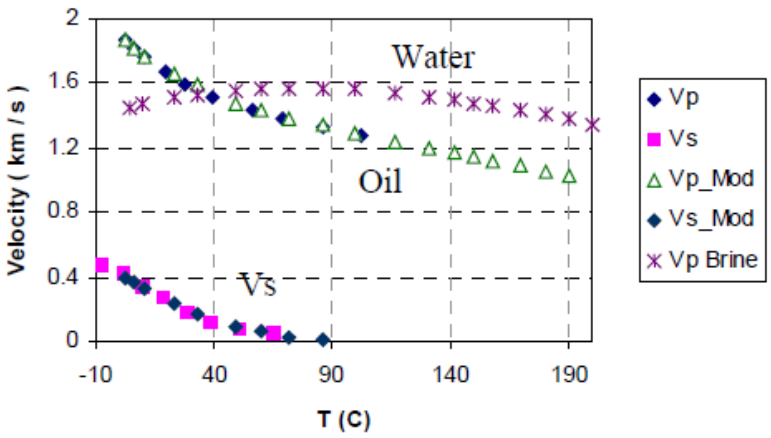

Figure 2.20. Measured and modeled velocities of heavy oil (API: 9.2) and water (Han et al. 2007)

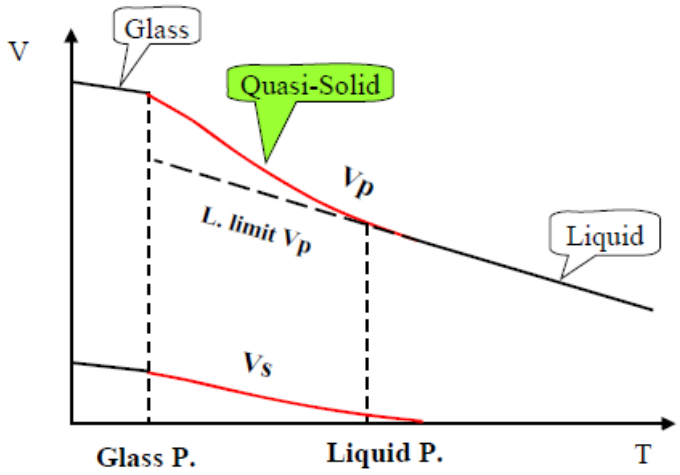

Figure 2.21. Schematic of phase change of heavy oil with temperature from (Han et al. 2007). Glass and liquid points represent the change from solid (glass) to viscoelastic (quasi-solid) and from viscoelastic to fluid (liquid) respectively.

These phase transitions between solid and liquid states, have been measured by several researches among them Han et al. (2007) generalized the onset of the liquid and glass points in a heavy oil sample shown in Figure 2.21. Batzle et al. (2004) also show the decrease of the shear modulus of a heavy oil sample when increasing temperature (Figure 2.22).

2.3.5. Shear modulus dependence on composition

Many authors have observed important variations on the elastic properties for different heavy oils. Abivin et al. (2011) studied different heavy oils through DSC and show how the temperature of the glass

point decreases with the API of the crude (Figure 2.23). The relation is not strong since relationships with density are not the most appropriate (as demonstrated in Figure 2.18a) but changes are evident.

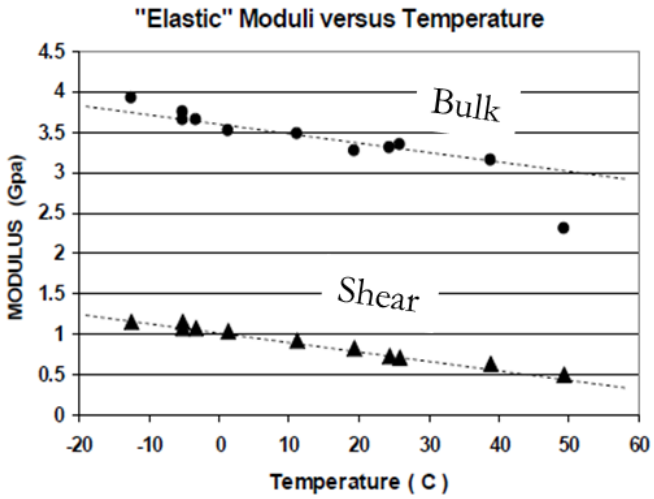

Figure 2.22. Elastic moduli of the GP007-Uvalde heavy oil (API: -5) from ultrasonic data. The effective shear modulus (triangles) drops toward zero as temperatures approach 80 C (Batzle et al. 2004).

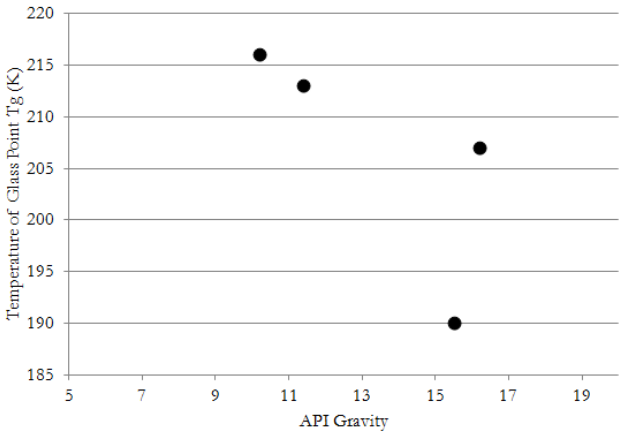

Figure 2.23. Temperature of glass point vs. API gravity of heavy oils data modified from Abivin et al. (2011).

Hasan (2010) studied Athabasca Bitumen and Maya crude oil and the results show how the temperature and frequency behavior changes between these two oils that have different composition. The Athabasca oil (Figure 2.24) has asphaltenes plus resins content equal to 35 percent while for Maya crude oil (Figure 2.25) this value is 26 percent. Comparing these two figures at a constant temperature (i.e. 270K), we can see that the Athabasca oil behaves like a viscoelastic material with a strong frequency dependency, while at the same temperature the Maya oil has a phase angle greater than 80 degrees and it is behaving like a liquid with almost no frequency dependency. The larger content of asphaltenes plus resins in the Athabasca bitumen is responsible for this behavior.

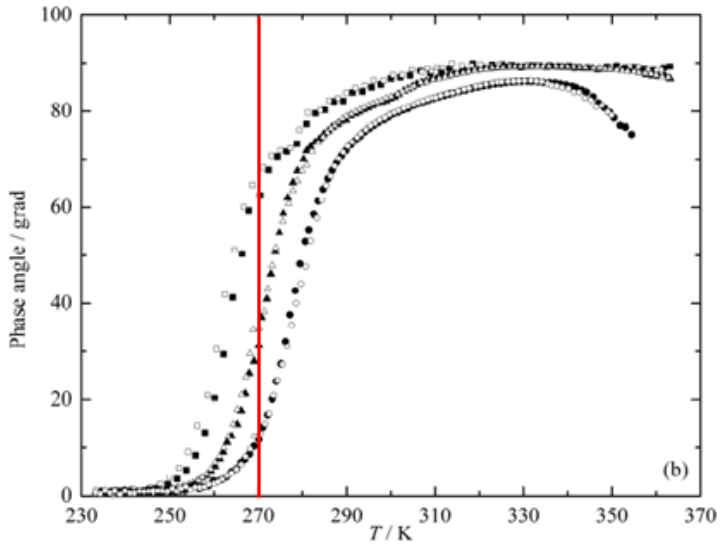

Figure 2.24. Frequency and temperature dependency of phase angle between stress and strain for Athabasca bitumen at three different frequencies, 0.1 (squares), 1 (triangles) and 10 Hz (circles) (Hasan 2010). At 270K the heavy oil is in the viscoelastic regimen with phase angles ranging from 70 to 15 degrees for the different frequencies tested. Asphaltenes plus resins = 35 percent.

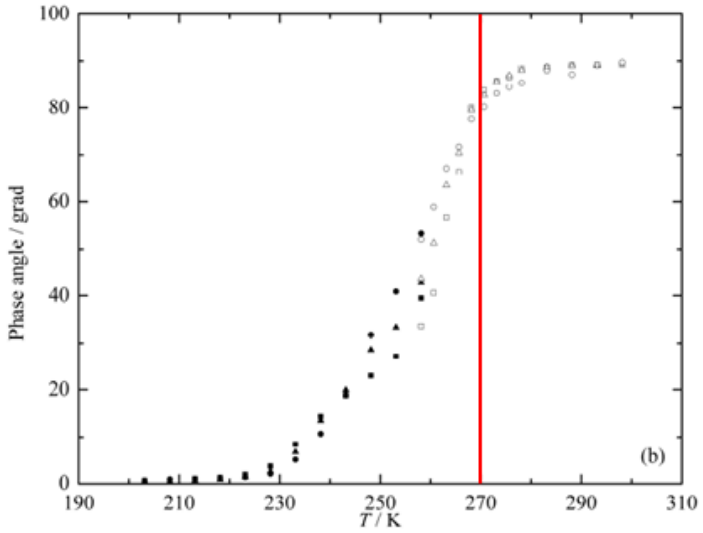

Figure 2.25. Frequency and temperature dependency of phase angle for Maya crude oil bitumen at three different frequencies, 0.1 (squares), 1 (triangles) and 10 Hz (circles) (Hasan 2010). This oil is "lighter" (lower Asphaltenes plus Resins content, 26 percent) than the one shown in Figure 2.24. At 270K this crude oil has a phase angle above 80 degrees and with not much variation between the three frequencies tested.

Similarly the association between resins and asphaltenes was considered responsible for the increase in viscosity from different samples around the world by Hinkle et al. (2008) and shown in Figure 2.18b.

The above description of the dependence of the shear modulus of heavy oils with composition is given at a macro scale where the bulk properties of the material are studied. However, to better understand how the components of heavy oils influence their viscoelastic behavior I will explain viscoelasticity on a molecular scale. For this, I need to introduce the concept of relaxation time. A simple explanation of relaxation time given by Matsuoka (1992) is that relaxation time is the time necessary for a system to "forget" the configuration it had prior to a perturbation. In shear modulus terms, it refers to how fast a molecule, particle or aggregate that was subject to shear deformation can come back to its original configuration. The relaxation process is then associated to some kind of molecular motion. In pure viscous-fluids there is enough space between molecules and the relaxation process is very fast; as a result, this process depends only on the properties of the fundamental molecule. As we lower the temperature, increase molecular size or increase interaction between molecules, the distance between molecules is reduced and cooperative process begins to act (Matsuoka & Hale 1997). A cooperative process refers to the fact that when molecules are densely packed they need to relax simultaneously and "cooperate" between them in order to change their configuration.

From Matsuoka & Hale (1997) it can be interpreted that in heavy oils, the association between molecules in the solid-like state is mainly due to the polar nature of its heavier components (asphaltenes and resins) and a secondary effect is the molecular weight of these components. However in the liquid state, when the interaction between components is reduced, the characteristic of the individual molecule becomes more relevant and not as much the interaction between them. Subsequently, it is expected that the effects of molecular weight becomes more important for liquid-like materials. Even though the above explanation is given in terms of molecules, same effects are also present in aggregates or macromolecules present in heavy oils.

The aggregates present in heavy oils need more time to "relax" in the presence of shear deformation and this time will depend on composition as when asphaltenes and resins concentrations increase the number of small molecules in the system is reduced. A reduced number of small molecules and an increase in polar components, translates in reduced free molecular motion and requires larger synchronization. Large synchronization translates in a broader distribution of relaxation times and so an increased frequency dependency.

2.3.6. Shear modulus dependence on frequency

In the previous sections, we described the temperature and composition dependence of the viscoelastic properties of heavy oils. The examples provided in Figure 2.20 and Figure 2.22 where the temperature dependence is evident, were collected at a single ultrasonic frequency. However, the viscoelastic behavior of materials is also highly dependent on frequency, which is also referred to as frequency dispersion. Frequency dependence is of great interest in geophysics as many of the geophysical measurements are collected at different frequencies. Being able to characterize the

frequency dispersion is key in order to interpret and compare results that were acquired a different frequencies.

At a fixed temperature and low frequencies a heavy oil system may behave like a viscous-liquid since the relaxation time of the fluid system may be fast enough to respond to the slow dynamic perturbation. As frequency is increased, the time of the perturbation decreases and the system does not have time to respond and it enters the glass transition zone. If frequency is increased further, the system enters the glassy state and behaves as a solid at high frequencies. This dependence was measured by Batzle, et al. (2006a) in a heavy oil of API of -5 (Figure 2.26) using a low-amplitude tension/compression technique.

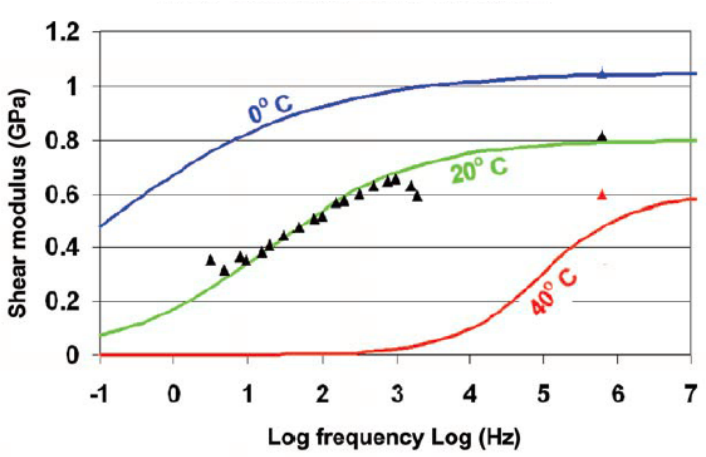

Figure 2.26. Measured (triangles) shear modulus in the GP007-Uvalde heavy oil (API: -5). High-frequency shear modulus comes from ultrasonic data. Low-frequency data were measured using a low-amplitude stress-strain technique. Solid lines are from Cole-Cole dispersion model (Batzle, et al. 2006a)

Rojas (2010) also measured frequency dependant shear modulus of several heavy oils observing large variations with frequency and temperature (Figure 2.27). She used rheology and ultrasonic measurements on different samples. Hinkle et al. (2008) also characterized the shear behavior of heavy oils with frequencies using rheological measurements (Figure 2.28). These results both indicate that the liquid and glass points of heavy oils depend not only on temperature but also on frequency.

2.3.7. Frequency dispersion models

Dispersion models are used to describe the elastic or dielectric behavior of any material with frequency with the use of a limited number of adjusting parameters. The focus of my work is the shear modulus of heavy oils so I will describe the dispersion models in terms of shear modulus. The simplest model to describe the dispersive behavior is Maxwell's model which was also described by Debye as a system with a single relaxation mechanism (Cole & Cole 1941). Equation 2.13 describes the Debye

behavior as a function of three parameters: G_0 which is the modulus at zero frequency, G_∞ is the modulus at infinite frequency and τ_0 is the relaxation time or its inverse, which is called the peak frequency.

$$G^* = G_\infty - \frac{(G_\infty - G_0)}{(1+iw\tau_0)} \qquad (2.13)$$

Batzle, et al. (2006a) described Maxwell's model as providing the proper trends but with curves too steep as they account for only one relaxation time. Figure 2.29 shows Debye's behavior as function of normalized frequency (a) and its complex plane representation (b) as a perfect semicircle.

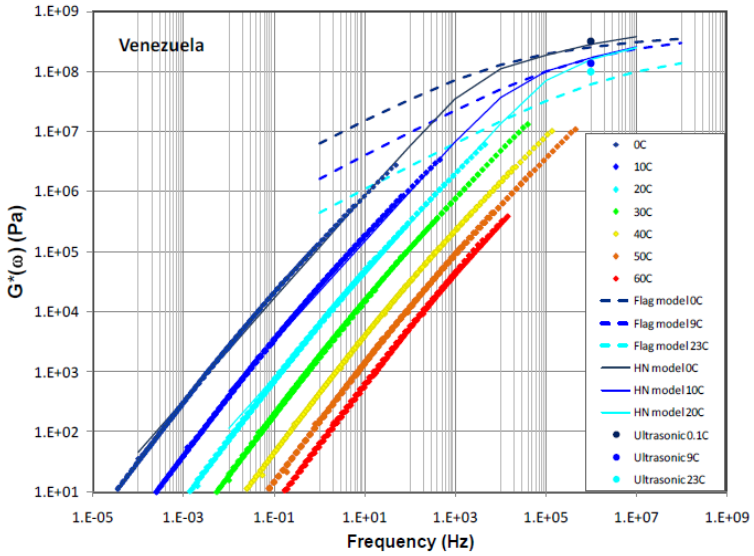

Figure 2.27. Comparison of complex shear modulus at ultrasonic and low frequencies for Venezuela heavy oil sample (Rojas 2010).

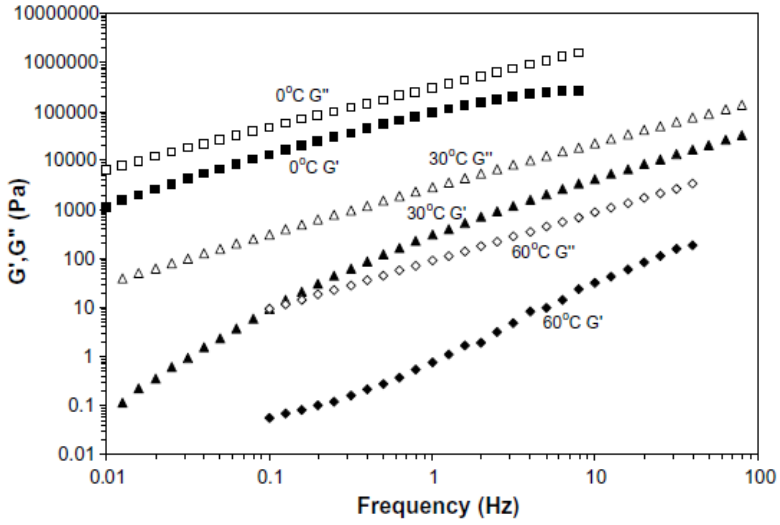

Figure 2.28. Storage modulus (G') and loss modulus (G") measured as a function of temperature (Hinkle et al. 2008)

As explained in the previous section, heavy oils are composed of a wide range of molecular sizes and varying molecular structures and they are expected to have a distribution of relaxation times in place of a single relaxation time described by Maxwell. The distribution of relaxations times expected in heavy oils is better described by models derived from Cole-Cole's equation (Cole & Cole 1941). The Cole-Cole model adds one parameter (α) to Maxwell's model to describe the spread in relaxation times, thus the number of adjusting parameters increases to four (equation 2.14)

$$G^* = G_\infty - \frac{(G_\infty - G_0)}{(1+(iw\tau_0)^{1-\alpha})} \qquad (2.14)$$

This equation shows as a circular arc with the center of the circle lowered when plotted in the complex plane (Figure 2.30).

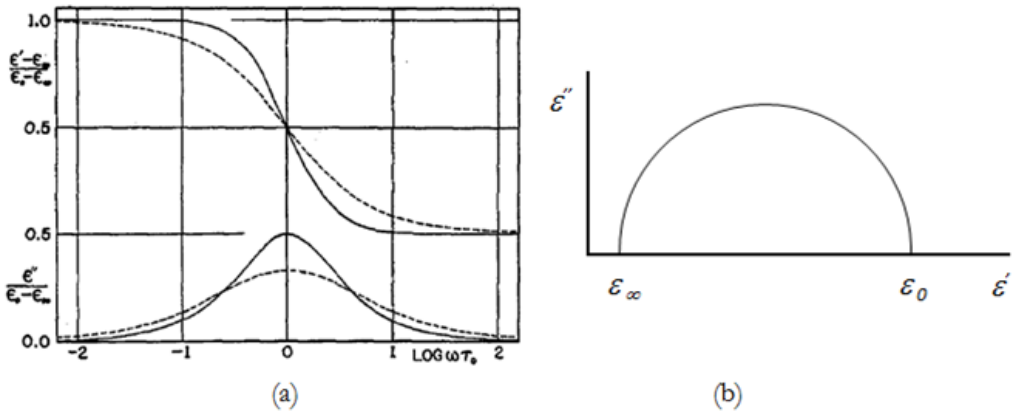

Figure 2.29. (a) Debye's real and imaginary part (continuous lines) vs., experimental (dashed). (b) Real vs. Imaginary part Debye's behavior. ε stands for the dielectric constants studied in the cited work (Modified from Cole & Cole (1941).

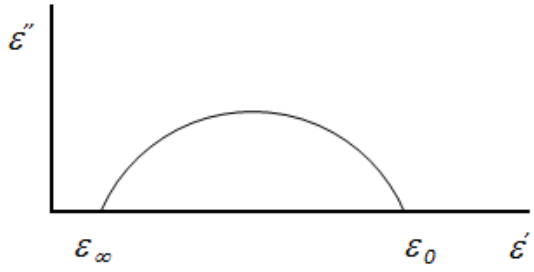

Figure 2.30. Complex plane representation of Cole-Cole's model. The complex behavior is represented by a circular arc with depressed center. ε stands for the dielectric constants studied in the cited work (Modified from Cole & Cole (1941))

The Cole-Cole fit to the frequency dispersion of the real part of the shear modulus (storage) of a heavy oil is shown by the continuous line in Figure 2.26.

Other models are available to describe frequency dependence. Rojas (2010) in Figure 2.27 and Han et al. (2007) used a modification of the Cole-Cole model proposed by Havriliak & Negami (1967) (HN model). This model adds a parameter (γ) to account for deviations in the behavior of the material at low frequencies (equation 2.15).

$$G^* = G_\infty - \frac{(G_\infty - G_0)}{(1+(iw\tau_0)^{1-\alpha})^\gamma} \quad (2.15)$$

Besides the HN model there are many other dispersion models that try to adjust the frequency behavior in different parts of the curves. Friedrich & Braun (1992), for example, separate the alpha term in the Cole-Cole model into two parameters which allows adjusting the behavior at high frequencies. In this case, the behavior at low frequencies remains the same and when both terms are equal, the model is equivalent to the Cole-Cole model. They designed their model to correlate with a "flow region" at low frequencies and a "glazzy zone" at high frequencies. Bergman (2000) studied the contribution of many of these models and summarized the behavior of the imaginary part in a single equation with five adjustable parameters. These five parameters are the slope at low (a) and high frequency (b), the peak frequency (ω_p), value of the peak ($G_p^{''}$) and width of the peak (C) (equation 2.16).

$$G'' = \frac{G_p''}{\frac{(1-C)}{a+b}\left[b(\omega/\omega_p)^{-a} + a(\omega/\omega_p)^{b}\right] + C} \quad (2.16)$$

This equation reduces to the imaginary part of the Cole-Cole equation when $a = b = \alpha$ and $\omega_p = 1/\tau_0$. The value of the peak (in the *G''* vs. frequency plot, attenuation peak) can be described in terms of the values at zero and infinite frequencies (equation 2.17).

$$G_p'' = [(G_\infty - G_0)/2]\tan(a\pi/4) \quad (2.17)$$

And the C term is described as follow (equation 2.18)

$$C = \frac{1}{2}\left[1 - \tan^2\left(\frac{a\pi}{4}\right)\right] \quad (2.18)$$

Bergman's equation adds more flexibility to analyze the imaginary behavior in detail to obtain a good representation of the heavy oil system. However, we must be careful when adding parameters just to fit the experimental data, since these new parameters may have no physical significance. On the other hand, a correct description of the imaginary part is significant as the attenuation magnitude can be obtained by the ratio of the imaginary to the real part of the shear modulus (equation 2.6).

The significance of the dispersion models relies on the fact that many of the geophysical measurements are done at different frequencies, and in order to compare or validate them we need to

consider how the property changes with frequency. In this work, I will use only the Cole-Cole model to provide some guidance in this comparison as the main objective of my research is not to model the details of the frequency dispersion but to understand the behavior of the heavy oils.

Dispersion models also can be used to correlate the shear modulus with composition as it was tested by Das (2010) when trying to link the modulus at infinite frequency with the fraction of asphaltenes plus resins in the heavy oils (Figure 2.31). This connection between the theory of dispersion models and chemical composition of heavy oils has not been done before. Even though at that time Das (2010) was discouraged with his findings, the visible trend observed in Figure 2.31 gives an indication that the fitting parameters of the dispersion model can be related to composition.

Even though the use of extended dispersion models to model the shear modulus from composition is outside the scope of my project, it is important to understand the significance and applicability of each of the parameters of the models to heavy oils. For this, I will use the Bergman model as it summarizes many of the existing dispersion models and mention the equivalent description to the Cole-Cole model. It is important to note that the Bergman model uses a large number of fitting parameters which may not be necessary to fit the experimental data. This is significant as the experimental error may be larger than what the additional parameter can add to the data fit. In the following paragraphs, I will analyze the connection between the chemical composition and the fitting parameters of the dispersion model.

I will begin with the slope at low and high frequencies (in the *G'* vs. *G''* plot). Bergman (2000) explains that for glass-forming materials it is expected that at low frequencies the behavior be described by a single exponential, which will be the equivalent to $\alpha = 1$ in the Cole-Cole model and $a = 1$ in Bergman's model. A single relaxation behavior is expected for materials with simple composition. In this case, all molecules are the same and the type of interaction between them is unique, occurring at a single frequency. In heavy oils, at low frequencies (or high temperatures) the molecules have enough time to relax after a perturbation, however, due to the complex composition a distribution of relaxation times is expected ($a = \alpha \neq 1$). In this manner, α (Cole-Cole) or a (Bergman) describes the chemical diversity of the system.

At high frequencies (or low temperatures) the time between perturbations (or the distance between molecules) is reduced, under this condition molecules have less time to relax. If this effect is combined with the presence of molecules with high polarity (resins and asphaltenes), the capacity of the system to relax decreases even further. The effect of the high polarity molecules may be different at low frequencies when the distance between molecules is greater and can move more freely. The difference between the effect of the polarity at low and high frequency may require $b < a$ in the model. As "a" represents the slope at low frequencies and "b" the slope at high frequencies. When "a" is different than "b" two different relaxation mechanisms are expected.

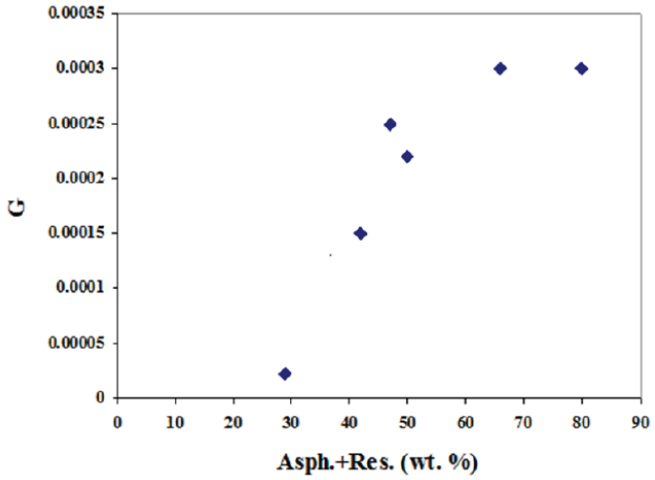

Figure 2.31. Storage modulus at extrapolated infinite frequency (G_∞) vs. Asphaltene + Resins for a set of heavy oils (Das 2010).

The C term describes the coupling between the relaxation mechanisms at low and high frequencies. A system that relaxes completely differently at low and high frequencies will have a value of $C = 0$, assuming no coupling between the low and high frequencies. In contrast, if $C \neq 0$, as in the Cole-Cole model, a synchronized process is described. The coupling effect refers to the synchronization occurring in the system as the individual units (or components) in the system need to interact with each other in order to relax.

2.3.8. Shear modulus dependence on amplitude

The relation between stress and strain in *linear* viscoelastic materials depends only on frequency (or time) and not on stress or strain magnitude (Ferry 1980). However, materials behave linearly depending, not only on the sample itself but also on the magnitude of the strain they are subjected to, in this case materials present nonlinearity. In the rheometer experiments pertaining to my work, strain amplitudes are selected to ensure that the experiments are performed under the Linear Viscoelastic Regime (LVR). The LVR is the region in which the storage modulus stays constant with increased strains. The common behavior of the storage modulus is to decrease as the strain reaches the critical strain (Figure 2.32a) called strain thinning; yet the reverse behavior can be seen in some materials that increase their modulus as they reach their critical strain (Figure 2.32b), this is called strain hardening or stiffening. Materials in general behave linearly for a limited range of amplitudes after which nonlinearities in the material appear.

Under strain magnitudes used in the rheometer (order of 10^{-4}) heavy oils have a strain thinning behavior. For strain amplitudes greater than the critical strain, a rupture in the structure of the fluid occurs and the shear modulus decreases.

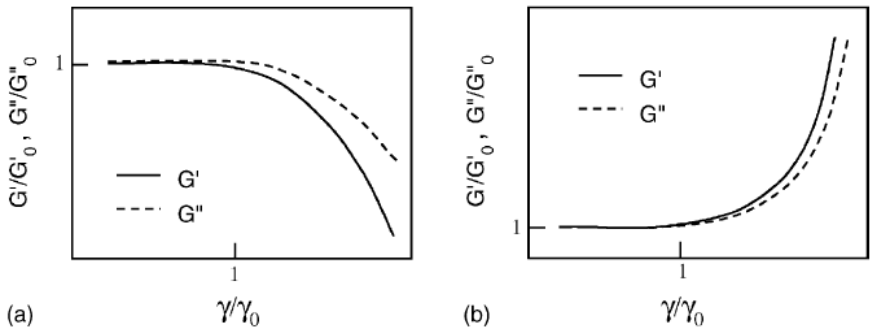

Figure 2.32. Large amplitude oscillatory shear (LAOS) behavior (a) strain thinning; (b) strain hardening (Hyun et al. 2002). G'/G'$_0$*, normalized storage modulus;* G"/G"$_0$*, normalized loss modulus and* γ/γ_0*, normalized critical strain.*

Heavy oils form large aggregates due to association between components with large polarity (asphaltenes and resins). Under large strains these structures can break down into smaller structures resulting in a decrease in the shear modulus. Figure 2.33, modified from Li et al. (2009), shows a schematic representation of this phenomenon in which several macrostructures of aggregates are broken down under the effect of shear.

A constant storage modulus (G') measured within in a region of strain amplitudes does not prove that the presence of another region of different constant storage modulus at lower or higher amplitudes could exist. Amplitude dependence is a key subject for my research and more explanations will be given in the results section 4.3.

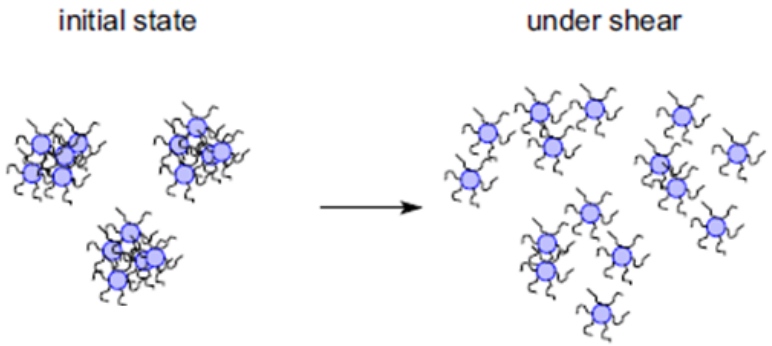

Figure 2.33. Schematic of aggregate break down. Expected behavior of heavy oil aggregates under large strains. Modified from Li et al. (2009).

2.4. Additional concepts

As part of this background I will introduce some additional concepts that are helpful in understanding the behavior of heavy oils during shear measurements. These are adhesion, cohesion, adsorption and slip.

2.4.1. Adhesion

The concept of adhesion differs depending on the source, but one clear definition is that adhesion is the state in which two bodies are held together by interfacial contact, and forces can be applied to that interface without necessarily causing separation (Drew & Myers 1999). Adhesion can refer to the intermolecular forces acting in the interface that allows the two bodies to remain together, but it also refers to the mechanical adhesion caused by interlocking of microscopic roughness between the two materials.

2.4.2. Adsorption at solid-liquid interfaces

Adsorption can be defined as the preferential concentration of certain components in an interface creating different concentrations at the interface from that of the "bulk". In the case of a solid-liquid interface, the adsorption of the liquid in the solid creates a transition zone in the order of molecular dimensions. In a simple liquid, there may be a greater concentration of molecules near the solid surface, but if there are interactions between the solid and the liquid (like in the case of surface active materials), reorientation of the molecules can occur near the surface possibly changing the density, dielectric constant or other physical characteristics of the liquid (Drew & Myers 1999). Figure 2.34 shows the increase on the interfacial region between a simple liquid with no interaction with the surface (a) versus a liquid that oriented itself due to the presence of the solid surface (b).

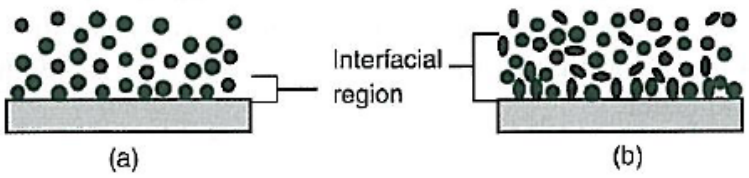

Figure 2.34. At a solid-liquid interface two types of adsorption scenarios may be present: (a) quasi-uniform molecular distribution (pure liquids), or (b) extensive adsorption in the case of surface active molecules. In this case the interfacial region is much wider than in pure liquids (Drew & Myers 1999).

2.4.3. Slip or wall slippage in rheology measurements

In rheology measurements, all calculations consider that the velocity of the fluid close to the wall equals zero, also called a condition of no-flow or no-slip. However, in many materials and for diverse reasons this condition is not maintained and a value of velocity at the wall can be measured, which is called slip. If slip is present, rheology measurements read lower values of viscosity and shear modulus. Slip can be classified in "true" slip, when there is a real discontinuity of the velocity at the solid surface, or as "apparent" slip when a layer of higher velocity builds near the solid surface (Yoshimura & Prud'homme 1988). True slip occurs when the adsorbed material to the surface "slides" along the wall, which is usually present when the interaction with the wall is weak. In the case of adsorbed polymer chains with stronger interaction with the wall, the polymer chains can experience a stretch phenomena and

disentanglement (“apparent slip”). When the bonding with the walls is very strong, slip will only occur at very high stresses (Dorgan & Rorrer 2013). For materials with suspended particles or emulsions, a “depleted” layer can appear near to the wall, creating a high velocity layer. Independently of the mechanism of slip, it always translates in a reduction of viscosity or shear modulus when increasing stress for values greater than a certain yield stress.

In the case of oscillatory measurements, a sign of true slip can be identified by a distortion in the sinusoidal response of the strain. This distortion can include asymmetric periodic, non-periodic, quasiperiodic or chaotic responses (Graham 1995). The deviation from a pure sinusoidal response of the strain (or stress) is then a strong evidence of slip (Adrian & Giacomin (1992), Lan et al. (2000)). Note that this can lead to particular problems in automated systems where the results are given under the assumption of a pure sinusoidal behavior.

2.5. Applications of my research

In this section, I will give some examples were better knowledge of the shear properties of heavy oils as those provided by my research can have direct impact.

2.5.1. Seismic monitoring of thermal EOR operations of heavy oil reservoirs

Thermal EOR methods aim to increase the temperature of the reservoir in order to reduce the viscosity of the heavy oil and improve production. Examples of thermal EOR include continuous steam injection or steam flood in which steam is injected in one well and production occurs in nearby wells; cyclic steam injection, in which steam is injected in one well for a period of time and the same well is put on production afterwards; steam assisted gravity drainage (SAGD), which consist of two horizontal wells collocated on top of each other, steam is injected in the shallower well and oil is produced from the deeper well. Success of all these methods is based on the ability of the steam to sweep and heat the entire reservoir. The efficiency of the process depends primarily in reservoir heterogeneity and placement of injector and production wells is designed to optimize the recovery. Steam injection produces three new stages in the reservoir, a hot oil zone, a hot water zone and the steam chamber behind these two (Figure 2.35).

The efficiency of thermal EOR processes is measured by the advance of the hot oil front as it is the heated oil with reduced viscosity that is produced. Even though the efficiency of the process is actually the advance of the hot oil front, the advance of the steam chamber is easier to identify in 3D and 4D seismic studies due to the sharp change in velocities with the presence of steam. Jenkins et al. (1997) were able to map the steam chamber thickness using simulation of P-wave velocity reduction due to the presence of steam. In their work, they did not consider any changes in S-wave velocity or the effect on P-wave due to changes in the shear modulus of the fluid as it could be expected in thermal operations with heavy oil (Figure 2.36).

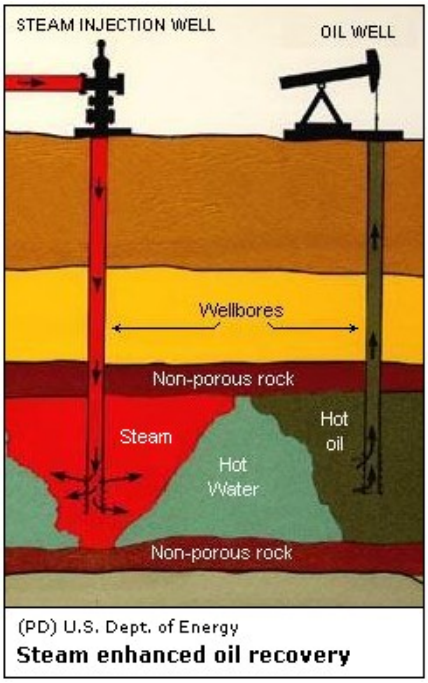

Figure 2.35. Schematic of steam injection EOR process showing the three stages in the reservoir, hot oil, hot water and steam (image from United States Department of energy)

Recently, geophysicists begin exploiting the changes in S- wave and Vp/Vs ratios to identify the hot oil front in the seismic monitoring studies. The understanding of the behavior of the S-wave in heavy oil reservoirs have also increased due to the increasingly availability of multicomponent 3D and 4D studies in heavy oil reservoirs. Kato et al. (2008) calculated the changes in P-wave, S-wave and Vp/Vs ratio due to steam injection (Figure 2.37) considering the effects of temperature. Velocities were calculated from rock physics models calibrated with ultrasonic measurements of reservoir rocks at different pressures and temperatures. These velocities were corrected for dispersion effects between the ultrasonic and seismic frequencies. The rock physics models and dispersion corrections used in this work have a limited applicability as they were developed for the specific field in study but they represent an adequate workflow to account for the changes in heavy oil acoustic properties in steam flood operations.

Another study that incorporates the changes in shear wave velocity of heavy oils in thermal EOR operation was presented by Wolf et al. (2008). In their work, the authors study the feasibility of monitoring the steam injection production of bitumen sands using converted P-to-S wave elastic impedance. This technique allowed distinguishing the hot reservoir from the cold reservoir and steam chamber. The authors did not explain how they chose the values of P-wave and S-wave of the hot reservoir but they acknowledged the difficulty of modeling heavy oil reservoir due to the lack of robust rock physics models and importantly due to the lack of calibration data (Figure 2.38).

Bianco et al. (2008) performed numerical simulation of a SAGD process in the McMurray formation in Canada. This formation is known for its unconsolidated rock frame and heavy oils of less

than 10 API gravity. The authors focused their work in the effect of the steam stimulation on the rock-frame of the unconsolidated rock, which strongly affects the bulk modulus and velocity of the rocks. In their conclusions, they emphasize that the ideal simulation should include shear wave and dispersion information to achieve a more realistic picture of the wave propagation. However, they did not include these types of information because of large uncertainties on the shear modulus and dispersion information at seismic frequencies.

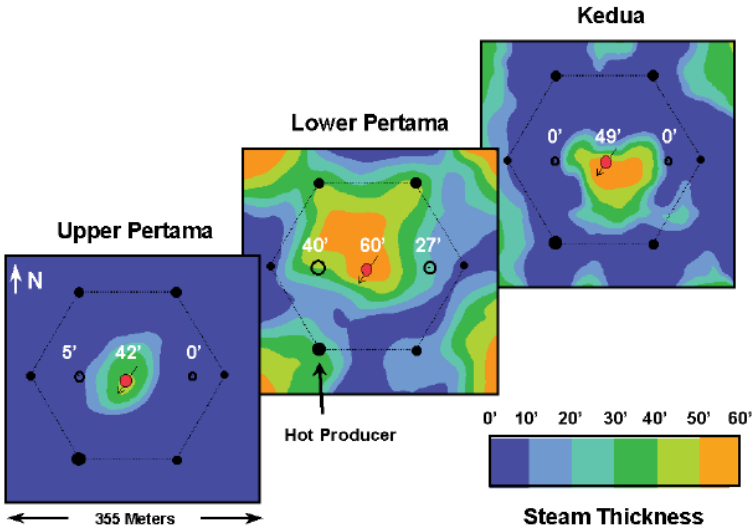

Figure 2.36. Steam thickness maps in the three Duri pilot reservoir intervals from Jenkins et al. (1997). The steam chamber was mapped in this work modeling changes in P-wave velocity.

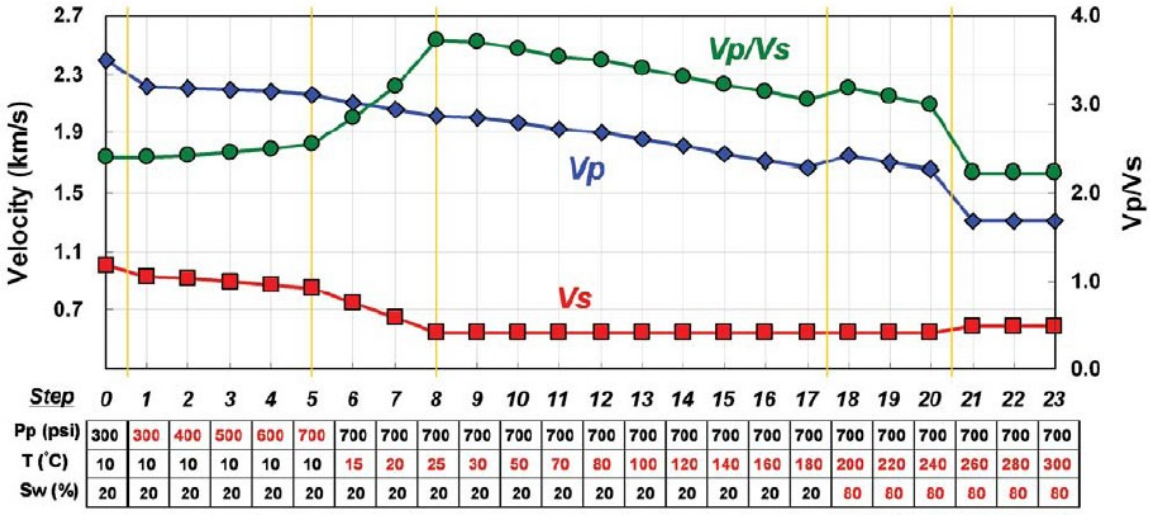

Figure 2.37. Sequential P- and S- wave velocities and Vp/Vs ratio changes induced by steam injection. Sequential reservoir condition changes are represented by 23 steps. Pore-pressure changes occur from step 1 to 5, and temperature changes from step 5 to 23. In addition, adjacent to the injector well, the movable bitumen is largely replaced by hot water at step 18 and water phase changes from liquid to steam at step 21. A sharp change in S-wave and Vp/Vs ratio is observed when temperature increases in steps 5 to 7 (Kato et al. 2008).

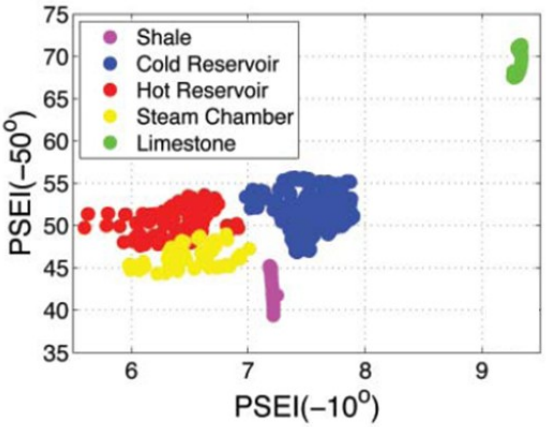

Figure 2.38. Heated reservoir with results of steam chamber inversion plotted in P-to-S Elastic Impedance (PSEI) space. The hot reservoir can be distinguished from the cold reservoir and steam chamber (Wolf et al. 2008).

Seismic monitoring is not the only technique that would benefit from a deep understanding of the behavior of the shear modulus of heavy oils across frequencies. Monitoring techniques of thermal applications are also performed at higher frequencies from VSP and cross-well seismic applications. Tendel et al. (2011) completed a feasibility study to monitor SAGD operations in the Fort McMurray formation in Canada with a permanent cross-well seismic system. They based their properties simulation on data published by Kato et al. (2008) and adapted for their area. Their model emphasized the changes in S-wave velocity due to early heating of the reservoir that travels in front of the steam chamber.

Another application that will directly benefit from a thorough understanding of the shear modulus of heavy oils at varying frequencies and compositions is the monitoring of THAI operations. THAI stands for Toe-to-Heel Air Injection, which is an in-situ combustion process that cracks, upgrades and mobilizes the heavy oil (Kendall 2009). In this process, several phases are added to the reservoir: compressed air, a combustion zone, a coke zone and an upgraded oil zone. The upgraded oil zone can signify an increase of 10 API gravity units with respect to the original oil. Changes of 10 API degrees imply an important change in P-wave and S-wave velocities. Kendall (2009) and Kendall & Wikel (2011) explain the possibilities of monitoring THAI operations using 4D-3C data and emphasize the changes in S-wave as a main indication of the advance of the upgraded hot oil. In these papers, the authors quote the changes in velocity of heavy oils with temperature but did not highlight the added velocity decrease due to the reduction in API gravity which implies a change in composition. A schematic example of this operation is shown in Figure 2.39.

Other studies that will benefit from my research work are those that have to deal with acoustic (seismic, VSP or log) characterization of reservoir with natural changes in heavy oil properties. Examples of these are the oils sands in the Canada, North Sea and China and the tar mats in the Gulf of Mexico. Figure 2.40 shows data from two different regions indicating the range or variation in API gravity (Larter et

al. 2006). Figure 2.41 shows and schematic of processes involved in vertical and lateral variations of viscosity and API gravity in heavy oil reservoirs (Larter et al. 2008).

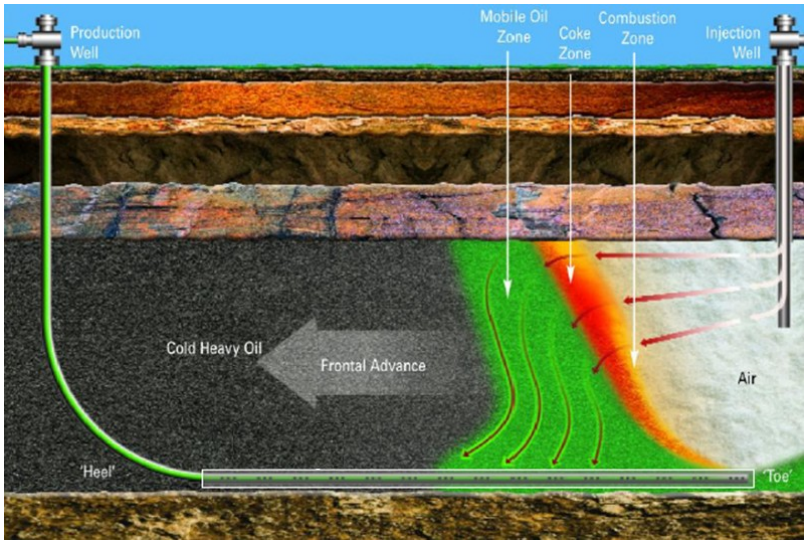

Figure 2.39. Schematic representation of the THAI process showing the vertical air injector, combustion zone, coke zone, mobilized oil zone and horizontal production well (modified from Kendall (2009)).

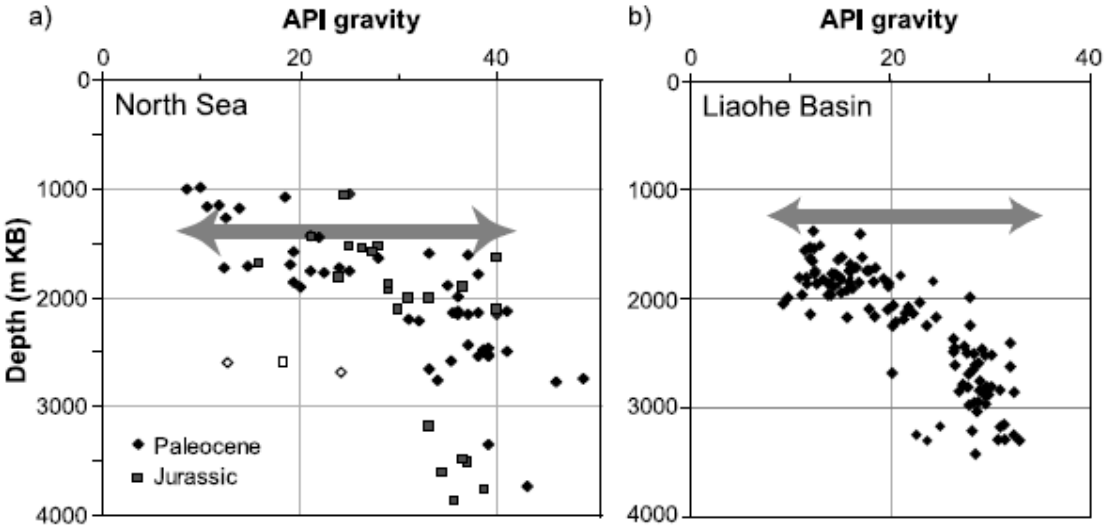

Figure 2.40. Vertical variations of oil API gravity with reservoir depth. (a) marine North Sea oils (b) lacustrine oils (China). Low-API-gravity oils are increasingly dominant in shallower reservoirs with large variations in API gravity and viscosity (Larter et al. 2006).

2.5.2. Steady shear viscosity estimation from seismic data

The high viscosity of heavy oils has been linked with transmission and attenuation of acoustic waves which brings the possibility to estimate the viscosity from seismic data. This is especially relevant as I emphasized in the previous section how important are the viscosity variations to production of heavy

oil reservoirs. It is important however to distinguish between the viscosity values that could eventually be estimated from the seismic, from the viscosity values used by engineers to design pipelines and surface facilities. The main distinction between them is that the viscosity "sensed" by geophysical acoustic measurements is dynamic, which means that is measured through a sinusoidal load (i.e. the pass of seismic waves through a rock). In contrast, the viscosity needed by engineers is measured through steady shear flow which mimics the flow in pipelines and tubing. In this section, I will relate the two viscosities and speculate how we can obtain these values from seismic.

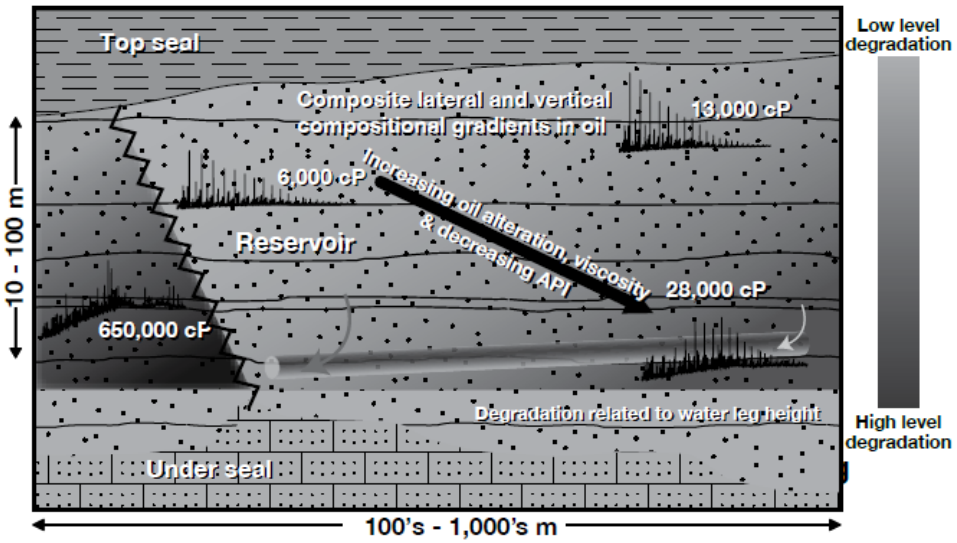

Figure 2.41. Vertical and lateral compositional gradients that may be present in super heavy oilfields, related to biodegradation at the base of an oil column, fresh oil charge mixing and reservoir compartment (Larter et al. 2008).

The steady shear viscosity is measured in a rheometer using the constant flow mode. Viscosity in this case is the resistance of fluid to flow under a constant shear rate and it is expressed by Twardos & Dennin (2003):

$$\eta = \frac{\sigma}{\dot{\varepsilon}} \qquad (2.19)$$

Where η is the steady viscosity, σ is the stress and $\dot{\varepsilon}$ is the strain rate. On the other hand, "Dynamic" viscosity is measured under oscillating shear force at varying frequencies and it was described in equation 2.8 in terms of shear modulus. Here it is expressed in terms of stress and strain (Li et al. 2005):

$$\eta^* = \frac{\sigma^*}{\varepsilon^*} \qquad (2.20)$$

Where σ^* is the complex stress described in equation 2.1 by $\sigma(t)$, and ε^* is the complex strain described in equation 2.2 by $\varepsilon(t)$. Cox & Merz (1958) proposed that the functional dependence of the

complex viscosity magnitude as a function of frequency is identical to the functional dependence of the steady shear viscosity as a function of the shear rate which is now called the Cox-Merz rule:

$$|\eta^*(\omega)| = \eta(\dot{\varepsilon})|_{\dot{\varepsilon}=\omega} \tag{2.21}$$

However, Li et al. (2005) explained that the Cox-Merz rule is valid only for fluids where the fluid-viscous component (η' or G'') is much larger than the solid-elastic component (η'' or G'). In the case of heavy oils, there are many cases where the elastic component is larger than the viscous component and it is under this condition that seismic waves are most affected. This means that for geophysical application the assumption of the Cox-Merz rules may not be completely valid.

For this cases, Li et al. (2005) theoretically deduced that for fluids where the elastic component cannot be neglected the steady shear viscosity can be estimated from the viscous component of the dynamic viscosity at low frequencies. This relationship can be described as follow:

$$\eta'(\omega \to 0) \approx \eta(\dot{\varepsilon})|_{\dot{\varepsilon}\to 0} \tag{2.22}$$

For applications to geophysics, P-wave and S-wave velocities are a function of the elastic component of the shear modulus, which means that if we are able to extract the shear modulus of the fluid from seismic data it will be related to the elastic component of the viscosity, which is expressed by:

$$G' = \frac{\eta''}{\omega} \tag{2.23}$$

This implies that we cannot use only the shear modulus from seismic to estimate the steady viscosity of that fluid, as we will detect only the *elastic* part of the viscosity and the steady viscosity is related to the *viscous* component expressed in equation 2.10. In order to have the complete information we will need to have a measure of the intrinsic attenuation which relates the viscous and elastic components as shown by equation 2.6 and here expressed also in terms of viscosity.

$$\frac{1}{Q} = \frac{G''}{G'} = \frac{\eta'}{\eta''} \tag{2.24}$$

If we have the attenuation ($1/Q$) and the shear modulus (G') from seismic, we could then use equation 2.23 to convert the shear modulus to storage viscosity (η'') and use equation 2.24 to calculate the loss (or viscous part) viscosity (η'). If the storage viscosity (η'') is larger than the loss viscosity (η'), is then related to the steady viscosity through equation 2.21; if the loss viscosity (η') is larger than the storage (η'') then the steady viscosity is calculated using equation 2.22.

As seen in the above explanation, estimation of the viscosity of the heavy oil directly from seismic seems cumbersome and it assumes that the fluid effects can be separated from the rock and wave propagation effects. In any case, two important points to remember are, first, that the viscosity "sensed"

by the seismic is different than the one applicable to fluid flowing through pipelines, and second, that the viscosity that directly relates to the shear modulus in the P and S-wave equations corresponds to the storage (or elastic part of the) viscosity (η'').

2.5.3. Shear behavior of other viscoelastic materials studied in geophysics

The present work is focused on the understanding of heavy oils, however, the findings of this work can have applications to other viscoelastic materials that are either directly studied by geophysics or that their presence affects geophysical acoustic measurements.

Examples of those materials are soft unconsolidated sediments, which are found at the bottom of any water body like lakes, estuaries and the ocean. Even though inter-particle forces are smaller than the molecular forces seen in heavy oils, these sediments can present similar shear behaviors of those from heavy oils described in the previous sections, as they also act as aggregates than can flocculate, settle and breakup due to strain. Hamilton (1971) and Chou et al. (1993) extensively studied the behavior of marine sediments to strain and other authors have studied similar effects at earthquake scales (Sumita & Manga 2008).

3. SHEAR MODULUS EXPERIMENTAL METHODOLOGIES

My experimental work consisted in selecting three samples which are solid-like at room temperature and measured its composition and shear properties. The shear properties were compared between different techniques using a Cole-Cole fit dispersion model.

In this chapter, I will explain the rheometer measurements and tension/compression techniques, which are the two main techniques I used in my research to analyze the shear behavior of heavy oils. These two techniques come from different disciplines, as the rheometer is mainly used by chemical engineers, while the tension/compression technique is used by geophysicists. Even though both techniques come from different disciplines, they are based on the same theory but differ in the geometry or state of the samples and amplitudes used.

I will describe the two shear modulus methodologies beginning with rheometer measurements, briefly describing the main calibration and quality control steps, followed by specific steps needed to perform gap thickness variation measurements and finally I will describe the effect of temperature on the measurements as it is key to understand possible experimental errors. Following this, I will focus on the tension/compression technique, describing the methodology and listing specific steps that were needed in my research for the calibration of new equipment. I will end up the chapter, explaining the modifications that I needed to implement to work with soft samples (heavy oils) which are unique and have not been tested before. Results of the analysis are explained in chapter 4 and additional results are shown in appendices A and B. A brief description of the three samples I measured is also given in appendix C.

For other analyses which were conducted by third parties, such as SARA and pyrolysis analyses, a brief description of the procedures can be found in section 4.1. Water content and API gravity analyses were used as references and were performed using standard procedures described in Appendices D and E respectively.

3.1. Rheometer measurements

Rheometer measurements constitute a simple technique to measure shear properties of heavy oils at low frequency. It is considered simple as it does not require much time for sample preparation compared with the case of tension/compression measurements in which sample preparation can take up to a week. The technique is also considered to be “standard” as such equipment is amply available and there is wide experience among chemical engineers who have study many type of materials for many years.

The study of dynamic elastic properties in the rheometer can be done at frequencies between 0.01 to 100 Hz which are in the range of seismic frequencies. Demonstrating that the rheometer is an adequate technique to characterize heavy oils at low frequency can help to advance the understanding of the behavior of heavy oils in seismic applications.

3.1.1. Rheometer technique description

I performed the rheology experiments in an ARG2 system from TA instruments, Inc. company. The rheometer has an upper rod connected to a "geometry" and the lower piece is a Pettier plate which provides the temperature control. Different geometries are available and are selected depending on the viscosity of the sample. The sample is placed between the two plates and a sinusoidal force is imposed by the upper rod displacing the sample, when force is released the response of the sample is recorded by the same rod. The response of the sample can be elastic, viscous or viscoelastic as described in section 2.1. The rheometer measures the magnitude of the strain and the phase lag between stress and strain; storage and loss modulus are then calculated from equations 2.4 and 2.5.

One important step during the rheology measurements is the calibration which needs to be performed daily. The five main calibration steps include: instrument inertia, geometry inertia, zero gap setting, bearing friction, rotational mapping and oscillatory mapping. The oscillatory mapping is recorded by the equipment and the user just verifies that the oscillatory mapping is saved before performing the experiments. After the initial calibration, the sample is placed on the Peltier plate and temperature is increased to ensure the sample is melted and thoroughly mixed. The geometry is lowered slowly until the desired gap is reached (commons gaps are 0.5 and 1 mm). The sample should remain strictly between the geometry and the Peltier plate, therefore the geometry is lowered to a thickness close to the testing gap (0.05 to 0.1 mm more) and the sample is trimmed carefully to remove any excess. The temperature of the Peltier plate is set to the required temperature and the normal force is set to zero to ensure the sample is relaxed before performing the experiment. Even though a systematic assessment of errors was not conducted, repeatability errors are in the order of less of 1 percent if test is repeated immediately one after the other. Repeatability errors increase up to 5 percent if the test is repeated under the same conditions but is conducted at a different time.

3.1.2. Selection of the geometry

The geometry is normally chosen based on the viscosity of the sample; the more solid the sample the smaller the geometry. For the tests performed in my research, the smallest available geometry was used: parallel plate with 8 mm diameter. For geophysical applications, we are interested in conditions under which the samples are found: such that have a large storage modulus (solid-like), which translates in the requirement of using the smallest geometry available. Larger geometries need many corrections when the sample is too stiff and can give incorrect results.

3.1.3. Types of tests

The rheometer allows for different types of tests, specifically changing the independent variable. Among the more important ones are: temperature, frequency and strains sweeps. Temperature sweeps are done keeping the frequency and strain constant and changing the temperature at a constant rate. These tests are interesting in heavy oils as they show when the sample stops behaving like a solid and changes to a liquid. However, care must be taken since if we are using a small geometry when increasing temperature the viscosity lowers significantly and the geometry is no longer adequate, giving many errors. If the user wants to do a temperature sweep, it should be done changing the geometries at intermediate or several temperatures to ensure good quality results.

Frequency sweeps are performed at a constant temperature and strain, varying the frequency. Frequency steps are defined by the number of steps per logarithmic decade required by the user. Usually five or ten points are adequate to describe the behavior with frequency.

Finally strain sweeps are performed at a single frequency and temperature. These tests are important and need to always be performed to the sample before performing any other tests. The experiments in the rheometer are usually conducted at a strain level in which nonlinearities are avoided which means they have to be performed within the Linear Viscoelastic Regime (LVR). Within the LVR there are no variations of the shear modulus with strain level. To ensure this, the strain sweeps are performed at different frequencies and temperatures to ensure that the measurements remain in the LVR during the duration of the experiment. It is recommended to select the smallest value of strain within the LVR tested as the regime gets shorter when increasing frequency or reducing temperature. Figure 3.1 from TA Instruments, Inc. shows the decrease in the LVR with frequency.

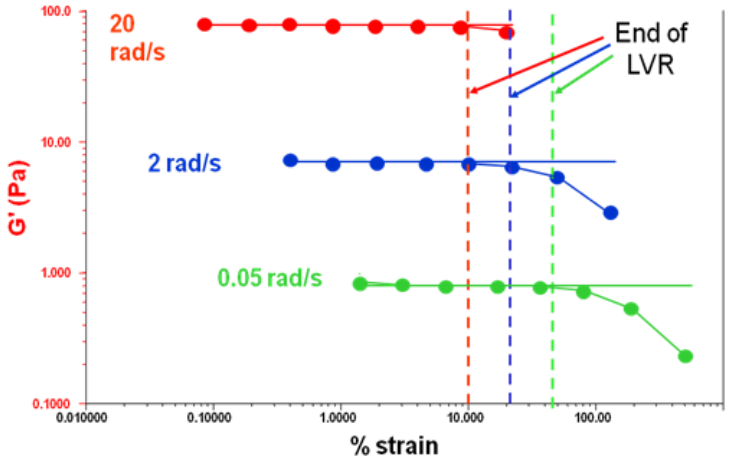

Figure 3.1. Variation of Linear Viscoelastic Regime (LVR) with frequency (TA Instruments). The region of LVR gets shorter as the frequency of the measurement is increased.

3.1.4. Quality Control

A detailed quality control of the output data generated by the rheometer is needed in order to have confidence in the results. A direct way to assess the quality of the data is to review the phase measurements. The rheometer measures the phase lag between the stress and strain (raw phase) and then generates a corrected phase lag (delta). The corrections made by the rheometer were primarily designed to account for inertia effects during oscillation tests of low viscosity fluids. Other corrections done to the measured phase when samples have high viscosity are related to the compliance of the motor and equipment. When large corrections are made by the equipment, they are due to inappropriate measurement conditions, either too large or too small plate geometry. Under the adequate conditions the raw and corrected phases are similar and data is reliable. Any data for high viscosity oils with differences of more than ten degrees between the raw and corrected phases should be considered with care. For light oils the correction due to inertia can be allowed to be greater than ten but the raw phase should not be greater than 120 to remain valid.

3.1.5. Effect of temperature

Temperature effects are of high relevance for the rheometer measurements. As it was mentioned above, the source of heat in the rheometer comes from the lower plate which creates an internal temperature gradient within the sample. In the case of the GP029-Asphalt Ridge sample, the tests were performed at -6.5C while room temperature was at 22C approximated. The parallel plate geometry is made of stainless steel which has a heat transfer coefficient approximately twenty times larger than asphalt at room temperature ("The Engineering ToolBox", 2014). So it is to expect that with an upper contact with stainless steel which has contact with the room temperature and a heat removal at -6.5C below the sample, there should be an important temperature gradient within the sample. Figure 3.2 shows a schematic representation of the temperature differences in the testing of GP029-Asphalt Ridge sample. Even after reaching complete stationary conditions, the gradient will cause the overall viscosity to decrease.

The effect of the temperature gradient has been measured and reported in the literature. Figure 3.3 from Barker and Wilson (2006), shows the thermal gradient created within the sample. Barker and Wilson (2006) reported in their experiments a gradient as high as 55C within the sample for a temperature difference of 170C between the Peltier plate and room temperature for a polymer sample and 1 mm gap thickness. They explain that the thermal conductivity of the sample is key in the generation of the thermal gradient.

In the case of the heavy oils tested in this research a thermal gradient during testing is expected as the thermal conductivity of the material is very low. The conditions of the experiments are not as extreme as reported by Barker & Wilson (2006) since the temperature differences between the testing

and room temperature ranged between 20C and 26C and gap measurements varied between 0.07 and 1.3 mm.

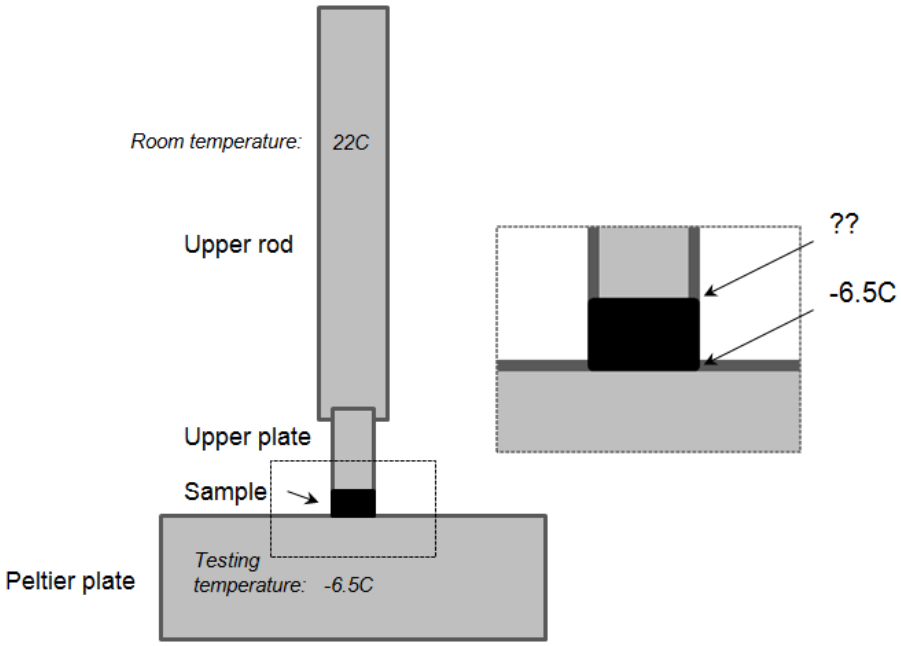

Figure 3.2. Schematic representation of temperature variations in the rheometer for sample GP029-Aspahlt Ridge testing conditions. Detail shows the lower part of the sample is in contact with the Peltier plate at -6.5C but the upper part of the sample is in contact with the upper plate which is at a higher unknown temperature.

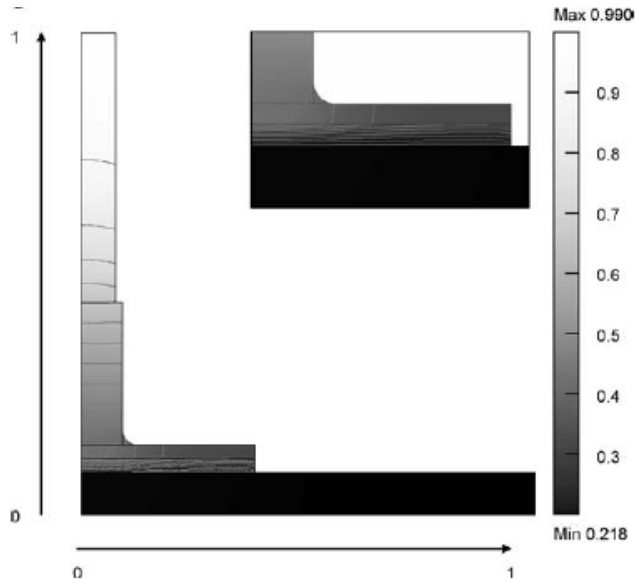

Figure 3.3. Dimensionless temperature distribution for simulations showing the thermal gradient in the equipment and within the sample (inset) from Barker & Wilson (2006). Simulation were done for a polymer with a 1 mm gap and 170C temperature difference. The thermal gradient within the sample is as large as 55C.

Variations of modulus during testing due to temperature variations in the rheometer have been reported in the literature for asphalts. Petersen et al. (1994) reports variations of up to 40 percent in the modulus due to conditioning time, in Figure 3.4 they show the effect of temperature on the complex modulus of asphalts plotting the change in the complex modulus by degree C vs. complex modulus. For a sample like GP007-Uvalde, with a modulus in the order of 10^8-10^9 variations of modulus with degrees C can be expected in the order of five to ten percent per degree. Petersen et al. (1994) recommend having a fluid bath or air oven to keep the temperature uniform and constant around the sample (Petersen et al. 1994). This type of setting was not available for the tests performed in my research.

To assess the effect of temperature, I tested the GP007-Uvalde sample decreasing the temperature in small steps and comparing the modulus. Figure 3.5 shows the change in modulus with temperature performed at a fixed frequency of 1.25 Hz. Results indicate that the Uvalde sample experienced a change in modulus in the order of 7 percent per degree C. In this figure, a repeated test is shown by the green triangle and another test performed at the same conditions in a different rheometer is shown by the red square.

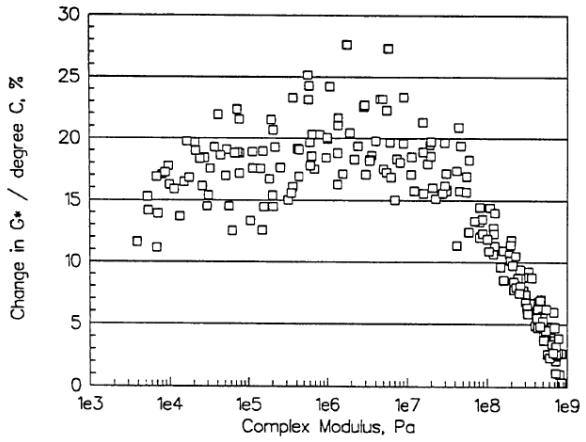

Figure 3.4. Temperature effect on the complex shear modulus of asphalts. Percent change in complex modulus per degree C as a function of complex modulus (Petersen et al. 1994).

Differences between tests performed in different rheometers can be due to temperature stabilization problems or the effects of the Peltier plate surface which is explained in section 4.2.5.

Temperature stabilization is in particular important in temperature sweeps. Figure 3.6 shows the modulus versus temperature while heating or cooling the GP007-Uvalde sample. Detail of the figure is show in Figure 3.7. Below 40C, a heating lag can be identified because the two curves separate. This lag occurs due to the diminished thermal conductivity of the sample at lower temperatures. This lag results in a variation of the shear modulus of 12 percent at 30C.

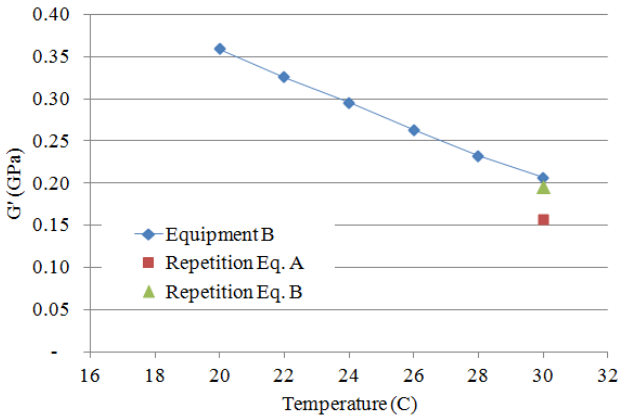

Figure 3.5. Storage modulus vs. temperature at 0.5 mm Gap and 1.25 Hz. A repetition of the experiment is shown by the green triangle and a test performed at a different rheometer is shown by the red square.

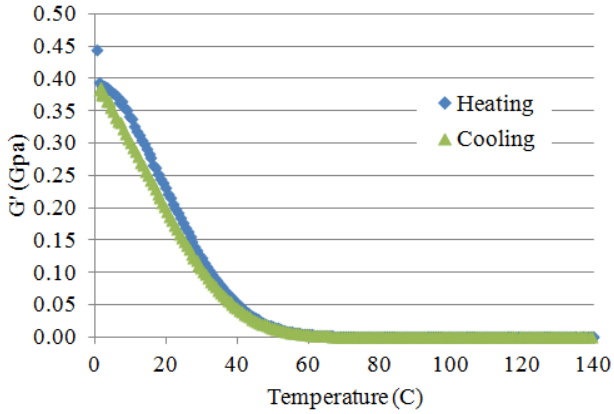

Figure 3.6. Storage modulus vs. Temperature. Green triangles represents the data obtained when heating the sample from 0 to 140C. Blue diamonds represents the data when cooling from 140 to 0C.

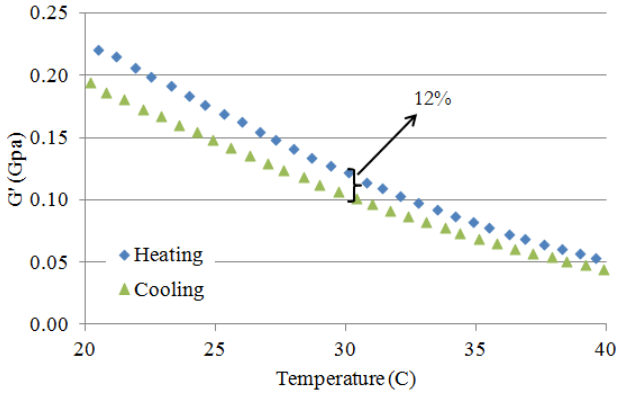

Figure 3.7. Detail of Figure 3.6 between 20 and 40C indicating a 12 percent difference in storage modulus at 30C between the heating and cooling cycles.

Lastly, it is important to consider that when working at high temperature there can be a loss of sample by evaporation or thermal cracking. For the samples I tested, pyrolysis analysis showed that there is loss of hydrocarbons until temperatures values well above 100C. For the main tests of my work samples were never heated above 100C.

3.1.6. Gap thickness tests

One important result of my research is the finding that the properties of the heavy oils vary depending on the gap or film thickness. Gap thickness tests can be performed in the rheometer but they cannot be automated as the other test mentioned above. One should start at the maximum gap and decrease the gap in each step. After all tests have been performed at the first gap, temperature should be slightly increased to facilitate the reduction of the gap. The new reduced gap is set at a higher temperature, the reduction of the gap can be done with no normal force control to expedite the process. While the gap is decreased there will be an increase in normal force, the user has to wait until the normal force is back to zero to ensure the sample is relaxed before performing any additional tests, this process can take 30 min to an hour. While the normal force reaches zero again, the sample is trimmed and after the normal force reaches zero, the temperature is lowered again to the testing temperature and the sample is left to equilibrate for enough time to ensure proper temperature equilibrium before all tests are performed.

3.2. Tension/Compression measurements to estimate dynamic elastic properties of heavy oils at low frequencies

As it was explained in section 2.3.6, the shear modulus of heavy oils is highly dependent on frequency. Scientists (Spencer 1979; Batzle, et al. 2006a) have developed models and techniques to measure the elastic properties of hard materials (i.e. rocks) at wide frequency ranges, including lower frequencies within the range of seismic data. The tension/compression technique consists of applying axial deformation to the sample and measuring the resulting strain at frequencies between 3 to 3000 Hz. Amplitudes are kept in the 10^{-6}-10^{-7} range, and are a tradeoff between measurements at low amplitudes (to stay in the linear regime) and interference noise levels.

The sample has to be in cylindrical shape and strain gauges are attached to the sides of the sample. Ultrasonic crystals can also be included at the end of the sample to measure ultrasonic velocities. A detailed description of the experimental procedure can be found in Das (2010) and Batzle, et al. (2006b). The equipment works well for solid or solid-like samples to which strain gages can be attached, but for softer samples such as heavy oils, hydrates and loose sediments important only limited efforts have been done. In my research I extended the technique to work with softer samples, like heavy oils.

Besides a strong dependence of the elastic properties with frequency, heavy oils present a strong dependence with temperature. This introduces the need of assuring a temperature close to constant during the length of the experiment which was achieved by the introduction of a new acquisition system and a temperature control bath. Errors were not assessed directly but subsequent measurements of the same sample indicate repeatability errors of less than 5 percent.

In the following sections, I will summarize the advances made during my research in order to measure the elastic properties of soft samples at low frequencies. I will begin with changes in the acquisition system, calibration, and finish with sample preparation and temperature control.

3.2.1. New acquisition system

In the Center for Rock Abuse (CRA) at Colorado School of Mines, data used to be collected using digital oscilloscopes. These scopes had a limited number of channels and poor dynamic range. A LabVIEW™ controlled acquisition system based on a National Instruments (NI) digitizing card replaced the original system, improving time and increasing the number of channels that could be simultaneously recorded. Before, we also used a bank of phase lock amplifiers controlled by a MATLAB® program. These amplifiers proved to be much slower, had low reliability, and developed communication issues. A complete sweep of frequencies and channels took several hours. The new acquisition system developed using LabVIEW™ reduced this time (and became more stable), this new acquisition system was used for the tension/compression tests in my research.

The new system is a LabVIEW™ controlled program based on a multichannel NI high resolution digitizing card. Several new aspects of this system are:

- Allows phase measurements
- Calculates of standard deviation for both amplitude and phase
- Allows for variable amplitude
- Stores wave forms for each frequency
- Filters signals
- Works with up to twelve channels simultaneously

3.2.2. Calibration and validation of the new acquisition system

The new acquisition system was connected to a new equipment assembly which required a combined calibration and validation process to verify the results I obtained are valid. The calibration and validation I performed included:

1) Comparison to oscilloscope amplitudes: In order to verify that the new acquisition was reading the right amplitudes, I performed several tests comparing the amplitudes read manually in a oscilloscope to those measured by the new acquisition system.

2) Test of the Wheatstone bridge: To test the correct functioning of the Wheatstone bridge, I compared a pair of gages the amplitudes for each half bridge channel to those of a quarter bridge configuration. The quarter bridge configuration considers only one gage a 1000 ohm resistor connected to the bridge. The quarter bridge configuration should give half the amplitude than the one measured with the half bridge configuration using the two gages but it is sensitive to the results from a single gage.

3) Estimation of channel multipliers: Even though the Wheatstone bridge is built equally for each channel; it is expected that the amplitudes at each channel to read slightly different. To reduce this error, I calculated channels "multipliers" to make all amplitudes the same. For this process, I measured a frequency sweep using the same pair of gages in an aluminum standard using each of the twelve channels in the Wheatstone bridge.

4) Noise suppression: Initial tests performed to the aluminum standard showed significant amounts of ambient noise which affected the low frequency data. Noise reduction has been achieved by introducing the testing equipment inside a pressure vessel, even when the tests are performed at atmospheric pressure. The noise outside the pressure vessel was primarily found at low frequencies (below 1 Hz) and at multiples of 60 Hz. Another significant disturbance to the signal is found above 1000 Hz when the resonance frequency of the system is reached. Figure 3.8 provided by Mathias Pohl (also from the Center for Rock abuse at CSM), shows the amplitude of a vertical strain gage between 0.2 and 2000 Hz in the aluminum standard obtained outside and inside the pressure vessel. The noise is reduced significantly but, as expected, the resonance peak is maintained.

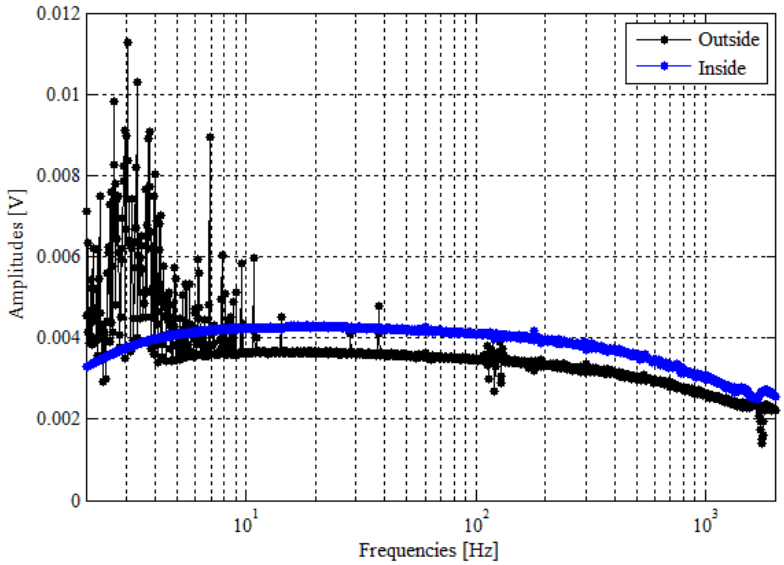

Figure 3.8. Amplitude of a vertical gage in an aluminum standard, outside (black) and inside (blue) a pressure vessel. Significant reduction in noise is achieved by performing the test inside the pressure vessel (figure provided by Mathias Pohl).

5) Calibration with standard material: in parallel to the aluminum standard tests, I measured a sample of Poly Ethylene Ether Ketone (PEEK). Measurements to this standard were done outside the pressure vessel. However, even with the important amount of noise observed in the vertical and horizontal gages, Young's modulus obtained for the PEEK sample is consistent with ultrasonic results with minor dispersion effects observed.

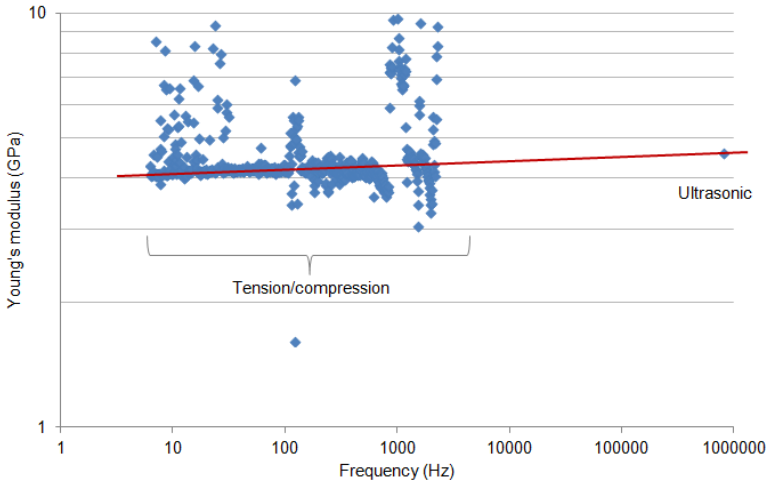

Figure 3.9. Young's modulus of PEEK at intermediate and ultrasonic frequencies collected outside the pressure vessel. Even with the presence of noise, there is consistency between the low frequency and the ultrasonic results. Minor effects of dispersion are observed and were expected for the sample.

3.2.3. Soft samples preparation

Measuring elastic properties of soft samples (heavy oils) at low frequencies presents a major challenge. Batzle, et al. (2006b) measured a heavy oil sample at low frequency attaching strain gages to the surface of the heavy oil after it was molded into a cylinder shape (see Figure 3.10 from Behura et al. (2007)). This procedure was possible due to the extreme high viscosity of the sample (API -5) at room temperature. However, the majority of the heavy oils of commercial interest have lower viscosity at room temperature which makes the process of attaching strain gages impractical, if not impossible.

For these reasons I had to modify the gages positioning. The first and major modification was the need to use a jacket to contain the heavy oil. The jacket which is made of a material resistant to high temperatures (kapton) and flexible enough to allow contraction and deformation of the sample is attached to the aluminum standard. The jacket material has to be "softer" that the material being tested (see properties of testing materials in APPENDIX F). Strain gages with pre-attached wires are attached to the jacket, or positioned inside the jacket with wires through the jacket and sealed. For heavy oils, the samples are heated above the liquid point and poured into the jacket. Heating temperature should be kept below 100C to avoid loss of material; 100C is the temperature below which the pyroloysis tests did not show any production of hydrocarbons. After cooling, the upper part of the sample is capped with another aluminum standard. The aluminum standard and the upper part of the sample are heated with a

heat gun, to facilitate the sealing of the sample and reduce the possibility of air getting trapped between the sample and the aluminum standard. After sample if cooled to room temperature, epoxy is added to seal the upper connection between the jacket and the aluminum standard. Aluminum standards may or may not have ultrasonic crystals to allow for ultrasonic measurements in the sample. One of the jackets used in this work with inside gages is shown in Figure 3.11. The jacket in this particular configuration has twelve strain gages, three horizontal pairs and three vertical pairs and four pairs of semiconductor gages, two at each end (not shown in the picture). Because of the large strain amplitudes expected in heavy oils, foil gages must be used to measure the oil instead of semiconductor gages which are used to measure the low amplitudes in the aluminum standards.

Figure 3.10. Heavy oil (GP007-Uvalde) sample with semiconductor strain gages attached to the surface (from Behura et al. 2007)

Figure 3.11. Example of jacket design to measure elastic properties of soft samples. The jacket is made of kapton which is resistant to heat and flexible enough to allow deformation of the soft sample. The jacket is attached to an aluminum standard, six pair of gages, three vertical and three horizontal are inserted in the jacket.

To improve adherence of the sample to the strain gages, a film of epoxy was added to the surface of the gages before inserted in the jacket as it is shown in Figure 3.12.

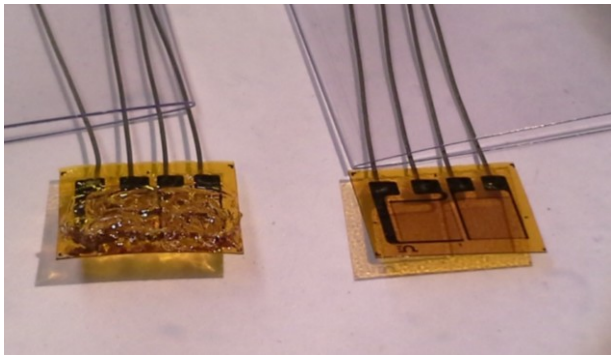

Figure 3.12. Example of used strain gages with (left) and without (right) epoxy layer to increase adherence of the sample to the gages and prevent slippage

3.2.4. Temperature control

Temperature control is very important for heavy oils as I have shown that the shear properties are largely dependent on temperature. For this reason, a thermocouple is inserted through the jacket and sealed to be able to measure the temperature inside the sample. Measurements were conducted inside a pressure vessel equipped with a temperature bath which allowed working at constant low temperatures for a long period of time. Samples were put in inside the pressure vessel 24 hours prior to testing to ensure the temperature had equilibrated throughout the sample. Temperature measurements were taken periodically during the duration of the experiments. Experiments were kept to a very short time, since the heat induced by the components of the equipment and the strain gages were increasing the temperature during the experiment. After each experiment, temperature was allowed to equilibrate before acquiring additional data. Thanks to the new acquisition system it was possible to acquire a significant amount of data in a short period of time to reduce variations in temperature.

4. RESULTS AND DISCUSION

In this chapter, I summarize and analyze the experimental results that cover three aspects of heavy oils key to understand its elastic behavior.

In section 4.1, I first provide evidence and theory that connect the elastic properties of heavy oils to its composition. Then I will describe a quantitative correlation between SARA analysis and programmed pyrolysis that has not been established before. Establishing this relation gives pyrolysis a large potential to be used as a quantitative predictor of elastic properties of heavy oils.

In section 4.2, I analyze the shear modulus results obtained using the rheometer at different gap thicknesses. These results give new insights into the properties of heavy oils in confined spaces, and have important implications in geophysics and engineering.

In section 4.3, I compare the results obtained with the rheometer to those obtained with tension/compression techniques and explain the changes in properties of heavy oils under different amplitude regimes. The comparison and theory of the shear modulus measured at different amplitude regimes has not been established before and the work I present here represents the first effort on the field in understanding this behavior.

4.1. Potential use of SARA analysis and programmed pyrolysis to predict elastic properties of heavy oils

One purpose of measuring the elastic properties of heavy oils at different testing conditions (frequency, temperature and amplitude), is after all to be able to create models to predict the shear properties at reservoir conditions. Having the capacity of predicting the elastic properties of heavy oils allows interpreting diverse measurements done in the field and inverting from seismic. Therefore, a deep understanding of the heavy oils composition is needed as it remains one of the most important properties of the heavy oil that highly affects its elastic properties and that has not been fully studied. In my research, I was not able to explore in detail the effects of composition on the elastic properties, but nonetheless, I provide a qualitative comparison analysis showing evidence and theory of the composition dependency of the elastic properties and I propose an alternative to describe the composition of the heavy oils.

4.1.1. Techniques to characterize heavy oils composition

There are many techniques that have been used in the industry to chemically characterize in detail heavy oils, among them Fourier Transform Infrared Spectroscopy (FTIR), Molecular Beam Mass

Spectroscopy (MBMS), Carbon 13 Nuclear Magnetic Resonance (^{13}C NMR), and Proton Nuclear Magnetic Resonance (^{1}H NMR). However, we are interested in techniques that have the potential to quantitatively predict the elastic properties of heavy oils. One chemical characterization very common in the oil industry is the SARA fractionation which consists of separating the heavy oil into its Saturates, Aromatics, Resins and Asphaltenes fractions. These fractions are obtained after separating the heavy oil sample using solvents with different polarities. Fractions obtained have polarities increasing from saturates with less polarity to asphaltenes with the largest polarity. There is also an increase in the average molecular weight of the SARA fractions from Saturates to Asphaltenes. However, the polarity of the molecules (strength of molecular bonding) is a major driver of the elastic properties of the heavy oils as it was measured by Hinkle et al. (2008) and this relationship will be described in the next sub-section. Even though SARA analysis could have the potential to predict elastic properties, SARA analysis can be expensive, time consuming and prone to significant human error, as described in detailed by Wu et al. (2012) and explained later in this section. For this reason, in addition to SARA analysis, I identified an alternative technique that could potentially be used as a predictor of the elastic properties which is less expensive and could be more reliable than SARA fractionation.

With this purpose in mind, I decided to test programmed pyrolysis as an alternative to SARA analysis. Programmed pyrolysis consists in a decomposition of the sample using heat while registering the hydrocarbons released or the weight loss of the sample. Comparing the results of programmed pyrolysis to SARA and establishing quantitative correlations between the two techniques is an indication of the potential of pyrolysis to also predict the elastic properties of heavy oils. Before I do this comparison, I first analyze the relation between SARA analysis and molecular polarity with the shear modulus of heavy oils. Following, I will describe the programmed pyrolysis technique and its connection to molecular polarity and SARA fractions. I will then describe the methodology used to correlate the two techniques and show the correlation results. Finally, I will compare the two techniques and summarize the findings.

4.1.2. SARA analysis, polarity and its connection to elastic properties

SARA analysis is considered an industry standard for heavy oil characterization. Many companies and laboratories request this type of analysis to help classification of their heavy oils. Fractions obtained during SARA analysis have different polarities and molecular weights (MW), increasing from saturates with less polarity/MW to asphaltenes with the greatest polarity/MW. Molecular polarity is directly related to molecular interaction (molecular bonding) which is an important factor controlling the shear properties of the heavy oils as I explained in detail in section 2.3.5.

SARA analysis can be summarized as follows: First step in the analysis consists of precipitating and filtering the asphaltenes using a low polarity solvent (i.e. heptanes, pentanes or iso-octane). Precipitated asphaltenes trapped in the filter are dissolved using a high polarity solvent (i.e. chloroform)

and the remaining fractions, maltenes, are run through a chromatographic column. The chromatographic column allows separating the other three fractions. Saturates fraction is separated using a non-polar solvent (i.e. heptanes, pentanes or iso-octane), the aromatics fractions is obtained using an aromatic solvent such as benzene, and finally the resins are separated using a higher polarity solvent such as a mixture of benzene and methanol. Details of one methodology used at Colorado School of Mines can be found at Wu et al. (2012), however it is important to keep in mind that there are variations in this technique, in particular the solvents used. Different labs may use different solvents and ways to separate each fraction which can affect the results. These discrepancies are a major source of variations between SARA analysis from different labs as highlighted by Wu et al. (2012). Regardless of these differences, SARA fractions are always based on the solubility of the different components of the oil.

To expand what was described in section 2.3.5., it is important to highlight that solubility is related to polarity and polarity is the tendency of molecules to interact with surrounding molecules due to an imbalance of the electric charges. Resins and asphaltenes are the fractions with the highest polarity and tend to interact and form aggregates or macromolecules. Moschopedis & Speight (1976) investigated the interaction between resins and asphaltenes, and they proposed that it occurs due to the presence of hetero-atoms (nitrogen, oxygen and sulphur), which are capable of creating hydrogen bonds. They showed that the molecular interaction between resins and asphaltenes occurs primarily in the form of hydrogen bonds which are strong molecular connections where a transfer of charge occurs. They add that the presence of less polar and less aromatic fractions, interact with the aliphatic chains of the asphaltenes and create a smooth transition between the polar and non-polar regions of the oil, allowing the asphaltenes aggregates to stay in solution and not precipitate. These lighter fractions act like a solvent in a suspension.

The reason why the polarity is important in the study of elastic properties, is related to the capacity of a material to store or use energy to change the configuration of its molecules. Matsuoka (1992) describes this interaction in a simple way. When a shear stress is imposed in a material, the molecules try to move one pass the other, if the energy imposed in the material is high in comparison to the strength of the molecular bonds the energy is used to change the configuration of the molecules and the energy is “lost”. This constitutes the behavior of a pure fluid, this energy is quantified by the storage modulus (imaginary part of the shear modulus). If the molecular bonds are very strong, like in solids, the energy is not enough for the molecules to change the configuration and the energy is “stored” in the material, therefore when the stress is released, the material goes back to its original configuration. This represents the storage modulus (real part of the shear modulus). In the case of viscoelastic materials like heavy oils, part of the energy coming from the applied stress is used to change the configuration of the molecules while the other part is stored in the molecules with stronger chemical bonds like the hydrogen bonds created between resins and asphaltenes molecules. In this case, heavy oils have both a loss and a storage modulus giving it its viscoelasticity.

Viscoelasticity of heavy oils is dependent on frequency. As indicated above, the material uses the energy to change the configuration of the molecules, but as we increase the molecular size and the interaction between them (higher polarity), molecules need to relax simultaneously and "cooperate" between them in order to change their configuration (Matsuoka & Hale 1997). At low frequency, there is more time between perturbations allowing the re-accommodation of the molecules (high loss modulus), but at high frequency, there is little time for the molecules to "cooperate", the energy between perturbations is preserved and the material behaves more elastically (high storage modulus) causing the material to behave more elastically.

4.1.3. Programmed pyrolysis and its connection to polarity and SARA analysis

The term pyrolysis refers to the process in which a material (solid, liquid or gas) is thermally decomposed in the absence of oxygen (Horsfield et al. 1983). There are many versions of the technique but a common one is where the sample is heated from room temperature to a 600C or 700C at a constant rate in an inert atmosphere (i.e. nitrogen). Organic compounds produced during the heating are usually analyzed in a Flame Ionization Detector (FID). The next schematic figure provided by the vendor (Figure 4.1) shows the result from the programmed pyrolysis called the "pyrogram" (FID amplitude and temperature vs. time) and the information commonly reported by laboratories in the oil industry (S1, S2a, S2b, TmaxS2a, Tmin, TmaxS2b).

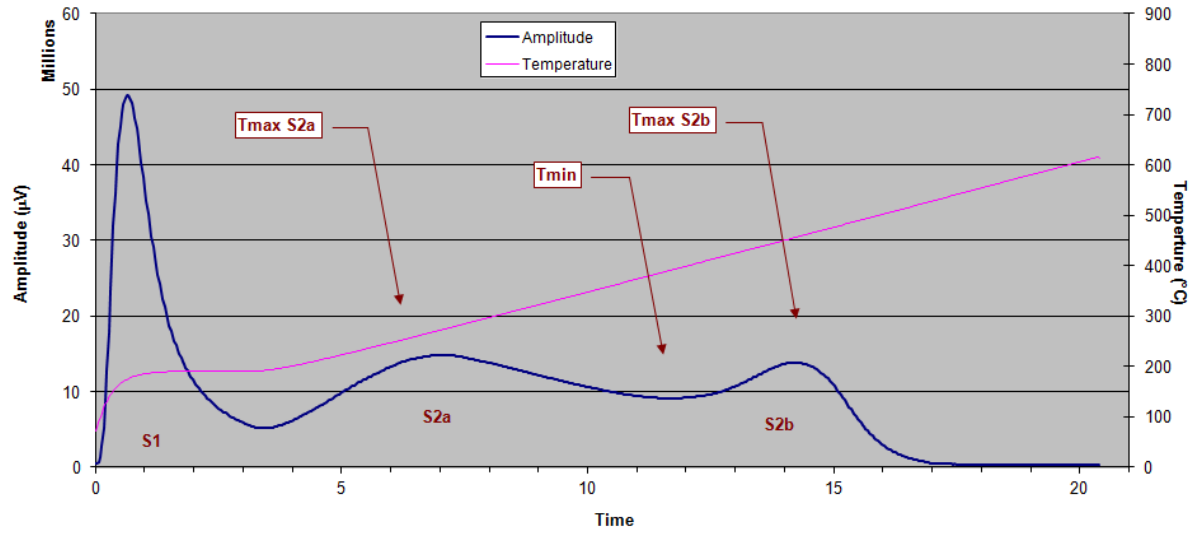

Figure 4.1. Description of pyrograms (provided by vendor).

When the programmed pyrolysis is performed in source rocks the peaks in the pyrograms are described by Horsfield et al. (1983) as follows: the first peak (S1) corresponds to the products evolved at temperatures approximated below 300C, the area under the curve corresponds to the yield of free organic matter. The second peak (S2), here separated as S2a and S2b, is referred to the products

evolved during the thermal decomposition of kerogen. TmaxS2a, Tmin and TmaxS2b are defined in Figure 4.1 and correspond to the temperature were the maximum of S2a and S2b and the minimum between them are reached. In the case of heavy oils the process is described by Ciajolo & Barbella (1984) as the volatilization of paraffinic and aromatic fraction below 400C, and above 400C some of the polar materials volatilize and the heavier components decomposed into smaller structures due to the breaking of molecular bonds. In their study, Ciajolo & Barbella (1984) used Thermo Gravimetric Analysis (TGA) which is a form of pyrolysis where the change in weight is registered instead of the organic compounds released. There is ample literature of TGA of heavy oils and they will be used as reference to analyze the thermal behavior of heavy oils.

Based on several authors experiences (Alvarez et al. (2011), Douda et al. (2004) and Kok et al. (1998)), the decomposition of polar fractions (resins and asphaltenes) depends on the technique variations used (atmosphere and temperature rate), but it seems to consistently occur for asphaltenes at temperatures larger than 400C. An example of this is shown in Figure 4.2 from Kok et al. (1998) and Figure 4.3 from Alvarez et al. (2011).

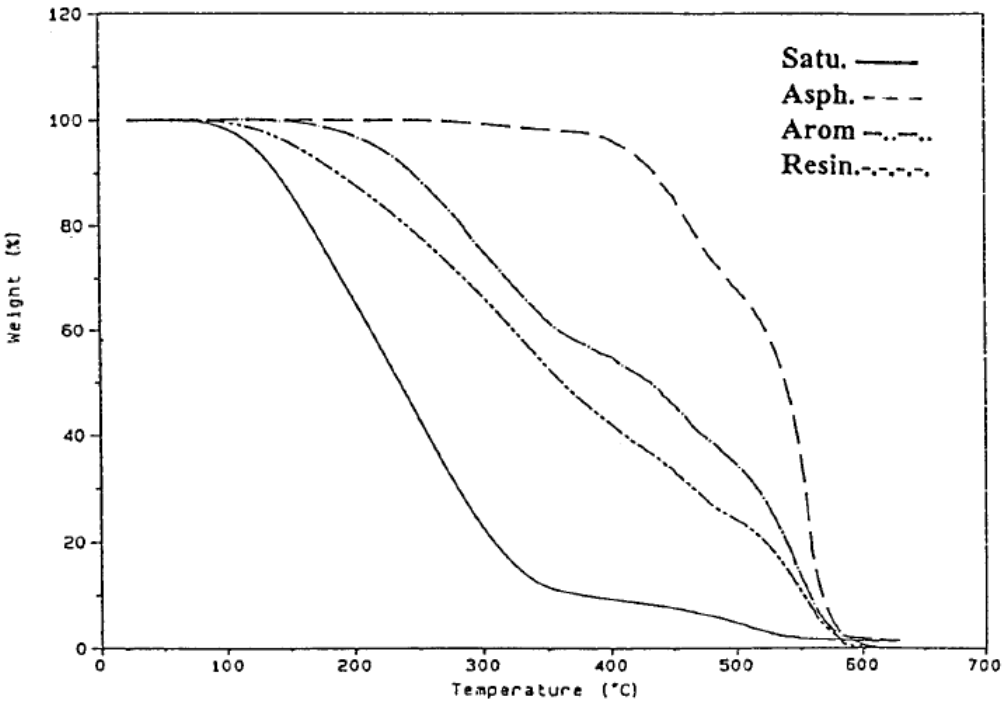

Figure 4.2. TGA curves of SARA fractions (Garzan crude oil) (Kok et al. 1998). Asphaltene fraction is released after 400C.

The effect of polarity in pyrolysis analysis is reflected by the amount of material released at each temperature. Heat breaks the molecular bonds with the stronger the molecular bond (high polarity) the more energy (heat) it needs to break. I expect therefore that the amount of material released at a certain range of temperatures to be proportional to the materials composition in terms of SARA fractions.

4.1.4. Other factors that affect SARA vs. Pyrolysis relation besides composition

The hydrocarbons released, or the rate of reaction with temperature, are a function not only on the properties and current temperature of the sample but also on the temperature rate (Urbanovici et al. 1999). An example of the dependency on the temperature rate is shown in Figure 4.3 from Alvarez et al. (2011), the difference shown in their work may not be significant for the rates tested but is something to consider when comparing experiments performed at different rates. The amount of hydrocarbons produced is also dependent on the atmosphere in which the analysis is performed. In the presence of air the sample can be oxidized and the pyrolysis reactions occur at a different rate than if the sample is pyrolyzed under an inert atmosphere like nitrogen. In Figure 4.4, Murugan et al. (2009) show a comparison of the pyrolysis of a heavy oil performed under inert atmosphere and in the presence of air.

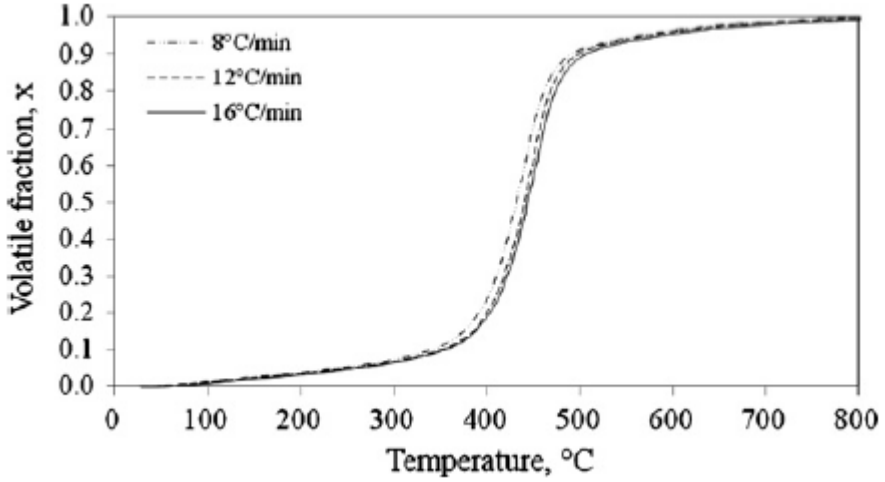

Figure 4.3. Volatile fraction of asphaltenes at different heating rates (Alvarez et al. 2011). The figure shows the shift in temperature at which the asphaltenes are released as the temperature rate changes.

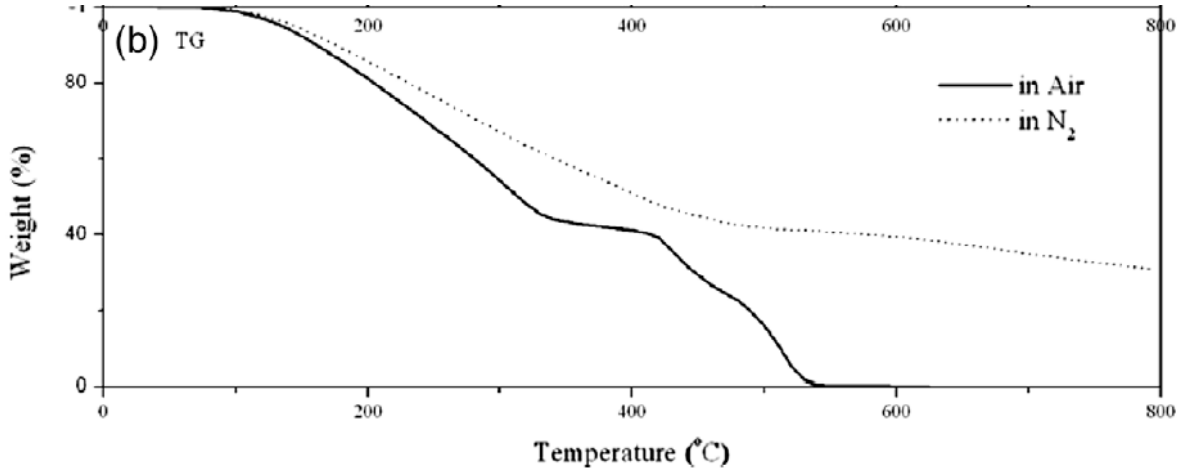

Figure 4.4. TGA curves of whole oil in N2/air atmospheres (Murugan et al. 2009). Changing the atmosphere under which the thermal analysis is performed changes the temperatures in which the products are released.

The thermal energy imposed on the sample by increasing the temperature is used to break the molecular bonds, so the amount of material released at each temperature is a measure of the molecular interaction existing in the sample. This is similar to the effect of using solvents with different polarities in SARA analysis to measure the quantity of the molecules with different molecular bonds strengths through solubility.

Due to the interaction between the different polarity fractions, I expect that the temperature of volatilization or decomposition of each individual fraction will be slightly different when they are analyzed together than what is seen individually. This was seen by Ritchie et al. (1979) with asphaltenes and bitumen and shown in Figure 4.5. All these factors indicates that even though we expect a good relationship between SARA fractions and pyrolysis results, there are many things to consider when comparing between different data sets. The size of the sample will directly affect the amount of hydrocarbons released or sample lost, for this reason many authors used the percent of weight loss change instead of the absolute weight loss as a better indicator. In the case of hydrocarbons released, the FID is directly proportional to the size of the sample.

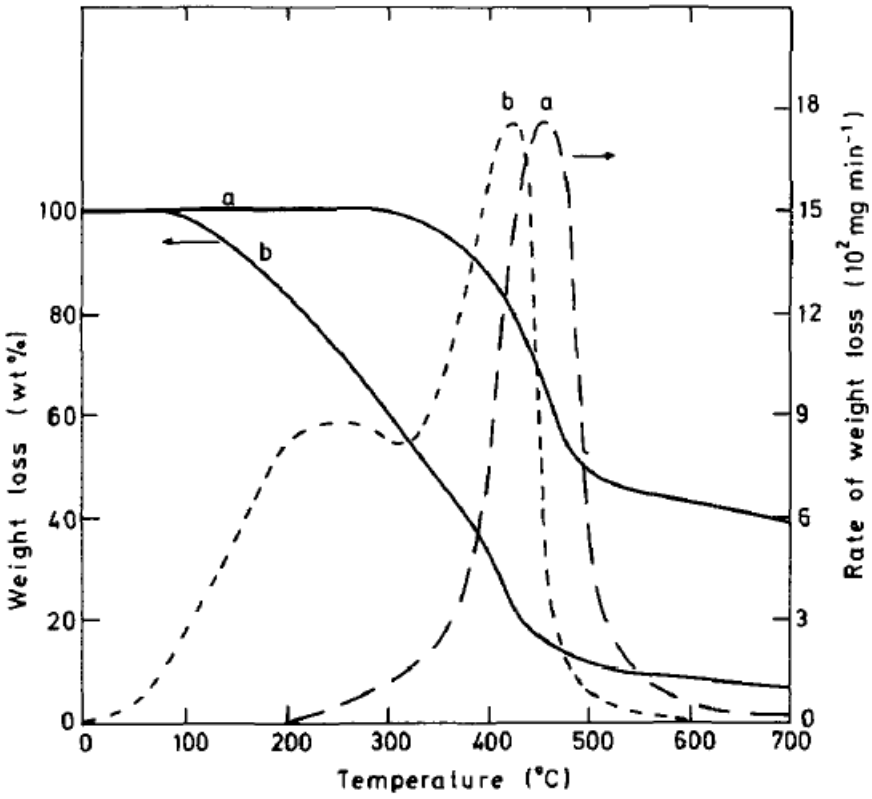

Figure 4.5. Integral and differential thermogravimetric traces for (a) asphaltene and (b) bitumen (Ritchie et al. 1979) showing shift in peak of asphaltenes due to the presence of other fractions.

4.1.5. Data

Samples used in this work are heavy oils from different parts of the world with API ranging from -6 to 14 API. Table 4.1 lists the samples used in this work together with SARA fractionation results, API gravity and water content when available. The samples were selected to cover a wide range of asphaltenes and resins contents. Asphaltenes vary from one to 78 percent and resins plus asphaltenes from 20 to 92 percent. Both SARA analysis and pyrolysis were performed by the same vendor. I performed the API and water content analyses at Colorado School of Mines. SARA analysis performed by the vendor uses heptanes for the precipitation of asphaltenes. Programmed pyrolysis was performed between room temperature and 560C under a nitrogen atmosphere at a constant rate of 25 C/min. Table 4.2 shows the pyrolysis results as reported by the vendor and Figure 4.6, shows the pyrograms vs. temperature of the eleven samples.

Table 4.1. List of samples used with SARA, API and water content results when available

	Oil Composition (wt%)				API	Water
Sample	Saturates	Aromatics	Resins	Asphaltenes	Gravity[1*]	Content[2*] (wt%)
GP003-2	26.62	52.54	16.67	4.17	12.95 ±0.4	0.58 ±0.4
GP003-3*	26.11	52.92	16.87	4.11	12.95 ±0.4	0.58 ±0.4
GP007-2	2.24	26.38	23.47	47.91	-5.00	NA
GP008-1	13.18	49.37	22.81	14.64	7.82	1.51 ±0.02
GP008-2*	12.46	47.80	24.72	15.01	7.82	1.51 ±0.02
GP009-2	11.37	20.67	36.43	31.53	3.26 ±0.2	NA
GP010-1	2.26	25.27	25.27	47.20	NA	NA
GP029-1	16.06	31.78	45.45	6.70	14.03 ±1	NA
GP029-2*	18.14	31.17	44.21	6.49	14.03 ±1	NA
GP030-2	14.54	38.26	25.82	21.38	6.59 ±0.5	NA
GP054-3	19.69	52.19	15.31	12.80	10.21 ±0.7	19.85 ±1.4
GP055-2	28.19	51.64	18.44	1.73	15.73 ±1.6	1.69 ±0.04
PE03-2	15.93	47.21	22.59	14.27	NA	NA
GP060-1	4.32	8.89	10.54	76.25	-5.96 ±0.5	NA
GP045	1.57	5.15	14.66	78.63	NA	NA
GP059-1**	19.34	39.51	27.74	13.41	9.58 ± 0.1	5.65 ± 0.7

*Duplicate, not used in correlations

**Blind test, not used in correlations

1* Methodology described in APPENDIX D

2* Methodology described in APPENDIX E

NA = Not Available

Table 4.2. Pyrolysis results for samples listed in Table 4.1 as reported by vendor

Sample	S1 (mg/g)	S2a (mg/g)	S2b (mg/g)	TMaxS2a (°C)	TMin (°C)	TMaxS2b (°C)
GP003-2	0.01	306.66	184.12	256.9	401.7	478.1
GP003-3*	0.02	153.36	122.85	256.2	397.3	481.6
GP007-2	0.01	200.06	106.25	256.7	474.4	475.0
GP008-1	0.02	70.46	80.09	256.7	375.4	471.6
GP008-2*	0.01	65.86	115.47	256.4	367.6	476.2
GP009-2	0.01	286.70	122.85	256.8	470.5	472.6
GP010-1	0.01	301.47	179.97	257.0	467.7	467.6
GP029-1	0.02	69.74	162.23	256.6	381.5	482.3
GP029-2*	0.00	82.80	186.12	256.8	384.5	482.1
GP030-2	0.01	711.39	227.13	256.7	480.3	480.2
GP054-3	0.02	221.09	259.02	257.1	384.1	476.7
GP055-2	0.01	481.68	294.71	257.0	413.2	482.6
PE03-2	0.02	111.06	159.56	256.9	377.4	477.7
GP060-1	0.07	27.69	133.18	234.0	315.2	478.6
GP045	0.02	397.91	345.32	254.9	478.6	481.5
GP059-1**	0.12	181.37	213.63	305.4	385.2	472.5

*Duplicate, not used in correlations

**Not used in correlations

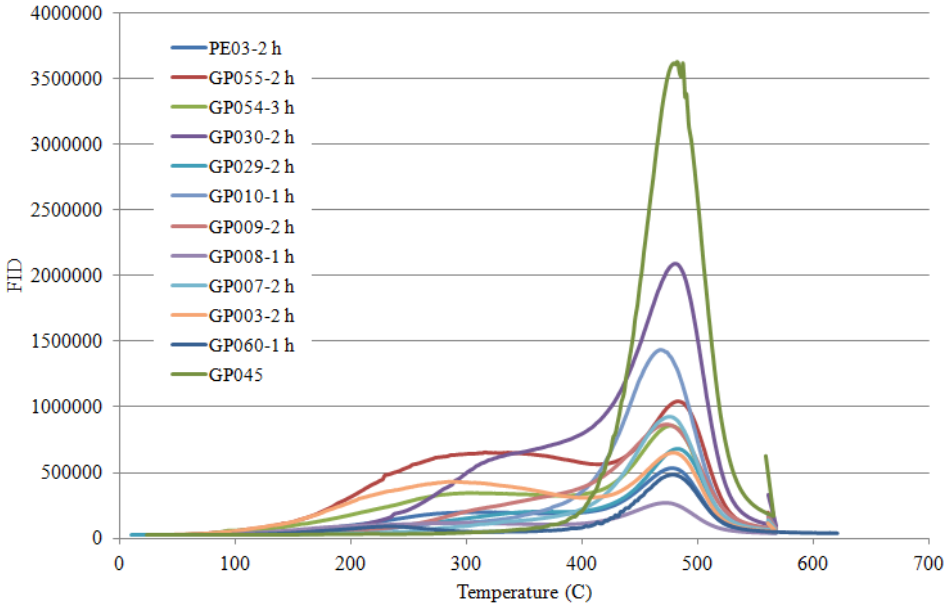

Figure 4.6. Pyrograms of heavy oil samples at a heating rate of 25 C/min under nitrogen atmosphere

4.1.6. Methodology and Results

The first step was to normalize the Flame Ionization Detector (FID) signal to the total of the FID signal measured during the experiment, in this manner, I eliminated differences between signals due to differences on the size of the sample. The normalized signal corresponds to the percentage of hydrocarbons produced at a certain temperature independent of the total amount produced. Figure 4.7 shows the normalized pyrograms for all samples. After normalization the similarities and differences between samples were easier to recognize. Based on the pyrograms we can see two groups of samples (Figure 4.8 and Figure 4.9). In the first figure (Figure 4.8) the samples with larger content of resins and asphaltenes (~50 to 93 percent) show a pronounced peak above 400C corresponding to the temperature of decomposition of polar components. In the second figure (Figure 4.9), the peak above 400C is much lower and a peak at lower temperatures between 200C and 400C increases, this group of samples corresponds to those with lower content of resins and asphaltenes (~20 to 40 percent). Just using the shape of the pyrograms a good classification can be made.

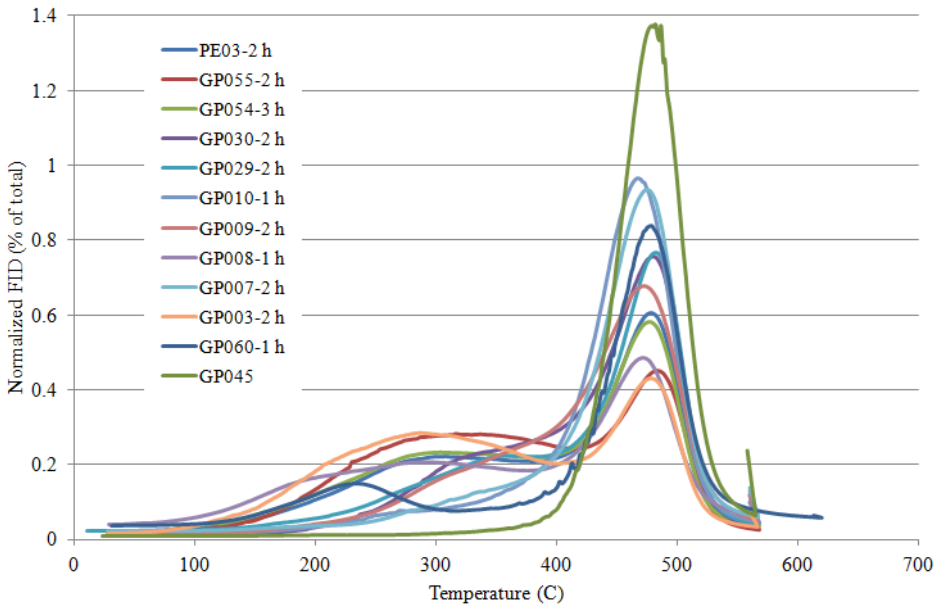

Figure 4.7. Data in Figure 4.6 normalized by the total amount of FID signal per sample

Instead of using S1 and S2 values as reported by the vendor, pyrolysis data was separated into temperature ranges every 100C as shown in Figure 4.10, and then each range and combination of ranges were correlated to the SARA fractions based on information from previous studies explained in section 4.1.3. Figure 4.11 and Figure 4.12 shows the correlations established between the fractions corresponding to the different temperature ranges and the SARA fractions. As expected from results reported from published TGA analysis, the FID signal coming from a temperature range between 200C and 400C correlates with the non-polar fractions, in particular a high correlation coefficient is obtained when correlating against the sum of the non-polar fractions (Figure 4.11) with a correlation coefficient of

91 percent. Signal coming from a temperature range between 400C and 560C, correlates strongly with the polar fractions (resins plus asphaltenes), with a correlation coefficient of 86 percent. Including the data below 200C did not improve any of the correlations and may be related with the water content of the samples.

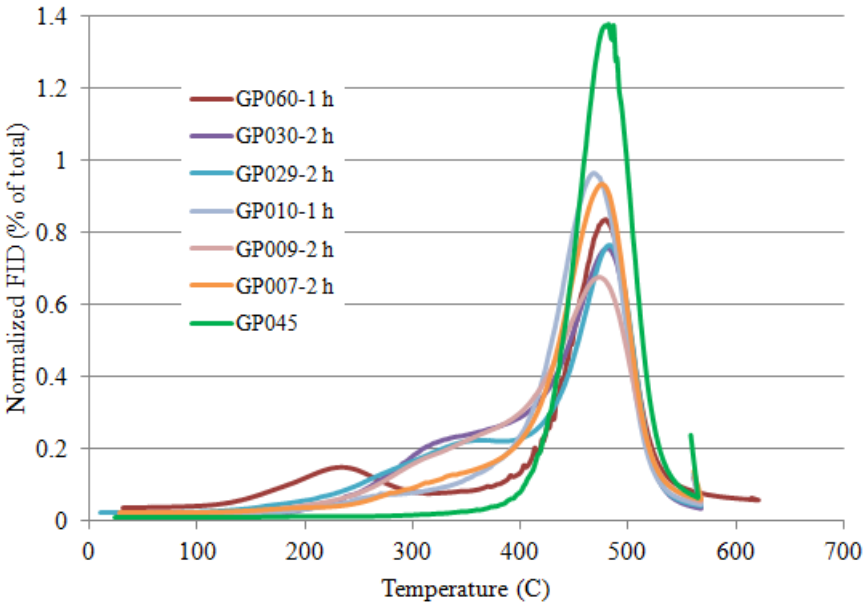

Figure 4.8. A sub-group of data from Figure 4.7, heavier samples API ranging from -6 to 14 API, resins plus asphaltenes ranging from ~50 to 93 percent. A clear distinctive peak from asphaltenes decomposition can be seen above 400C.

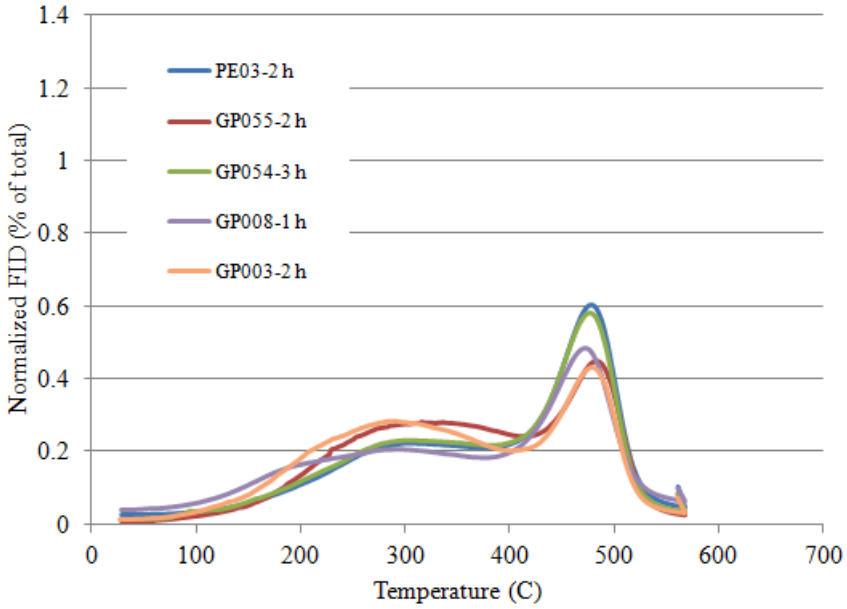

Figure 4.9. A sub-group of data from Figure 4.7, lighter samples API ranging from 10 to 15 API and resins plus asphaltenes from ~20 to 40 percent.

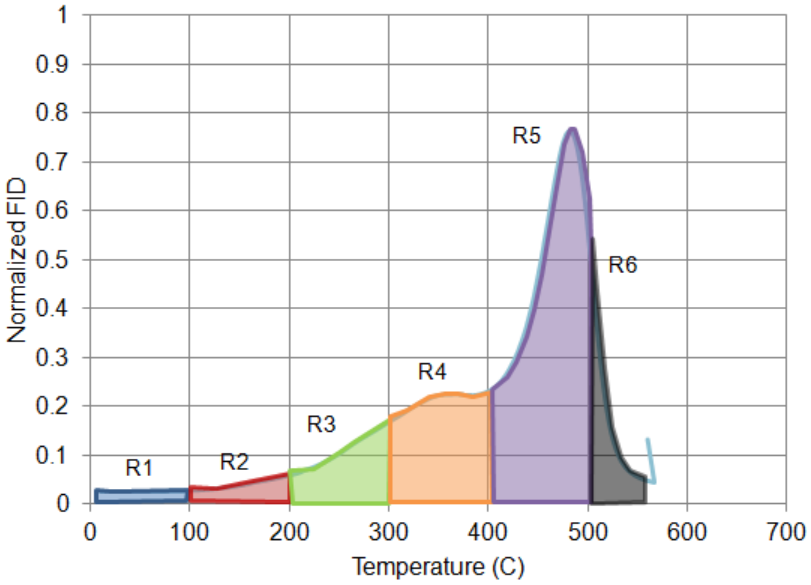

Figure 4.10. Schematic representation of temperature bins in which pyrolysis data was divided. Data from these ranges for each sample are listed in Table 3.

Even though there is dispersion in the correlation, there is a clear quantitative correlation between SARA and pyrolysis data. Error bars were added to reflect the uncertainty of the data. Errors bars for SARA fractions correspond to a standard deviation of ±5 percent which is an average value obtained by Johnston (2009) in our laboratory at Colorado School of Mines, however those values could go up to ±10 percent in many cases as reported in her work and the work of Wu et al. (2012). The error bars for the pyrolysis correspond to a value of standard deviation of ±1.2 percent and were calculated from the repeated samples used in this work. This value is probable a low value, as I am not comparing pyrolysis results between different laboratories or analysts as it was beyond the scope of this work.

Establishing a simple quantitative correlation between SARA and pyrolysis shown in Figure 4.11 and Figure 4.12 is a confirmation that both techniques are highly dependent of the polarity of the molecules present in the sample, which is related to the elastic properties of heavy oils. These results confirm the possibility of using pyrolysis analysis as a technique to predict the elastic properties of heavy oils. Table 4.3 lists the percent of hydrocarbons released by temperature range for all the tested samples.

4.1.7. Comparison between SARA and programmed pyrolysis procedures

There are three aspects that make pyrolysis a more convenient technique to quantitatively characterize heavy oils; cost, time and reliability:

1) Cost: in terms of cost SARA analysis costs approximately six times more than pyrolysis tests per sample.

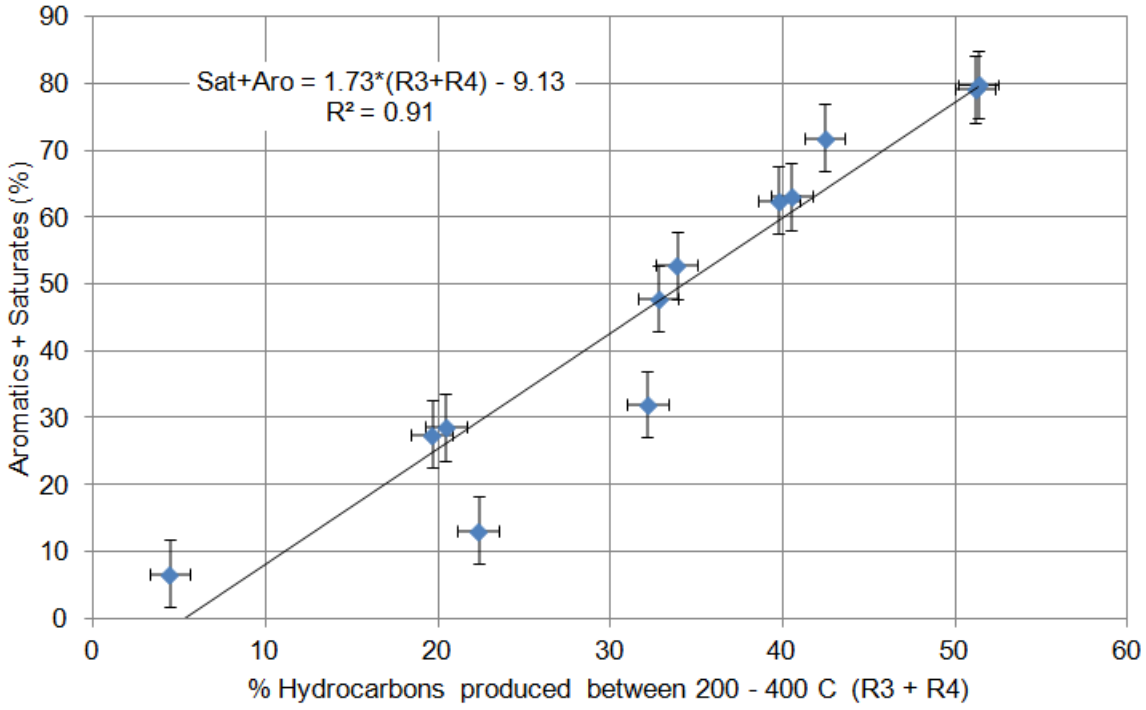

Figure 4.11. Correlation between pyrolysis temperature bin data and SARA fractions. Saturates plus aromatics vs. percent of hydrocarbons produced between 200C and 400C.

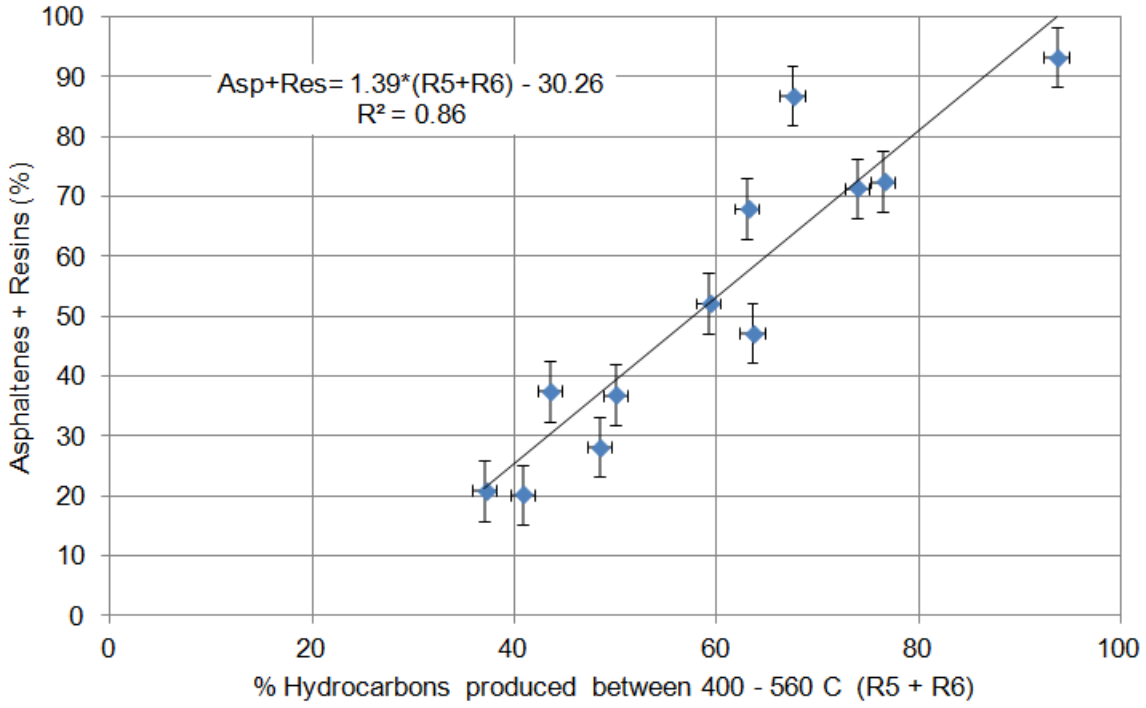

Figure 4.12. Correlation between pyrolysis temperature bin data and SARA fractions asphaltenes plus resins vs. hydrocarbons produced between 400C and 560C.

Table 4.3. Pyrolysis data for temperature ranges

	Percent of hydrocarbons released by temperature range					
	<100C	100 - 200C	200 - 300C	300 - 400C	400 - 500C	500 - 560C
Sample	R1	R2	R3	R4	R5	R6
GP003-2	2.402	9.455	25.811	25.337	36.655	0.340
GP003-3*	3.376	8.822	22.679	23.449	41.375	0.300
GP007-2	2.842	2.865	5.734	14.698	73.236	0.627
GP008-1	5.609	11.225	19.726	20.030	42.792	0.618
GP008-2*	4.563	7.043	16.859	20.805	50.233	0.497
GP009-2	2.243	2.634	8.862	23.267	62.431	0.563
GP010-1	1.895	2.079	6.073	13.546	75.908	0.500
GP029-1	3.689	4.383	10.987	21.763	58.630	0.548
GP029-2*	3.189	3.949	11.048	21.900	59.426	0.488
GP030-2	1.054	1.624	9.135	24.693	63.097	0.397
GP054-3	2.398	6.810	19.066	23.349	47.985	0.391
GP055-2	1.536	6.397	23.079	28.257	40.427	0.304
PE03-2	3.352	6.222	18.093	22.379	49.478	0.476
GP060-1	3.051	7.188	12.857	9.458	63.281	4.164
GP045	1.082	0.934	1.210	3.208	93.168	0.399
GP059-1**	1.649	7.566	19.118	22.353	47.010	2.303

*Duplicate, not used in correlations

**Not used in correlations

2) Time: SARA analysis, as it will be described in below, has different stages that in total per sample require between four to five days. If the analysis is required for several samples, samples can be tested in parallel and reduce the amount of time. How much this time is reduced will depend on the capabilities of the laboratory, and the availability of analysts. A good estimate is that between four to eight samples can be tested per week. Pyrolysis on the other hand, takes approximately 30 minutes in an automated machine, this time will vary depending on the heating rate and initial and final temperatures being tested. If we add the time required for sample preparation and cleaning, each pyrolysis sample takes maximum an hour for testing. Samples cannot be ran in parallel (unless more than one machine is available at the lab facilities), which gives a minimum of 40 samples per week, but it is known that this number is much higher in practice.
3) Reliability: the reliability of both techniques can be assessed analyzing the steps in the procedure and paying close attention to the human error. I will compare reliability in terms of the techniques procedure and which one is more prone to human error. Below there is a brief description of both techniques in which the intervention of the analysts in the case of the SARA analysis occurs at many steps while in the case of pyrolysis is limited.

SARA analysis: The first step in the analysis consists on weighting between 50 and 150 mg of sample and performing the topping, which consists in placing the sample for more than eight hours under nitrogen flow to evaporate the lighter component and water. The second step in the solubility analysis consists of precipitating and filtering the asphaltenes using an alkane (isooctane, n-heptane or pentane). For this, an alkane is added to the sample and mixed using a sonicator. The precipitated sample is taken with pipets and placed inside a syringe with a filter. The original vial is cleaned with the alkane until it looks completely clean, the cleaning solvent is also run through the filter. The maltenes are collected in a new vial, and the alkane solvent is run through the filter until it appears clear. The filter is then cleaned with a polar solvent (toluene or chloroform) and collected in a different vial. The new solvent is run through the filter until it appears clear. Asphaltenes and maltenes are then placed in nitrogen flow for more than eight hours to allow solvents to evaporate.

A chromatographic column is prepared with alumina and two different silicas which have to be pre-treated, the packing of the column is very important to get the proper retention and separation of the fractions. The maltenes, are run through the chromatographic column. The saturates fraction is separated using the simple alkane (isooctane, n-heptane or pentane), the aromatics fractions is obtained using benzene, and the resins are separated using a mixture of benzene and methanol. The separation of the saturates is done running a fixed amount of the simple alkane solvent, then benzene is added to the column and a color change occurs in the column, when the color change reaches the bottom of the column, the vial is changed to collect the aromatics. A fixed amount of benzene is added to the column to collect the aromatics. After this, the benzene/methanol mix is added to the column and a second color change occurs, when this color change reaches the bottom of the column, the vial is changed to collect the resins. A fixed amount of additional solvent is added to ensure full collection of the resins fraction. Each of the fractions is then placed in nitrogen for more than eight hours to evaporate the solvents. Vials have to be weighted before and after to calculate the amount of each fraction. The weighing is done using a micro-scale as the amounts of each fraction is very small.

Pyrolysis: Pyrolysis analysis consists in weighing 10 mg of sample and placing it in a pan inside the oven. The oven is programmed to change the temperature automatically as specified by the operator and register the hydrocarbons produced during heating. The hydrocarbons produced are registered using a FID (Flame Ionization Detector) from the machine.

As it can be seen by the above description, the SARA analysis requires many steps in which the analysts is actively involved. Many weights are taken and many transfers of materials occur between vials. Due to the small amounts of sample tested, any drops of sample falling outside the vials can cause important variations in the results. On the other hand, pyrolysis is an automatic process that once the sample is weighted and placed inside the oven, there is no human interaction and results are provided automatically. The reliability of the automatic equipment is not known, but from the point of view of experimental procedure, pyrolysis is less prone to human error than SARA.

4.1.8. Summary

Results shown in my work confirm that SARA fractions, divided as polar (resins and asphaltenes) and non-polar (saturates and aromatics), can be predicted from pyrolysis results performed at a constant temperature rate. This finding opens the possibility to use pyrolysis analysis to predict the elastic properties of heavy oils as both, SARA and pyrolysis, are related to the polarity of the molecules in the heavy oil sample. It is important to note that the errors in the prediction of the SARA fractions may also come from the errors on the SARA fractions estimation.

4.2. Rheometer measurements: liquid-solid transition due to confinement between solid surfaces

The main objective of my research was to validate the rheometer as a technique to measure the shear properties of heavy oils for geophysical applications. The rheometer allows measurement of the shear properties of samples at different temperatures, frequencies and strain/stress amplitudes. During this process of validation, I measured the effect of the solid-liquid interface in the heavy oil properties. This effect has not been extensively measured or explained before for heavy oils. These results have very important implications for geophysics that have not been considered before (further explain in chapter 5).

In this section, I will begin by showing the results of the shear modulus versus gap thickness for three different samples of heavy oils. Next, I will compare these results with similar observations found in the literature. Afterwards, I will give a theoretical explanation of these results supported by literature and I will explain the effect of slip at very low thickness values. I will end the section describing how the effect of the interface changes depending on the nature of the surface.

4.2.1. Effect of gap thickness on the shear modulus in rheometer measurements

Rodrigues & Batzle (2013), observed that as the gap between parallel plates was reduced, the shear modulus of the heavy oil increased until it reached a maximum. Figure 4.13 shows these results, which were taken for the GP007-Uvalde sample at a constant temperature and frequency. For this sample a limited number of gap thicknesses were tested, but results show how the modulus increases significantly when reducing the gap from 1 mm to 0.5 mm and reaches a maximum around 0.48 mm after which it begins to drop again.

I repeated the same experiment using a different sample (GP029-Asphalt Ridge), the experiments had to be conducted at a lower temperature (-6.5C) to ensure the sample has strong viscoelastic behavior and larger storage modulus than loss modulus. Gap thickness was decreased systematically from 1.5 mm to 0.07 mm and Figure 4.14 shows the change in shear modulus as changing the gap for different frequencies. The storage modulus increases three to four times when decreasing the

gap and this change varies with frequency with the largest changes observed at higher frequencies. The sample again reached a maximum value as it did for the GP007-Uvalde sample at a thickness of 0.11 mm after which the shear modulus begins to decrease.

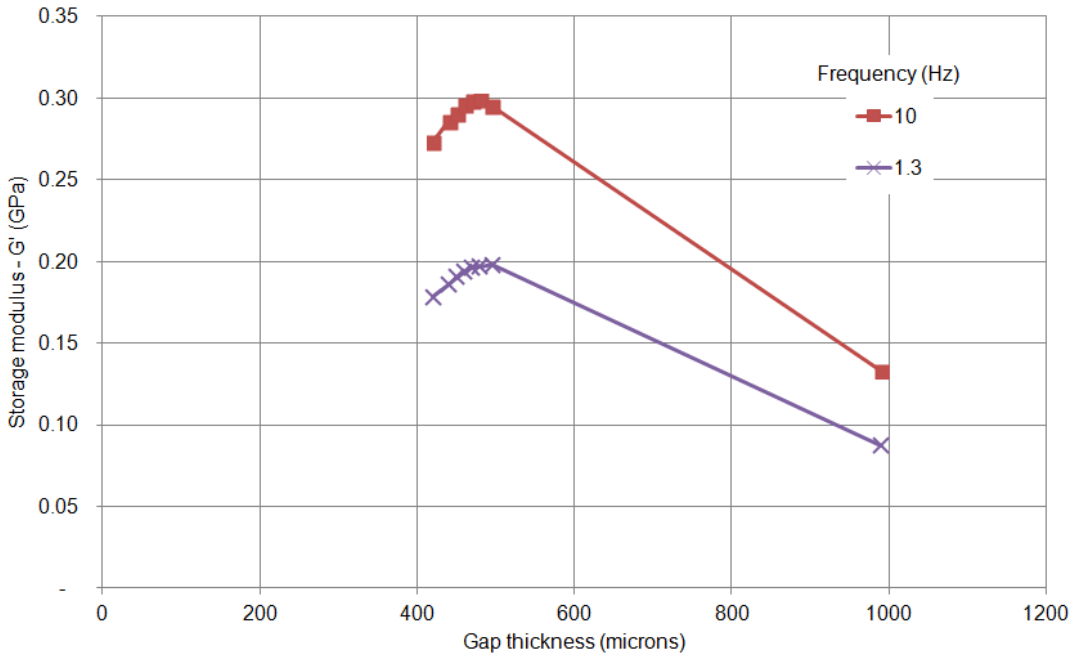

Figure 4.13. Storage modulus (G') vs. gap thickness at different frequencies for sample GP007- Uvalde (30C). A maximum value is reached at 0.48 mm gap.

To corroborate these observations, a third sample (GP010-Goleta) was also measured and results are shown in Figure 4.15, indicating a similar trend of increased shear modulus when reducing the gap thickness. For this sample a limited number of gaps were tested due to difficulties with sample handling. Tests were performed at a higher temperature (40C) as the sample is solid (perfectly elastic) at room temperature. The results show again an increase of the storage modulus when decreasing the gap and reached a maximum at 1 mm gap.

In Figure 4.16, I compare the three samples at a single frequency (10 Hz) and we can see that the three samples have comparable storage modulus even though the tests were performed at different temperatures and the three show an increase in shear modulus when decreasing the gap. The test temperatures were different between the samples to ensure all where in the viscoelastic regime yet closer to the solid state. The reason why the samples required different temperatures is due to the different composition among them. Table 4.1 from section 3.1 showed the SARA fractions and in Figure 4.17, I show the pyrograms of the three samples indicating clear similarities between GP007-Uvalde and GP010-Goleta samples, both having large quantities of asphaltenes and resins, and an obvious almost overlapping peak in the pyrograms. Sample GP029-Asphalt Ridge has a much larger content of lighter

components as reflected in the pyrogram showing an increased signal in the 300-400C temperature range and a reduction in the 400- 500C range. This explains the need to work at lower temperatures with the GP029-Asphalt Ridge sample, as reducing the temperature increases the shear modulus.

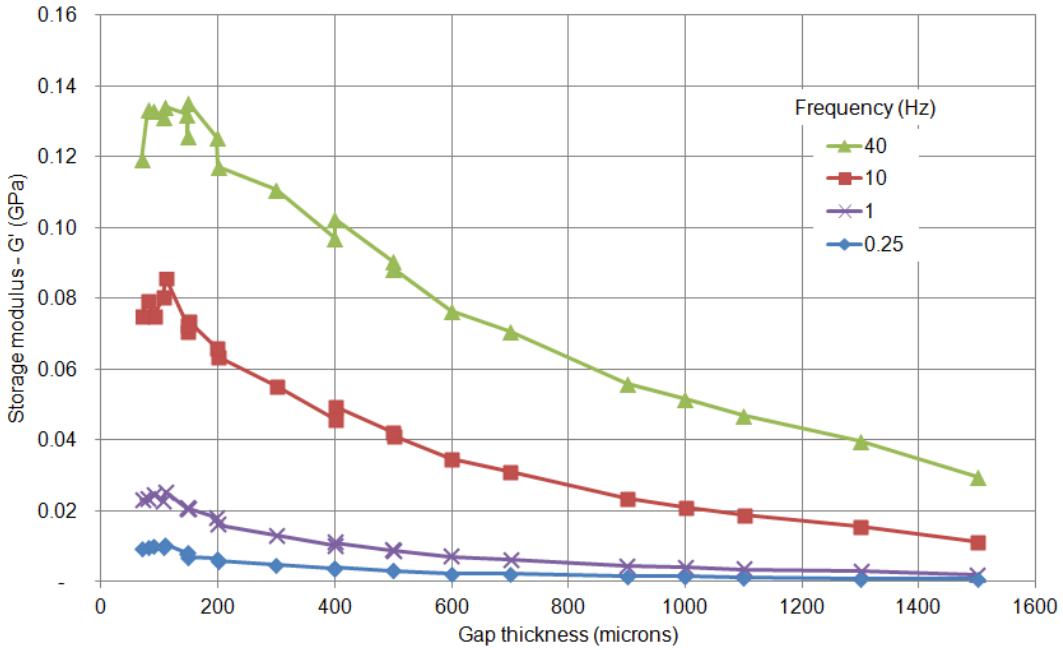

Figure 4.14. Storage modulus (G') vs. gap thickness at different frequencies for sample GP029- Asphalt Ridge (-6.5C). A maximum value is reached at 0.11 mm gap.

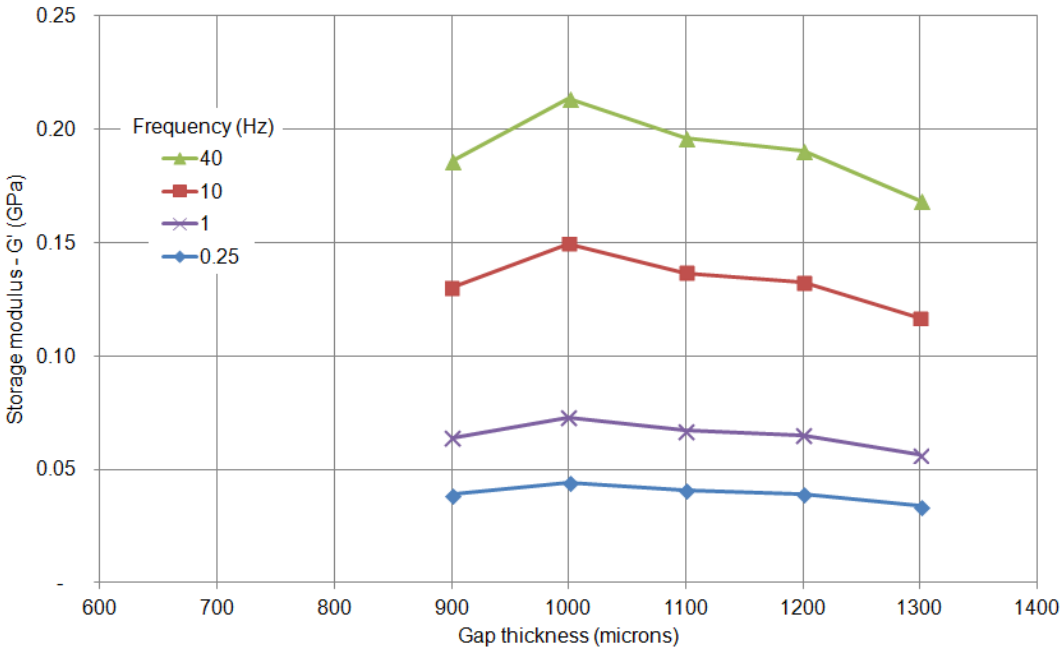

Figure 4.15. Storage modulus (G') vs. gap thickness at different frequencies for sample GP010 – Goleta (40C). A maximum value is reached at 1 mm gap.

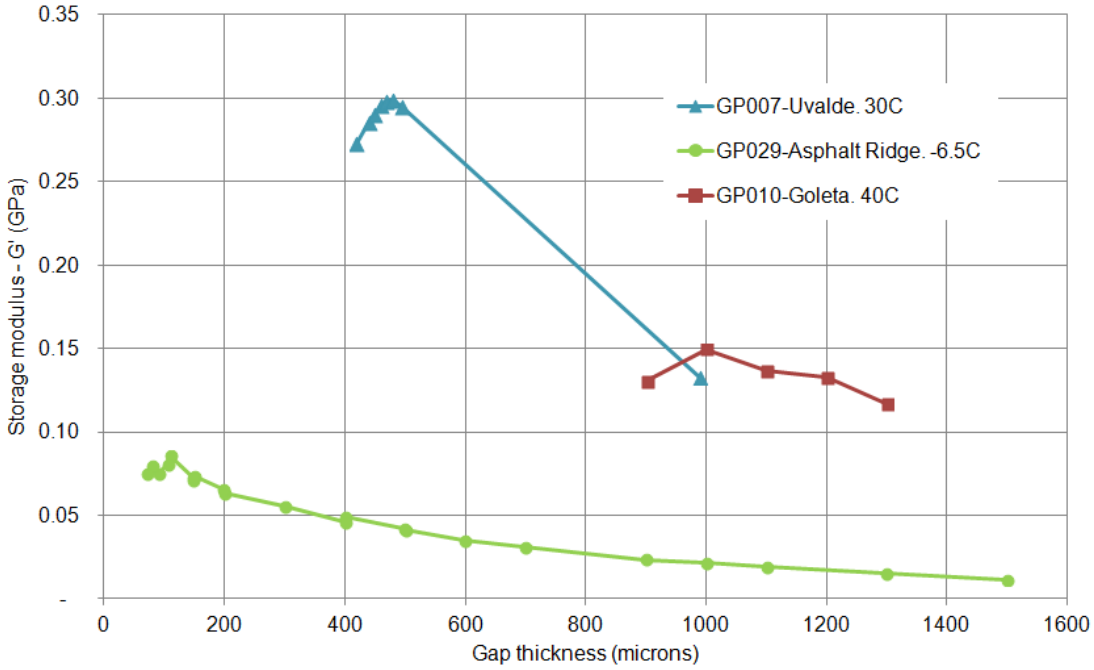

Figure 4.16. Storage modulus (G') vs. gap thickness for the three samples at a single frequency (10 Hz).

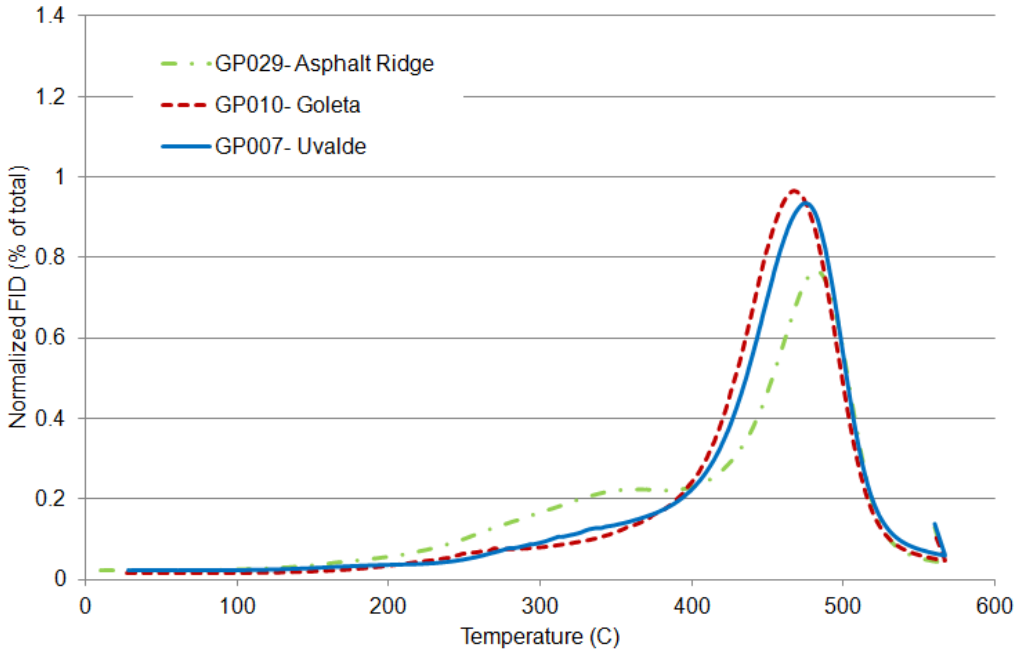

Figure 4.17. Pyrograms of the three samples tested in the rheometer.

4.2.2. Gap dependence reported in the literature

The variation of the shear properties of heavy oils (or asphalts) with thickness has been reported by only few authors (Qiu et al. 2011, Huang et al. 1998) as far as I know. From Qiu et al. (2011), Figure

4.18 shows that the complex shear modulus reached a maximum at 2 mm or 5 mm gap thickness depending if the sample was trimmed or untrimmed respectively.

However, in tensile regime, several authors in the road construction science have reported the increase in strength as we reduce the film thickness. Mack (1957) reported an increase in tensile strength of asphalt films as film thickness is reduced at 23 C, he obtained a maximum value varying from 33 to 50 microns (0.033 to 0.05 mm) depending on the sample, and he observed that the thickness at which the sample reached the maximum increased as the viscosity of the sample increased. Frolov et al. (1983) also showed a clear increase in film strength as thickness was reduced, reaching a maximum at approx. 25-51 microns (Figure 4.19). Majidzadeh & Herrin (1965) also reported an increase in tensile strength as thickness was reduced but were not able to see the maximum reported by Mack (1957). Figure 4.20 shows some of their results.

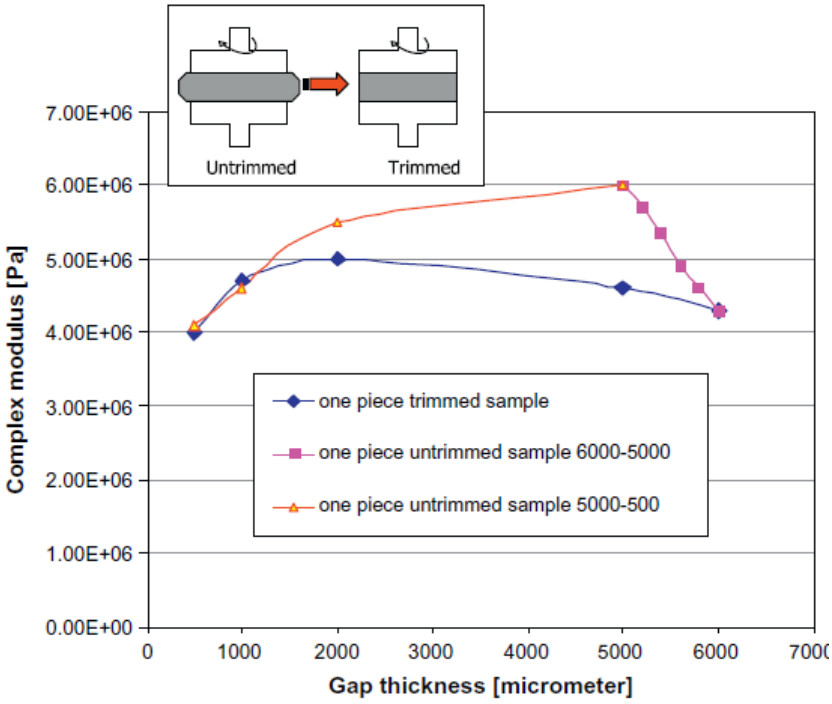

Figure 4.18. Gap effect on complex modulus from Qiu et al. (2011). A similar behavior observed in Figure 4.14 was described by the authors.

In the next sub-section, I will explain what are the mechanisms involved in this phenomenon were the sample becomes more solid-like as the gap between measuring plates is reduced. This type of phenomenon is called liquid to solid transition due to confinement.

4.2.3. Discussion of results: Liquid to solid transition due to confinement

Heavy oils, and in particular, those with a large content of polar fractions (resins and asphaltenes) are known for having strong intermolecular forces. These same molecular interactions can produce

changes in sample properties when in contact with a solid surface. In simple non-polar liquids, molecules are found in a disordered state when they are in bulk, dominated primarily by cohesion forces, the presence of a solid surface acts as an ordering mechanism which affects a layer of several molecules thick in the nanometer range (Hu et al. 1991) with sharp transition as seen in Figure 4.21 from Luengo et al. (1997). In this region the adhesive forces play the primary role in the behavior.

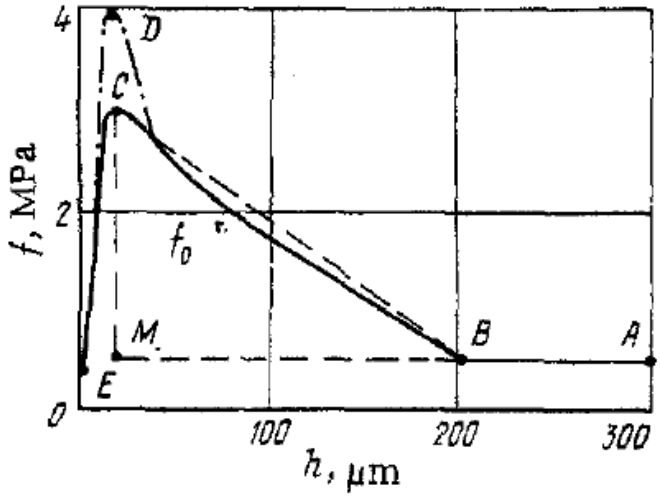

Figure 4.19. Tensile strength versus film thickness (Frolov et al. 1983)

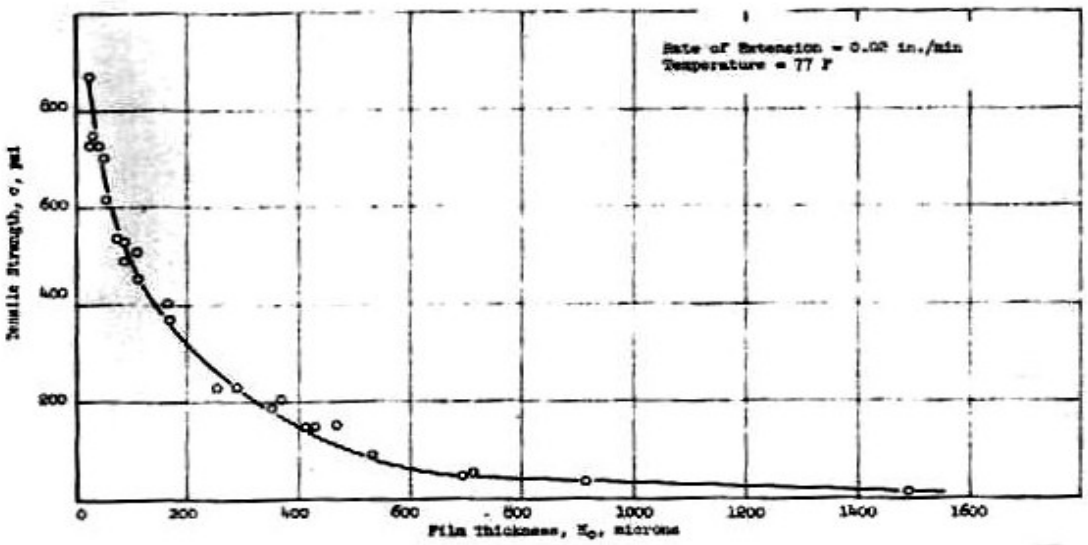

Figure 4.20. Tensile strength versus film thickness (Majidzadeh & Herrin 1965) (best image quality available)

As the molecular weight and polarity of the molecules increase, the effect of the solid surface can increase to the order of microns. Christenson & Israelachvili (1987) measured the viscosity of light oil samples between to surfaces, they concluded that the increased in polymer molecular weight extends the

thickness of the polymer layer immobilized by the surface. They pointed out that even small amounts of high molecular weight molecules (few ppms), especially those with polar components, can affect the interfacial properties of the sample and they proposed the effects of the surface to be even more pronounced for heavier oils. In the case of heavy oils, like the ones tested in my work, the majority of the sample is composed by high molecular weight-polar molecules, which means that the surfaces effects can extend to regions beyond what was measured by these authors.

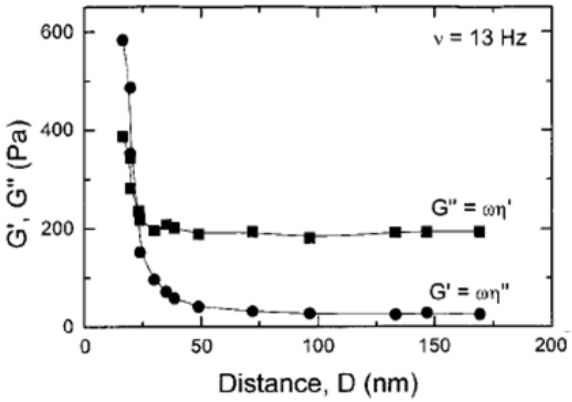

Figure 4.21. Effect of surface separation on storage and loss modulus at a constant frequency (Luengo et al. 1997)

Mack (1957) observed, while working with asphalts in tension, that the thickness of the region affected by the surfaces can be wide enough to be observed by macroscopic methods. The primary effects of the presence of this region are an increased viscosity and an increased elastic strength of the liquid. Some examples of these were shown in Figure 4.19 and Figure 4.20.

Described in chapter I, the larger more polar molecules within heavy oils (resins and asphaltenes) form large aggregates and the size of the aggregates are larger at lower temperatures what explains that the effects of the surface can be felt in the scale of the rheometer. The large aggregates adhere to the surface of the rheometer in a preferential orientation similar to the behavior of surfactants, the first layer which now is not randomly oriented, as we would expect in a bulk fluid, causes a second layer to stick to the first and so on until the effects of the re-orientation are lost far from the surface. This bonding of the molecules is stronger than the one observed in bulk and causes an increase in the viscosity of the sample near the surface. If the two surfaces are close enough, the effects of the surfaces become more important than those of the bulk and the sample behaves like a solid. The increase in modulus between the testing plates is extremely relevant, not only to the measurement itself but also to the fact that in porous media, heavy oils flow between grains and the presence of the surfaces create a confinement effect that can potentially modify the properties of the heavy oil.

In Figure 4.22, I show a schematic representation of this process, in (a) the heavy oil aggregates adhere to the surface and the effects are felt several layers away from the surface contact, the majority of

the sample is found in “bulk” state were the aggregates flow surrounded by the lighter components of the heavy oil (saturates and aromatics) and the sample has a liquid-like behavior. When the gap is reduced (b) the number of aggregates flowing freely is reduced and the effects of the surfaces can be measured, finally in (c), when the gap is reduced further the effects of the two surfaces begin to overlap and the entire sample is affected by the molecular reorientation caused by the two surfaces having a solid-like behavior.

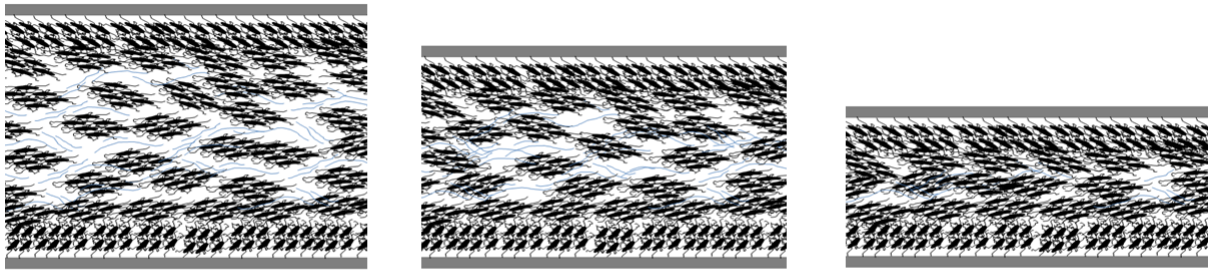

(a) Large gaps: properties of the bulk dominate (Liquid-like behavior)

(b) Intermediate gaps: effect of the liquid-solid interface begin to affect the properties

(c) Small gaps: effect of the liquid-solid interface dominate (Solid-like behavior)

Figure 4.22. Schematic representation of the liquid to solid transition of heavy oil aggregates due to the presence of the solid surface in the rheometer

The mechanisms of the surfaces effect on the properties of the heavy oils were described by Mack (1957) in tensile measurements, in his work he derived an equation based on the balance of repulsive and attractive forces. The equation relates the inverse of the normalized tensile strength to the inverse of the normalized thickness shown in equation 3.1.

$$\frac{T_m}{T} = \left(\frac{h_m}{h}\right)^a \qquad (3.1)$$

Where T and T_m represents the tensile strength and the maximum tensile strength respectively, h and h_m represents the thickness and the thickness where maximum occurs and the exponent (a), was described as a measured of the balance between attractive and repulsive forces.

Even though this equation described the behavior at small gaps, the validity of this equation for larger gaps was questioned by Majidzadeh & Herrin (1965), as in their work they show a change in slope at larger gaps (Figure 4.23) proposing different phenomena occurring at the two different scales (brittle failure vs. flow failure). Even though the phenomena occurring in a tensile regime differs from the shear regime, the change in slope is also seen in the results obtained for the GP029-Asphalt Ridge sample in my work (Figure 4.14). On the other hand, the balance of repulsive and attractive forces is still valid for shear measurements. To confirm this, I plotted the inverse of the normalized shear modulus versus the inverse of the normalized thickness (Figure 4.24). The plot shows a linear relation in logarithmic scale

near the maximum modulus (blue dots in the figure) as predicted by Mack (1957). This indicates that a similar equation can be used to describe the results obtained under shear.

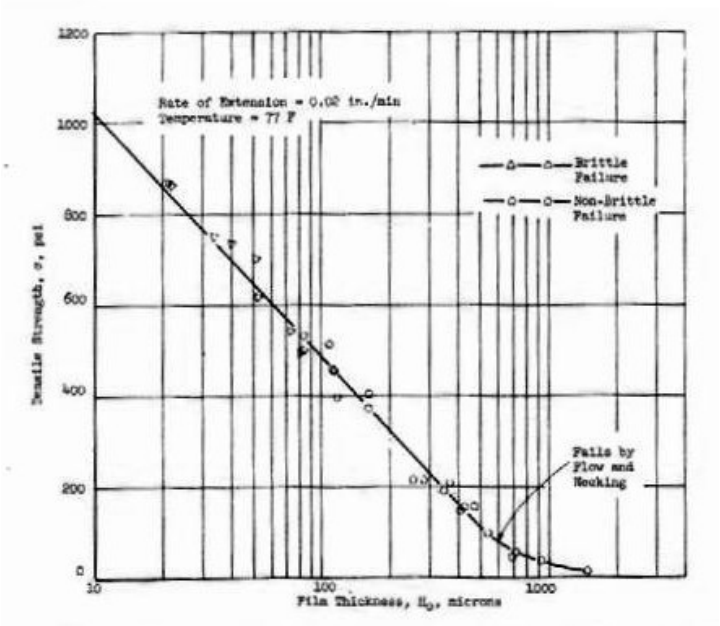

Figure 4.23. Influence of film thickness on tensile strength (Majidzadeh & Herrin 1965) (Quality of the figure is best available).

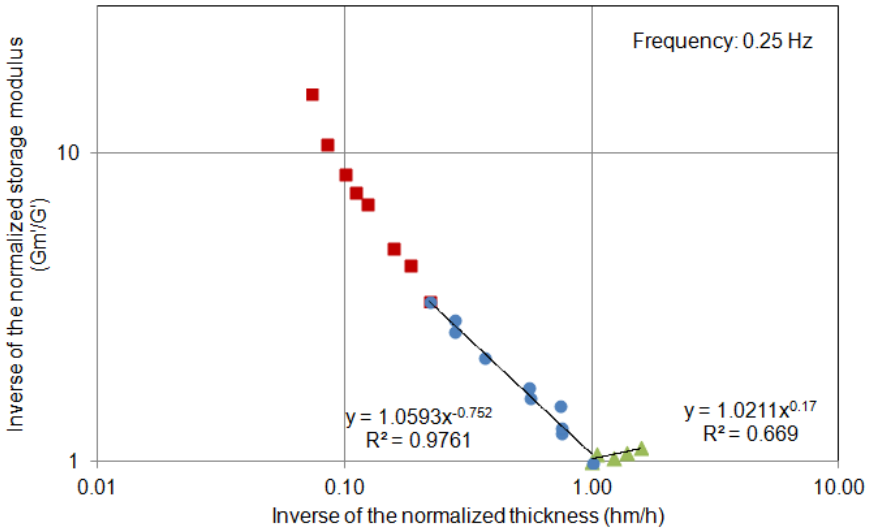

Figure 4.24. Normalized shear modulus vs. normalized thickness in logarithm scale showing a linear relation near the maximum modulus.

The physical presence of a maximum in tensile strength measurements was described and explained by Mack (1957). However, Frolov et al. (1983) and Majidzadeh & Herrin (1965) questioned the existence of that maximum and attributed the reduction in strength to a massive failure of the sample due to imperfections in the film preparation at very thin thicknesses. In shear measurements, the mechanisms

occurring below the maximum are different of those in tensile tests, since a massive failure is not expected. In the case of shear measurements, the decrease of values below the maximum can be attributed to slip, as I will describe in the next sub-section.

4.2.4. Slip at small gaps

In shear measurements, the theory of confined liquids does not predict the presence of a maximum close to small gaps, the theory predicts a continuous increase in modulus as the thickness is decreased until it reaches the behavior of a perfect solid. Therefore, the reduction in the shear modulus involves other mechanisms that can be attributed to slip. As described in section 2.4.3, slip is a plausible cause of shear modulus decrease when reducing the gap thickness in a rheometer. A sample under shear is subjected to an increased stress causing changes either to the sample itself near the surface ("apparent" slip) or causing a sliding movement or velocity discontinuity against the surface ("true" slip).

In my work, true slip is a plausible mechanism to explain the decrease in shear modulus at very small gaps, as the samples used have high viscosity and tests are performed at low temperatures. This type of mechanism has been reported by Luengo et al. (1997) when testing polymer melts and by Zhai et al. (2000) with asphalts at higher temperatures and strains. However, when true slip is present, there is a deformation of the sinusoidal signal read by the rheometer, the deformation can be visible either by the appearance of asymmetric responses or plateaus in the sinusoid. In the data I acquired there was no apparent deformation of the sinusoids that will indicate the presence of true slip. Some contribution of true slip, however, cannot be completely discarded but an additional mechanism of "apparent" slip is occurring.

With "apparent" slip in particular, the disentanglement mechanism does not apply directly to heavy oils, as it was described for polymers with long chains not reported in heavy oils. However, heavy oils aggregates can suffer similar decrease in modulus (or viscosity) due to an increased shear stress where aggregates that have been associated due to the surface effects are now disassociated due to the increase in stress. While molecular forces increase when decreasing the gaps, the stress also increases. The continuous increase in stress reaches a yield point where the new bonds created between aggregates are broken and a reversal of the shear modulus is observed.

The effect of slip was also observed at high frequency values for several gaps, as shown in Figure 4.25.

4.2.5. Surface type effect

As I explain in the previous sections, the gap effect occurs because of the presence of a solid-liquid interface. From this it can be clearly interpreted that the process of adhesion and reorientation of the molecules due to the presence of the surface will highly depend on the nature or quality of surface.

Certain surfaces may be more “attractive” to certain fluids than others, as well as surface roughness will prevent or cause increase slip. Huang et al. (1998) tested these effects when measuring the viscosity of different asphalt samples and confirmed that the surfaces tested (limestone and glass) had different effects on the viscosity measurements for several heavy oils. This confirms that both the surface and the nature of the heavy oil affect the measurement. Examples of this are shown in Figure 4.26 and Figure 4.27 from Huang et al. (1998). Figure 4.26 shows viscosity measurements for the same oil using two different surfaces, limestone and glass plates. Measurements done in limestone plates show an increase in viscosity, when reducing the gap, similar to the ones observed in my work. However, when changing the plates to glass, a slip behavior is clearly occurring with a decrease of viscosity with gap thickness. In the case of Figure 4.27 where a different sample of heavy oil was tested, slip occurs in both plates for gap values below 50 microns.

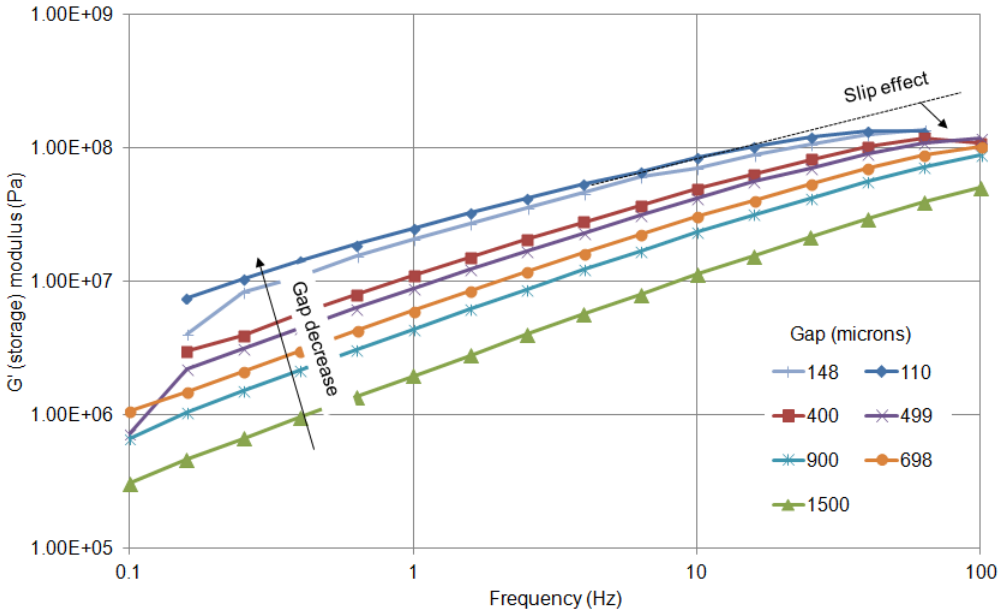

Figure 4.25. Storage modulus (G') versus frequency for seven gaps for sample GP029-Asphalt Ridge, showing the effect of decreasing the gap and the effect of slip at high frequencies.

Even though the effect of the type of surface was not tested in this work, it is an important factor that should be considered in future studies of the properties of heavy oils with the rheometer.

4.3. Comparison between rheometer, tension/compression and ultrasonic measurements: solid-liquid transition due to strain amplitude increase (nonlinearity)

In the previous chapter, I showed the results of measuring heavy oils in the rheometer and how the presence of the solid-liquid interface produces a liquid to solid transition in the sample. In this section, I will show the results of the shear modulus of the same oil sample measured with two different techniques more traditional to geophysics, tension/compression and ultrasonic velocities; and how these

results compare with the rheometer results. Based on the differences and similarities observed, I will explain the different regimes occurring in the sample due to changes in the amplitude between the techniques.

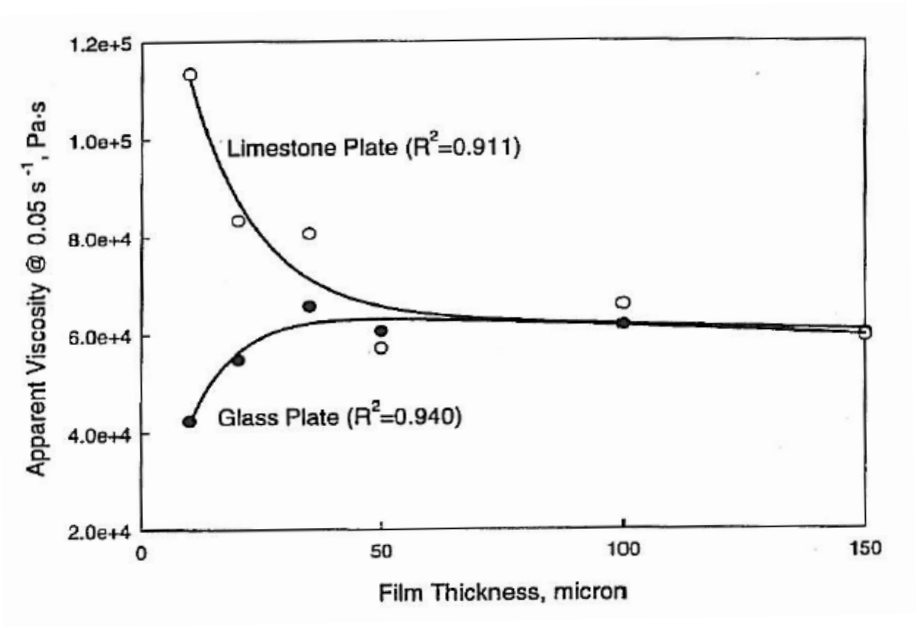

Figure 4.26. Apparent viscosity vs. film thickness in asphalt using two different test surfaces (Huang et al. 1998). An increase in viscosity when reducing the thickness occurs when using limestone plates while the contrary trend is observed for glass plates.

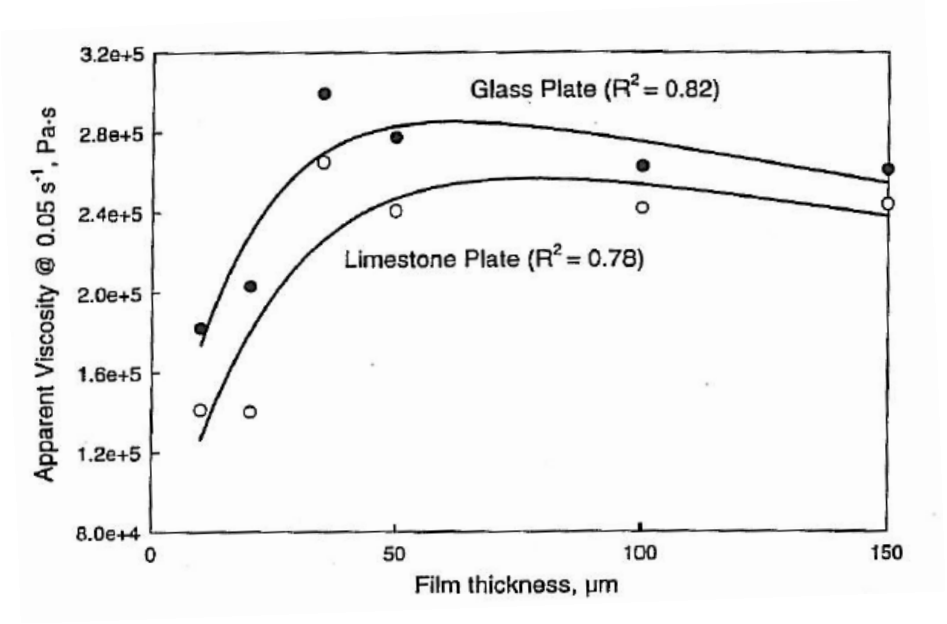

Figure 4.27. Apparent viscosity versus film thickness for asphalt (Huang et al. 1998). Similar data than observed in Figure 4.26 for a different asphalt sample. In this case the sample decreases the viscosity at very small gaps for both types of plates.

In chapter 2, I described the two main techniques used during this research to study the shear properties of heavy oils (tension/compression and rheometer). One main difference between them is the amplitude of the measurement which, as explained in section 2.3.8, may provide different results.

4.3.1. Comparison of results between the three techniques

Figure 4.28 shows the shear modulus of the heavy oil from the three techniques for the GP029-Asphalt Ridge sample. The rheometer results are shown only for the maximum values obtained at very small gaps (0.11 mm). As it can be seen, there is a good correspondence between the three techniques when compared using a Cole-Cole dispersion model, however there are still differences in particular for the rheometer results which are slightly smaller than expected. This becomes more significant when we compare the rheometer results with a sample prepared differently in the tension/compression (Figure 4.29). In this case, the heavy oil sample is the same, but the sample was prepared with the strain gages inserted inside (see section 3.2.3 with details on sample preparations) and with a layer of rough epoxy materials to improve adhesion and prevent slip.

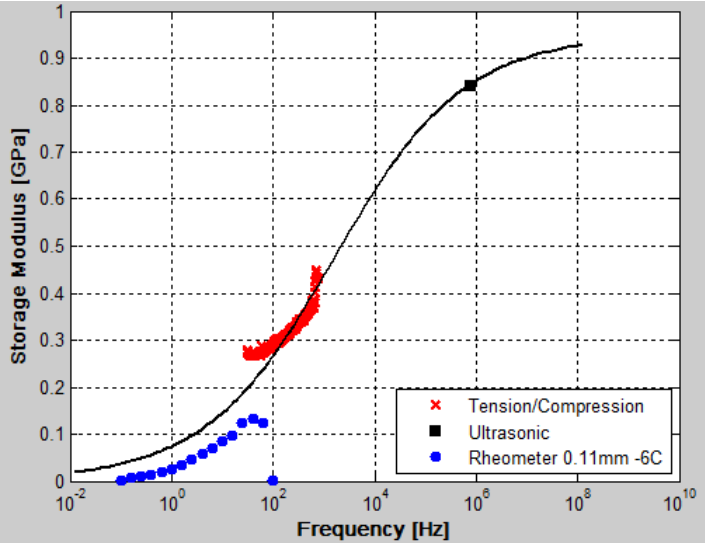

Figure 4.28. Storage modulus (G') vs. frequency for sample GP029 from three different techniques and Cole-cole dispersion model for reference. Strain gages were located outside the jacket. In these experiments the three techniques show a close match between the three techniques when compared with the rheometer results at a small gap (0.11 mm).

In both cases the rheometer results are lower than expected for that frequency range, but it is noticeable that the rheometer results that better "match" the tension/compression technique are the ones obtained at small gaps, which means that the shear modulus is larger due to confinement (explained in the previous section). This can be seen in Figure 4.30 when the same results shown in Figure 4.28 are compared to the rheometer results obtained with a large gap (1.3 mm). The rheometer measurements performed at large gaps correspond to properties of the sample closer to a "bulk" behavior, with no effect of confinement. Measurements performed with the tension/compression technique are performed at bulk

state, so a good match should be expected with the rheometer measurements done at large gaps which correspond to the bulk state. However, this is not the case here as shown in Figure 4.30.

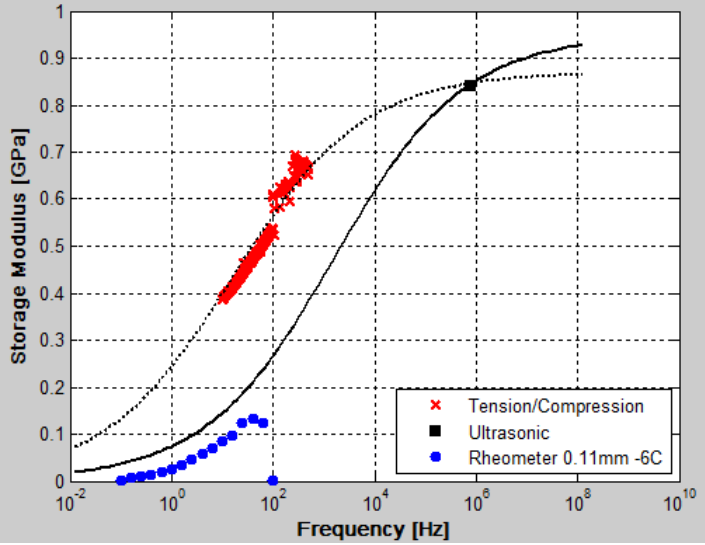

Figure 4.29. Storage modulus (G') vs. frequency for the heavy oil GP029 from three different techniques and same Cole-Cole dispersion model shown in Figure 4.28, continuos line and an alternative Cole-Cole model shown with a dashed line. Strain gages were located inside covered with a rough epoxy material to improve adhesion. In this case values of shear modulus are even larger than the ones shown in the previous figure.

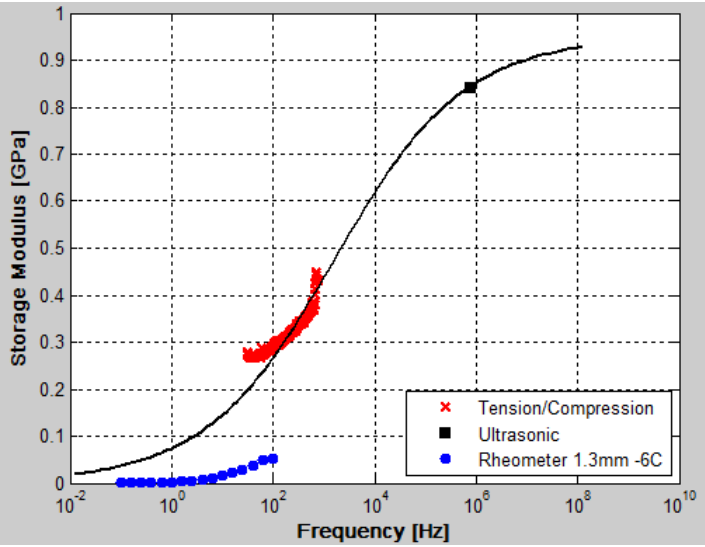

Figure 4.30. Storage modulus (G') vs. frequency for sample GP029 from three different techniques and Cole-Cole dispersion model for reference. Rheometer data shown corresponds to "bulk" values measued at 1.3mm gap thickness.

A similar comparison occurs for sample GP007-Uvalde shown in Figure 4.31 in which the three techniques compare well with respect to a Cole-Cole dispersion model. In this case the tension/compression (red crosses) and ultrasonic (black square) results were acquired by Batzle, et al.

(2006b) and the same sample was used to perform the rheometer measurements. The results shown for the rheometer correspond to the maximum values obtained in the rheometer using a 0.5 mm gap which corresponds to the confined state.

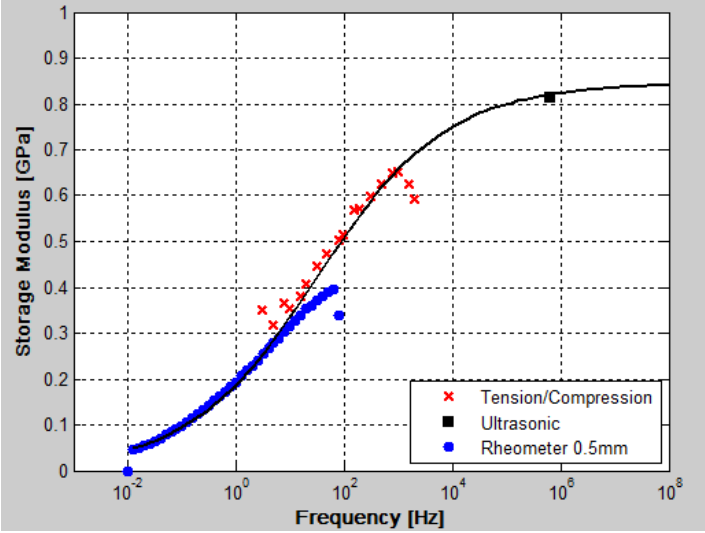

Figure 4.31. Shear modulus (G') vs. frequency (Hz) for the GP007-Uvalde sample at 30C, using three techniques and small gap thickness (0.5 mm). Data for tension/compression and ultrasonic taken from (Batzle, et al. 2006b) with outside gages. A very good match of the data is obtained using the Cole-Cole model.

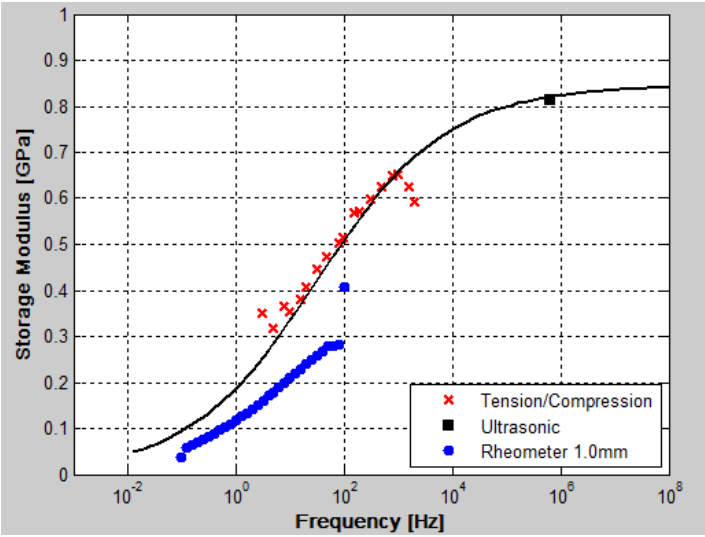

Figure 4.32. Similar plot as show in Figure 4.31 but at a 1 mm gap thickness for the rheometer results. In this case, the rheometer data does not match the expected Cole-Cole dispersion model fit for low frequency or the data at frequencies above 60 Hz which overlap with the tension/compression results.

When comparing the tension/compression results to the rheometer results at "bulk" obtained at larger gaps, the results do not match the expect trend from the Cole-Cole dispersion model as shown in Figure 4.32. The difference between the tension/compression and the "bulk" data from the rheometer can

be explained by changes in the sample due to the larger strain amplitude used in the rheometer. This phenomenon is called, solid to liquid transition due to amplitude, as it will be explained in the next section.

4.3.2. Discussion of results: solid-liquid transition due to amplitude

As described in chapter 2, heavy oils act as aggregates, these aggregates are internally strongly bonded due to the presence of polar molecules as asphaltenes and resins; while aromatics and saturates fractions act as a transition or "solvent" to the high polarity molecules. Each aggregate is composed of many molecules attached to others by strong intermolecular forces. If the sample is kept at a low energy level (low temperature, or low strain) there is not much energy and additional forces between aggregates become important and cause aggregates to associate and form microstructures that give a solid-like behavior to the heavy oil. The association forces are much weaker than the intermolecular forces forming the aggregates, so as long as the level of energy of the sample is kept low these structures subsist. When shearing the sample at a low strains (low amplitudes), the association between the aggregates do not break, but rather stretch and deform. This behavior is represented by (a) in Figure 4.33, the material acts like a solid and if the amplitude is slightly reduced or increased the shear modulus is constant and the material is in a linear viscoelastic regime (LVR). When the amplitude is increased (b), the weaker bonds are broken and the aggregates are separated and act like a suspension of polar aggregates (asphaltenes and resins) in a solvent (aromatics and saturates). The material still behaves linearly, and a second LVR develops. If the amplitude is increased further (c), aggregates begin to break and a non-linear shear behavior appears. This change in shear state with amplitude has not been previously measured or proposed for heavy oils to the extent that I know. The model shown in Figure 4.33 raises a major issue when comparing data from the rheometer with data from tension/compression or ultrasonic techniques, as the heavy oil is under a different strain regime in those techniques. This indicates that heavy oils have a nonlinear behavior with amplitude, however multiple regions of linearity may be present.

4.3.3. Multiple Linear Viscoelastic Regimes (LVR) in the literature

Even though the presence of multiple LVR has not been reported for heavy oils, it is well known for other materials like fresh cement paste. Figure 4.34 from the book of Ramachandran & Beaudoin (2000) shows the presence of two LVR for a cement paste as an example of typical behavior of cement suspensions with strain. For cement pastes the typical critical strain in which a transition from solid to liquid occurs is in the order of 10^{-4}.

Similarly, Chougnet et al. (2007) explained that aggregates at rest tend to form a single continuous phase and the material acts like a solid but when the strain is increased the material acts like a liquid. For two different materials, they showed that two different plateaus in the shear modulus occur. The change between the two LVR was described as a solid-liquid transition due to amplitude. The next figure (Figure 4.35) shows the results by Chougnet et al. (2007) in which they emphasize the fact that for the first LVR

the G' (storage) is larger than the G" (loss), which corresponds to a solid-like behavior, while in the second LVR at larger amplitudes, G" is larger than G' corresponding to a more liquid-like behavior.

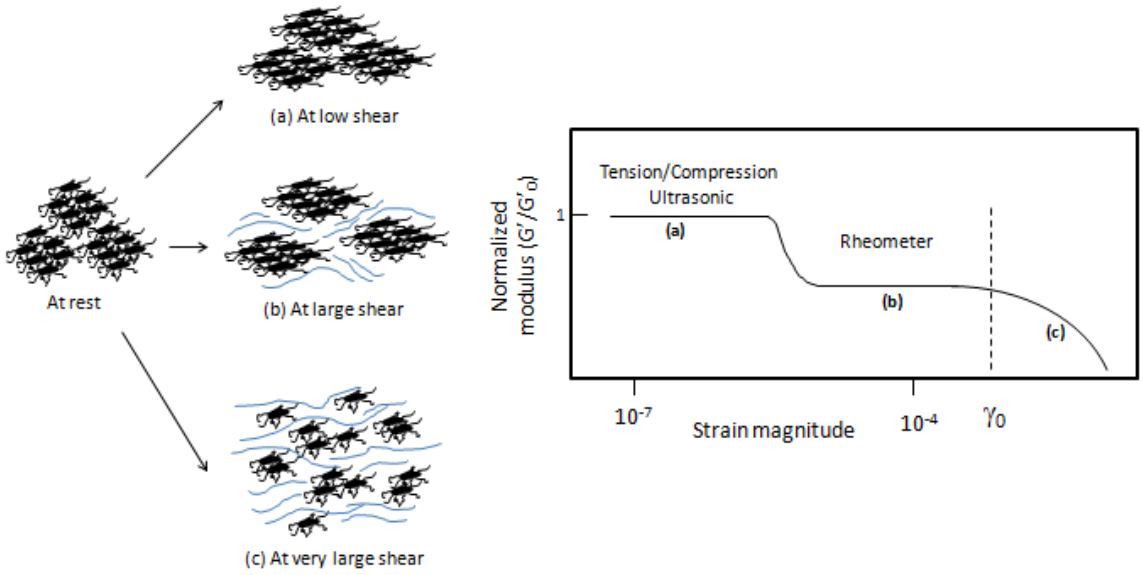

Figure 4.33. Schematic representation of heavy oil behavior under shear at different amplitudes. Left shows a representation of the molecular behavior, and the right side of the picture shows the corresponding expected shear behavior. (a) at low shear, aggregates stay together and bonds between aggregates only deform behaving like a solid, (b) at large shear, inter-aggregate bonds are broken, and the heavy oil acts like a suspension, (c) inter-molecular bonds are broken, aggregates break and a non-linear behavior develops.

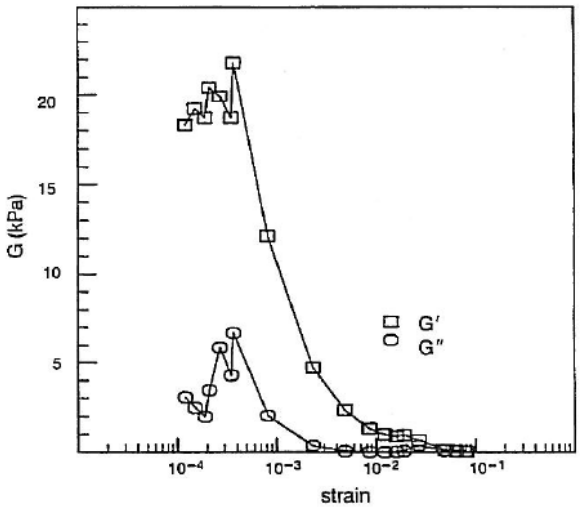

Figure 4.34. Storage modulus of cement paste vs. strain (Ramachandran & Beaudoin 2000).

Heymann et al. (2002), also measured similar results for spheres of polymer particles in concentrated suspensions. At low stress (low strains), the suspension behaved solid-like and shows a quasi-linear

viscoelastic regime, when increasing the stress (strain), they reported a sharp transition to liquid-like behavior and a secondary LVR appears at large stresses. The following figure (Figure 4.36) from Heymann et al. (2002) exemplified this. The figure shows the amplitude sweep for the suspension performed at different amplitude increase rates. Clearly from this figure the rate of amplitude increase affects the solid-like state while does not affects the liquid-like behavior.

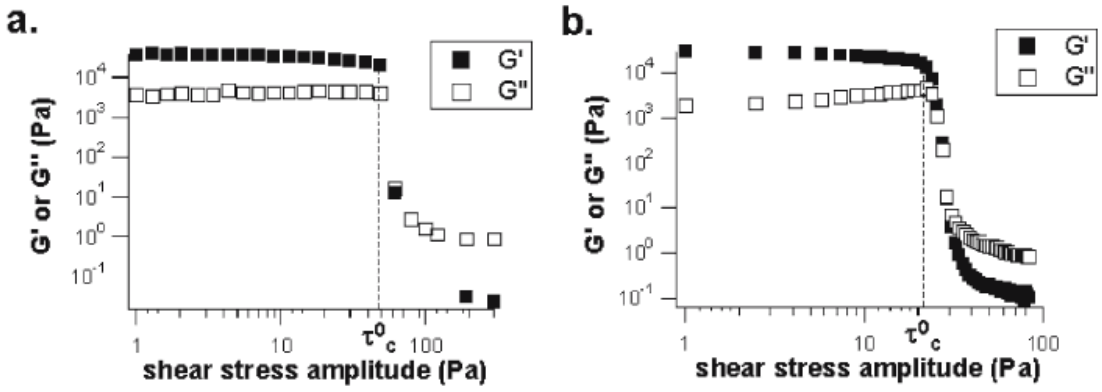

Figure 4.35. Shear modulus (G' and G") vs. stress amplitude for two different materials at 1 Hz (a) Cement, (b) Silica suspension (Chougnet et al. 2007). Two LVR are seen in the figures, the first one at low stresses showing a solid-like behavior (G'>>G") and a second one at large stresses, showing a liquid-like behavior (G">>G').

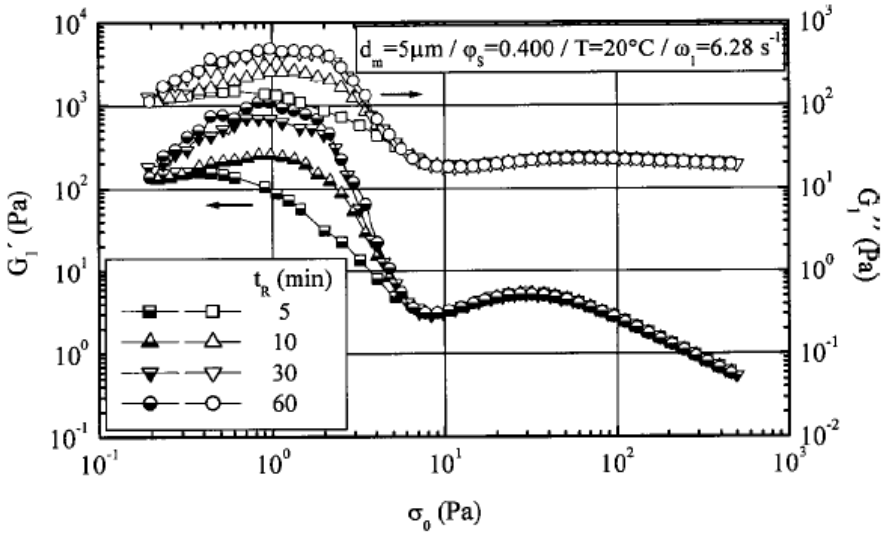

Figure 4.36. Shear modulus vs. stress for polymer spheres suspension at different rates of stress increment (Heymann et al. 2002). Here two quasi-LVR are observed at low and large stresses.

4.3.4. Opposing effects in the rheometer vs. tension/compression results: liquid to solid transition due to confinement vs. solid to liquid transition due to amplitude

At the beginning of this section, I showed how different the results from the "bulk" rheometer measurements were in comparison to the "bulk" tension/compression measurements. I also showed how

when comparing the same tension/compression results with the rheometer measurements done at small gaps the two data sets get very close and in some cases reach a perfect match.

As explained the presence of the two solid-liquid interfaces in the rheometer has a measurable effect on the shear modulus of the heavy oil sample. This effect produces an increase of the modulus as we reduce the gap between the parallel plates, changing the behavior of the sample from a liquid-like behavior to a solid-like behavior. On the other hand, also in the rheometer, there is a change from a solid-like behavior to a liquid-like behavior when the heavy oils are subjected to larger strains. These two effects are somewhat opposite and seem to compensate each other when we compare the tension/compression results with the rheometer measurements at smaller gaps.

In other words, rheometer measurements done in the "bulk" sample (large gaps), cause a transition from solid to liquid due to the increased amplitudes, but on the other hand, if the gap in the rheometer is reduced significantly, a transition from liquid back to solid is forced in the sample, explaining why a better match between the two techniques is obtained at small gaps. Figure 4.37 illustrates these changes. At low strains (a), in the tension/compression technique, the sample has a high modulus, when subjected to large strains in the rheometer, the sample reaches a secondary LVR with lower modulus (b). As we reduce the gap in the rheometer, the modulus increases due to the confinement effect between two solid surfaces. As the gap is reduced further, the modulus could (or not) reach a value that is comparable to that measured at lower strains (c). The reduced gap moved the sample to a similar b shear regime than the one measured at low strains in the tension/compression equipment.

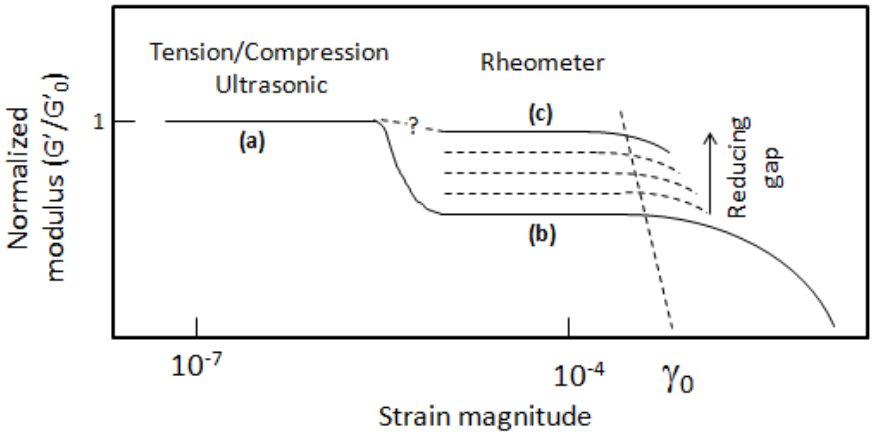

Figure 4.37. Modification to Figure 4.33 adding the appearance of an "equivalent" solid-like LVR with the rheometer after reducing the gap thickness.

The LVR at reduced gaps is similar to the solid-like state measured by the tension/compression technique, but is not the equivalent as in the rheometer the confined properties are a function of the nature of the solid surface material as it was seen in Figure 4.26.

To better describe the multiple LVR model shown above, in Figure 4.38 I added data to the schematic representation shown in Figure 4.37. The data was obtained at different frequencies and temperatures but help to visualize the schematic representation in terms of real data. Black squares corresponds to data taken in the tension/compression equipment at 40 Hz at different strains, at linear behavior con be observed on those five points which corresponds to the first LVR at low amplitudes. Since there was not a strain sweep available from the rheometer at 40 Hz, I include in this picture a strain sweep taken at 10 Hz and at small gap (0.11 mm), these are shown by the blue diamonds. It can be seen that they also behave linearly until approximately 10^{-2}, when it begins to behave non-linearly and decrease. For reference a single point taken at 40 Hz and 0.11 mm gap is shown in purple which corresponds to the location of the 40 Hz LVR comparable to the tension/compression data. Then, I added the "bulk" shear modulus at 40 Hz and 1.3 mm gap with a red square, which corresponds to the location of the LVR of the large gap measurement. All these tests were performed at -6.5C. Several tests were done trying to get data below 10^{-4} strain but too much noise did not allow for significant data to be collected at the temperature of interest. However, a strain sweep obtained at 30C for the same sample, shows a consistent increase of shear modulus at lower strain amplitudes (green triangles), this increase may be indicative of the transition between the two LVR proposed in my work.

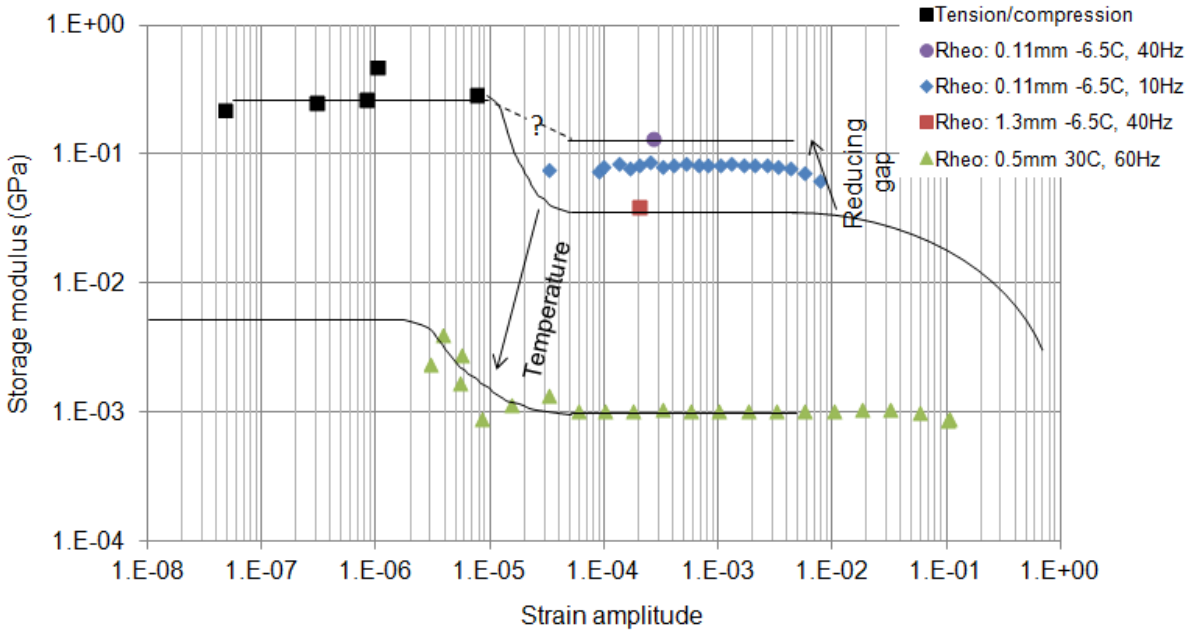

Figure 4.38. Storage modulus vs. strain amplitude at different gaps, frequencies and temperature with the schematic representation on top. Even though the data shown were taken at different conditions, all of them together help to explain the different behavior observed in the data and form part of the data used to build the schematic representation.

4.3.5. Other plausible explanations for the observed differences between tension/compression and rheometer measurements

The strain amplitude dependence showing two LVR in the behavior of heavy oils is a suitable explanation for differences observed between the two techniques; nevertheless, it is important to consider other plausible mechanism affecting the results.

Temperature inaccuracies

The properties of heavy oils are highly dependent on temperature as described in section 2.3.4. On the other hand, rheometer measurements are subjected to temperature variations as explained in section 3.1.5. Even though the tension/compression results were done at the same average temperature there is a great possibility that the temperature distributions of the experiments were different enough to explain some of the differences between the two techniques.

The presence of a temperature gradient within the sample in rheometer has been confirmed and modeled by other authors (section 3.1.5). The temperature gradient becomes more pronounced when the sample has more isolation capacity which is the case of the heavy oil samples at low temperatures. In the case of the GP029-Asphalt Ridge sample, there is a possibility that the average temperature of the sample, when set to be at -6.5C, was actually a value above that temperature due to the contact with the upper stainless steel rod which is in contact with the room temperature at 22C. However, the same temperature variations cannot explain the differences observed for the GP007-Uvalde sample. For the GP007-Uvalde sample at 30C in the rheometer, the temperature gradient should be opposite to the GP029-Aspahlt Ridge case, and the average temperature of the sample should be lower than the required temperature, some value between 30C and 22C (room temperature). This would imply that the temperature is lower than in the tension/compression experiment and then we should be measuring a higher modulus instead of the same or a lower one. Still, in the case of GP007-Uvalde there is also a large uncertainty in the temperature of the tension/compression results. The original results were published indicating a temperature of 20C, internal review of the data indicated that the measurements were done at 30C which is the value used during this research. It is believed however, that the experiment was done at room temperature with no control, which varies between 22C and 24C. In summary, the temperature uncertainties may be playing a major role in the differences observed between the two techniques.

The temperature variation alone cannot completely explain the variations observed between the two techniques. This variation can explain the differences between the tension/compression technique and the rheometer results obtained at the gap where the maximum value of modulus is achieved, but it does not explain why, to match the data, it is necessary to use the “confined” data from the rheometer.

In the section 4.2, I explained why the modulus increased with confinement between the rheometer plates, which implied that there is a different molecular regime occurring at confinement than in the bulk state measured with the tension/compression technique. If the differences between the two techniques are due only to temperature effects, then why would the data at a confined state in the rheometer would match the data in the tension/compression technique, which is measured at the bulk state with no surface effects?. The temperature effects can explain part of these differences but not completely, therefore there has to be other phenomena that cause the rheometer data to be significantly lower than the tension/compression measurements.

Slip phenomena in rheometer and tension/compression measurements

Slip phenomena was explained before, but to summarize, slip is the measurement of a lower modulus due to slippage of the sample across the solid surface. Even though slip cannot be considered the cause of all the changes of the modulus with gap in the rheometer, there is a possibility that there is some slip still present in the measurements done at all gaps and frequencies studied. If that is the case, then all the measurements done with the rheometer will be indicating much lower values than the real property which could be the cause of the discrepancies between tension/compression and rheometer measurements.

As explained before in sections 2.4.3 and 4.3.5, there are several mechanisms of slip usually classified as “true” and “apparent” slip. True slip was discarded based on the quality of the data, and “apparent” slip due to disaggregation can explain the reduction of modulus after the maximum in the rheometer measurements.

We could argue that some slip also occurs at every gap making the properties of heavy oils in the rheometer to measure lower than the tension/compression data. This is something that has been reported for emulsion or particle suspensions. In these suspensions, there is an effect of “depletion” were particles migrate away from the walls and create a “more liquid” layer near the walls causing the rheometer to measure a lower viscosity (modulus). Figure 4.39 from Barnes (1995), shows a the reduction of viscosity caused by wall slip in suspensions when increasing stress. Also picture in the figure is the measurements at different gaps, and it can be seen that as the gap is decreased the effects of slip are more pronounced. This is consistent with the fact that as we increase stress, slip increases.

This is not the case for the heavy oils I studied. I see a reduction on the modulus between tension/compression and the rheometer, which means that at an increased strain we have a lower modulus. This could be attributed to slip, but it will contradict the data measured in the rheometer. In the rheometer when stress is increased (reduction of gap), the modulus increases; it does not decrease as expected with slip. The “depletion” effects seen in suspensions, is not expected in heavy oils that like to adhere to solid surfaces due to the presence of surface active components like resins and asphaltenes.

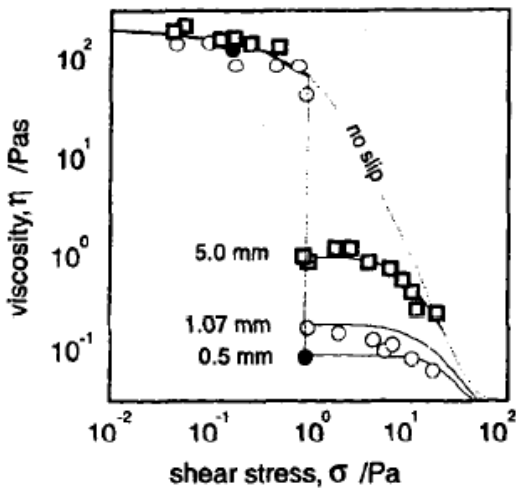

Figure 4.39. Slip effects on viscosity measurements of a suspension at different gaps. Suspension under shear can create a layer near the walls "depleted" of the suspended material and therefore of lower viscosity. The effect is further increased when reducing the gap (Barnes 1995).

5. CONCLUSIONS AND IMPLICATIONS OF THE RESEARCH

In this chapter, I summarize the conclusions of my work and describe potential implications of the results. I will begin with a general conclusion of the work and continue with more specific findings.

5.1. Conclusions

A general conclusion of this work is the fact that the answers to geophysical problems can highly benefit from other sciences that have work either similar problems or similar materials in a completely different context. That is the case in my work in which I had extensive support from chemical engineering, road construction science, and many areas of chemistry. Besides this general observation, below are the specific conclusions of my research:

My work qualitatively confirms the relation between SARA and pyrolysis and the elastic properties of heavy oils. It also provides a quantitative way to predict SARA fractions, divided as polar (resins and asphaltenes) and non-polar (saturates and aromatics), from pyrolysis results performed at a constant temperature rate. This finding opens the possibility to use pyrolysis analysis to predict the elastic properties of heavy oils as both, SARA and pyrolysis, are related to the polarity of the molecules present in heavy oils.

The presence of a solid-liquid interface can largely affect the elastic properties of heavy oils. Heavy oils composition includes molecules that are surface active which reorient in a preferential manner at the interface. This reorientation causes a change in the shear properties near the interface in a scale that can modify the macroscopic elastic properties of the heavy oil. This is the case of measurements done with the rheometer in which the presence of the two solid-liquid interfaces increased the shear modulus of heavy oils, an effect that is also called liquid to solid transition due to confinement. This was evidence by an increased of the shear modulus when reducing the gap between the rheometer plates.

Another important conclusion of my research is the presence of multiple LVR at different amplitudes of the shear modulus of heavy oils. Heavy oils are aggregates that at rest or under low shear, behave as a solid due to weak bonds between the aggregate particles. As strain amplitude is increased the weaker bonds are broken and the heavy oil behaves liquid-like. This was seen by the increased values measured by the tension/compression results at low amplitudes in comparison to the much lower values measured by the rheometer at higher amplitudes. This indicates that two linear viscoelastic regimes are present in the heavy oil at different amplitudes.

Finally, integrating the findings of the two last conclusions, when rheometer measurements are performed at reduced gaps, a solid-like behavior of the heavy oil can be achieved due to confinement between the two solid surfaces. The increased in shear modulus due to this transition almost reaches the values measured at much lower amplitudes in the tension/compression technique. It can be summarized that the effect of lowering the shear modulus by higher amplitudes in the rheometer is reversed by the confinement between the two solid surfaces of the rheometer plates. However, since the increase due to confinement depends also on the nature of the solid surface and not only on the properties of the sample, the confined behavior (rheometer) can be similar to the low amplitude behavior (tension/compression) but is not equivalent.

5.2. Implications

The main implications of this work can be divided into experimental and in the modeling or understanding of the rock physics and flow in porous media.

5.2.1. On geophysics experimental work

The rheometer has been proposed as an alternative technique to measure soft samples under shear, as the handling of soft samples in the tension/compression technique has many complications. There have always been doubts about the validity of the rheometer results due to the higher amplitudes and the present research confirms those issues. The rheometer is an appropriate technique to measure the properties of heavy oils for engineering applications, in which there is a constant flow at higher shear rates. Also, it could be argued that at high temperatures like those present in thermal EOR methods the heavy oil dynamic viscosity measured with the rheometer is close to that measured by the seismic. The argument comes by the fact that the effect of high temperature is equivalent to high amplitudes in which the heavy oil becomes more liquid-like. However, at colder reservoir conditions in particular in colder regions like Canada or Alaska, the seismic measures the heavy oil like a solid due to the low temperatures and low amplitudes of the seismic waves. Under these conditions, trying to predict the behavior of the seismic waves from heavy oil properties measured at the rheometer will likely give erroneous results. This implies that the use of the rheometer for geophysical characterization of heavy oils must be carefully employed or is only limited.

I recommend extending the work of handling soft samples in the tension/compression technique which will allow to better understand the heavy oil properties at low amplitudes. There is also a possibility that in the future rheometers are able to measure lower amplitudes and a better comparison could be made. However, even if that is the case the rheometer still presents the effect of the confinement between two solid surfaces that can affect the heavy oil elastic properties.

5.2.2. On rock physics models and flow in porous media

The results of my work also have important implications in the current and future rock physics models developed to predict the properties of rocks saturated with heavy oils and to study the flow in porous media. The most important aspect is the fact the shear modulus (or viscosity) of heavy oils can increase with confinement. This is the case of heavy oils confined between grains inside the rock and in reservoirs where precipitation of asphaltenes occur due to primary depletion or due to gas/CO2 injection. It is well known the effect of reduction of permeability (and changes in wettability) due to precipitation or adsorption of asphaltenes or resins on the grain walls. This decrease in permeability is attributed to the narrowing of the pore throats and changes in relative permeability; however, the effect that I am presenting here is an increase of viscosity near the walls that will further reduce the mobility on top of the narrowing of the pore throats. Figure 5.1 shows an schematic representation of this scenario, pore throats are "blocked" by asphaltenes but also the viscosity of the heavy oil in that area can increase significantly reducing mobility. The extent of the increased viscosity, and how much it will affect the bulk flow, will depend on the composition of the heavy oil and the temperature of the reservoir.

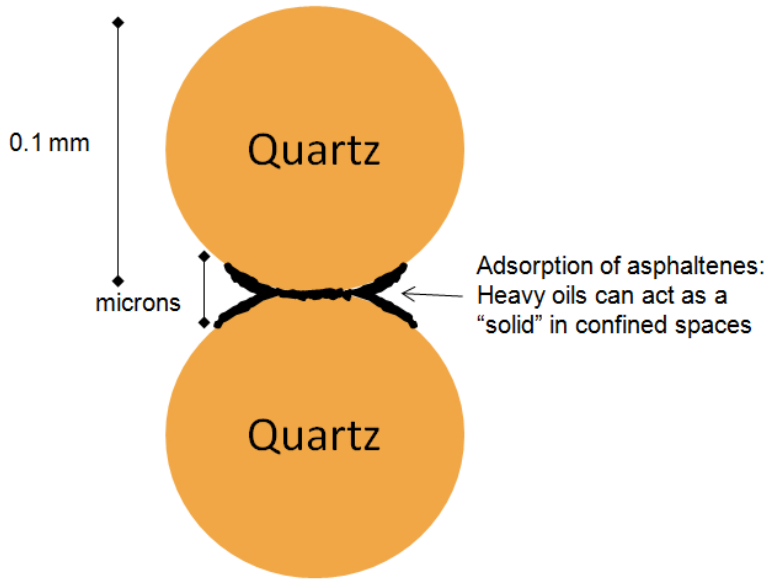

Figure 5.1. Schematic representation of heavy oils and asphaltenes in confined spaces.

REFERENCES

Abivin, P, Indo, K., Cheng, Y. Freed, D. & Taylor, S., 2011. Glass Transition and Heavy Oil Dynamics at Low Temperature. In World Heavy Oil Congress. Edmonton, Alberta.

Adrian, D.W. & Giacomin, A.J., 1992. The quasiperiodic nature of a polyurethane melt in oscillatory shear. *J. Rheol.*, 36(7), pp.1227–1243.

Alvarez, E., Marroquin, G., Trejo, F., Centeno, G. & Ancheyta, J., 2011. Pyrolysis kinetics of atmospheric residue and its SARA fractions. *Fuel*, 90, pp.3602–3607.

Barker, D.A. & Wilson, D.I., 2006. Temperature profiles in a controlled-stress parallel plate rheometer. *Rheol Acta*, 46, pp.23–31.

Barnes, H.A., 1995. A review of the slip (wall depletion) of polymer solutions, emulsions and particle suspensions in viscometers: its cause, character, and cure. *J. Non-Newtonian Fluid Mech.*, 56, pp.221–251.

Barre, L., Espinat, D., Rosenberg, E. & Scarsella, M., 1997. Colloidal Structure of Heavy Crudes and Asphaltenes Solutions. *Revue de L'institut Francais du Petrole*, 52(2), pp.161–175.

Batzle, M., Han, D.H. & Hofman, R., 2006a. Fluid mobility and frequency-dependent seismic velocity - direct measurements. *Geophysics*, 71(1), pp.N1–N9.

Batzle, M., Hofman, R. & Han, D.H., 2006b. Heavy oils - Seismic Properties. *The Leading Edge*, (June), pp.750–756.

Batzle, M., Zadler, B. & Hofman, R., 2004. Heavy Oils - Seismic Properties. In SEG Int. Exp. and 74th Annual Mtg. Denver, Colorado: SEG.

Behura, J., Batzle, M., Hofman, R. & Dorgan, J., 2007. Heavy oils: Their shear story. *Geophysics*, 72(5), pp.E175–E183.

Bergman, R., 2000. General susceptibility functions for relaxations in disordered systems. *J. Appl. Phys.*, 88(3), pp.1356–1365.

Bianco, E.M., Kaplan, S.T. & Schmitt, D.R., 2008. Seismic rock physics of steam injection in bituminous oil reservoirs. *The Leading Edge*, (September), pp.1132–1137.

Branco, V., Mansoori, G., De Almeida L., Parl, S. & Manafi, H., 2001. Asphaltene flocculation and collapse from petroleum fluids. *Journal of Petroleum Science and Engineering*, 32((2001)), pp.217–230.

Chou, H.T., Foda, M.A. & Hunt, J.R., 1993. Rheological Response of Cohesive Sediments to Oscillatory Forcing. *Coastal and Estuarine Studies*, 42, pp.126–147.

Chougnet, A., Audibert, A. & Moan, M., 2007. Linear and non-linear rheological behaviour of cement and silica suspensions. Effect of polymer addition. *Rheol Acta*, 46, pp.793–802.

Chow, R.S., Tse, D.L. & Takamura, K., 2004. The Conductivity and Dielectric Behavior of Solutions of Bitumen In Toluene. *The Canadian Journal of Chemical Engineering*, 82(August), pp.840–845.

Christenson, H.K. & Israelachvili, J., 1987. Direct Measurements of Interactions and Viscosity of Crude Oils in Thin Films between Model Clay Surfaces. *Journal of Colloid and Interface Science*, 119(1), pp.194–202.

Ciajolo, A. & Barbella, R., 1984. Pyrolysis and oxidation of heavy fuel oils and their fractions in a thermogravimetric apparatus. *Fuel*, 63(May), pp.657–661.

Ciz, R. & Shapiro, S.A., 2007. Generalization of Gassmann equations for porous media saturated with a solid material. *Geophysics*, 72(6), pp.A75–A79.

Cole, K. & Cole, R., 1941. Dispersion and Absorption in Dielectrics - I. Alternating Current Characteristics. *Journal of Chemical Physics*, 9, pp.341–351.

Costales, P., Tar: A Local Beach Tradition. *Edhat Santa Barbara*. Available at: http://www.edhat.com/site/tidbit.cfm?id=2603.

Cox, W.P. & Merz, E.H., 1958. Correlation of dynamic and steady flow viscosities. *J Polym Sci*, 28(118), pp.619–622.

Das, A., 2010. *The Viscoelastic Properties of Heavy-oil Saturated Rocks*. PhD dissertation. Denver, Colorado: Colorado School of Mines.

Dawe, R.A., 2000. *Modern Petroleum Technology*, Wiley & Sons Ltd. published on behalf of the Institute of Petroleum.

Dorgan, J. & Rorrer, N.A., 2013. Molecular Scale Simulation of HomopolymerWall Slip. *Physical Review Letters*, PRL 110(176001), pp.1–5.

Douda, J., Llanos, M., Alvarez, R., Lopez-Franco, C. & Montoya de la Fuente, J., 2004. Pyrolysis applied to the study of a Maya asphaltene. *J. Anal. Appl. Pyrolysis*, 71, pp.601–612.

Drew & Myers, 1999. *Surfaces, Interfaces, and Colloids* Second., United States of America: Wiley-VCH.

Eastwood, J., 1993. Temperature-dependent propagation of P and S waves in Cold Lake oil sands: Comparison of theory and experiment. *Geophysics*, 58(6), pp.863–872.

Espinat, D., Fenistein, D., Barre, L., Frot, D. & Briolant, Y., 2004. Effects of Temperature and Pressure on Asphaltenes Agglomeration in Toluene. A Light, X-ray, and Neutron Scattering Investigation. *Energy Fuels*, 18, pp.1243–1249.

Evdokimov, I.N. & Losev, A.P., 2010. Electrical Conductivity and Dielectric Properties of Solid Asphaltenes. *Energy Fuels*, 24, pp.3959–3969.

Fenistein, D. & Barre, L., 2001. Experimental measurement of the mass distribution of petroleum asphaltene aggregates using ultracentrifugation and small-angle X-ray scattering. *Fuel*, 80, pp.283–287.

Ferry, J.D., 1980. *Viscoelastic Properties of Polymers* Third., United States of America: John Wiley & Sons, Inc.

Friedrich, C. & Braun, H., 1992. Generalized Cole-Cole behavior and its rheological relevance. *Rheol Acta*, 31(4), pp.309–322.

Frolov, A.F., Vasileva, V. Frolova, E. & Ovchinnkova, V., 1983. Strength and Structure of Asphalt Films. *Yaroslavl' Polytechnic Institute (YaPI)*, 8, pp.35–37.

Goual, L. & Firoozabadi, A., 2002. Measuring Asphaltenes and Resins, and Dipole Moment in Petroleum Fluids. *AIChE Journal*, 48(11), pp.2646–2663.

Graham, M.D., 1995. Wall slip and the nonlinear dynamics of large amplitude oscillatory shear flows. *J. Rheol.*, 39(4), pp.697–712.

Gurevich, B., Osypov, K., Ciz, R & Makarynska, D., 2008. Modeling elastic wave velocities and attenuation in rocks saturated with heavy oil. *Geophysics*, 73(4), pp.E115–E122.

Hail Jr., W.J., 1957. Reconnaissance for Uranium in Asphalt-Bearing Rocks in the Western United States, Washington, DC: U.S. Atomic Energy Commision.

Hamilton, E.L., 1971. Elastic Properties of Marine Sediments. *J. Geophysical Research*, 76(2), pp.579–604.

Han, D.H., Liu, J. & Batzle, M., 2007. Shear velocity as the function of frequency in heavy oils. In SEG/San Antonio 2007 Annual Meeting. San Antonio, Texas: SEG, pp. 1716–1719.

Hasan, A., 2010. *Rheological Behavior and Nano-Microstructure of Complex Fluids: Biomedical and Bitumen-Heavy Oil Applications*. PhD Dissertation. Department of Mechanical Engineering, Edmonton, Alberta: University of Alberta.

Havriliak, S. & Negami, S., 1967. A Complex Plane Representation of Dielectric and Mechanical Relaxation Processes in Some Polymers. *Polymer*, 8, pp.161–210.

Heymann, L., Peukert, S. & Aksel, N., 2002. Investigation of the solid–liquid transition of highly concentrated suspensions in oscillatory amplitude sweeps. *J. Rheol.*, 46(1), pp.93–112.

Hiemenz, P.C. & Rajagopalan, R., 1997. *Principles of Colloid and Surface Chemistry* Third., United States of America: Marcel Dekker, Inc.

Hinkle, A., Shin, E., Liberatore, M., Herring, A. and Batzle, M., 2008. Correlating the chemical and physical properties of a set of heavy oils from around the world. *Fuel*, 87((2008)), pp.3065–3070.

Horsfield, B., Dembicki Jr., H. & Ho, T.T.Y., 1983. Some potential applications of pyrolysis to basin studies. *J. Geol. Soc. London*, 140, pp.431–443.

Hu, H.W., Carson, G.A. & Granick, S., 1991. Relaxation Time of Confined Liquids under Shear. *Physical Review Letters*, 66(21), pp.2758–2761.

Huang, S.C.. Branthaver, J., Robertson, R & Kim, S., 1998. Effect of Film Thickness on the Rheological Properties of Asphalts in Contact with Aggregate Surface. *Transportation Research Record*, 1638, pp.31–39.

Hyun, K., Kim, S., Ahn, K. & Lee, S., 2002. Large amplitude oscillatory shear as a way to classify the complex fluids. *J. Non-Newtonian Fluid Mech.*, 107, pp.51–65.

Jenkins, S.D., Waite, M.W. & Bee, M.F., 1997. Time-lapse monitoring of the Duri steamflood: A pilot and case study. *The Leading Edge*, (September).

Johnston, M., 2009. *Temperature and Frequency Dependence of Viscoelasticity in Bitumen*. Master of Science. Golden, Colorado: Colorado School of Mines.

Kato, A., Onozuka, S. & Nakayama, T., 2008. Elastic property changes in a bitumen reservoir during steam injection. *The Leading Edge*, (September), pp.1124–1131.

Kayser, R.B., 1966. *Bituminous Sandstone Deposits Asphalt Ridge*, Utah Geo. & Min. Survey.

Ke, G., Dong, H. & Johnston, M., 2010. Rock physics modeling of the frequency dispersion in bitumen saturated sands. In SEG. Denver, Colorado, pp. 2552–2556.

Kendall, R., 2009. Using Timelapse Seismic to Monitor the THAI Heavy Oil Production Process. In Houston, Texas: SEG, pp. 3954–3958.

Kendall, R. & Wikel, K., 2011. Multicomponent time-lapse monitoring of bitumen recovery and geomechanical implications. In San Antonio, Texas: SEG, pp. 4087–4091.

Kok, M., Karacan, O. & Pamir, R., 1998. Kinetic Analysis of Oxidation Behavior of Crude Oil SARA Constituents. *Energy Fuels*, 12(3), pp.580–588.

Lakes, R.S., 2009. *Viscoelastic Materials*, Cambridge University Press.

Lan, S.K., Giacomin, A.J. & Ding, F., 2000. Dynamic Slip and Nonlinear Viscoelasticity. *Polymer Eng. adn Sci.*, 40(2), pp.507–524.

Langevin, D., Poteau, S., Henaut, I. & Argillier, J., 2004. Crude Oil Emulsion Properties and their Application to Heavy Oil Transportation. *Oil & Gas Science and Technology – Rev. IFP*, 59(5), pp.511–521.

Larter, S., Huang, H., Adams, J., Bennet, B., Jokanola, O., Oldenburg, T. et. al., 2006. The controls on the composition of biodegraded oils in the deep subsurface: Part II— Geological controls on subsurface biodegradation fluxes and constraints on reservoir-fluid property prediction. *AAPG Bulletin*, 90(6), pp.921–938.

Larter, S, Adams, J., Gates, I. Bennet, B. & Huang, H., 2008. The Origin, Prediction and Impact of Oil Viscosity Heterogeneity on the Production Characteristics of Tar Sand and Heavy Oil Reservoirs. *JCPT*, 47(1), pp.52–61.

Li, S.P., Zhao, G. & Chen, H.Y., 2005. The Relationship between Steady Shear Viscosity and Complex Viscosity. *J. Dispersion Sci. Tech.*, 26, pp.415–419.

Li, X., Fang, Y., Al-Assaf, S., Phillips, G., Nishinari, K. & Zhang, H., 2009. Rheological study of gum arabic solutions: Interpretation based on molecular self-association. *Food Hydrocolloids*, 23, pp.2394–2402.

Luengo, G., Schmitt, F., Hill, R. & Israelachvili, J., 1997. Thin Film Rheology and Tribology of Confined Polymer Melts: Contrasts with Bulk Properties. *Macromolecules*, 30, pp.2482–2494.

Mack, C., 1957. Physical Properties of Asphalts in Thin Films. *Ind. Eng. Chem. Res.*, 49(3), pp.422–427.

Majidzadeh, K. & Herrin, M., 1965. Modes of Failure and Strenght of Asphalt Films Subjected to Tensile Stress. *Highway Research Record*, 67, pp.98–121.

Makarynska, D., Gurevich, B., Behura, J. & Batzle, M., 2010. Fluid substitution in rocks saturated with viscoelastic fluids. *Geophysics*, 75(2), pp.E115–E122.

Matsuoka, S., 1992. *Relaxation Phenomena in Polymers*, Munich, Vienna, New York, Barcelona: Hanser.

Matsuoka, S. & Hale, A., 1997. Cooperative Relaxation Processes in Polymers. *J. Appl. Polym. Sci.*, 64, pp.77–93.

Moschopedis, S.E. & Speight, J.G., 1976. Investigation of hydrogen bonding by oxygen functions in Athabasca bitumen. *Fuel*, 55(July), pp.187–192.

Murugan, P. et al., 2009. Pyrolysis and combustion kinetics of Fosterton oil using thermogravimetric analysis. *Fuel*, 88, pp.1708–1713.

Nielsen, B.B., Svrcek, W.Y. & Mehrotra, A.K., 1994. Effects of Temperature and Pressure on Asphaltene Particle Size Distributions in Crude Oils Diluted with n-Pentane. *Ind. Eng. Chem. Res.*, 33(5), pp.1324–1330.

Pacheco-Sanchez, J.H., Zaragoza, I.P. & Martinez-Magadan, J.M., 2003. Asphaltene Aggregation under Vacuum at Different Temperatures by Molecular Dynamics. *Energy Fuels*, 17(5), pp.1346–1355.

Peramanu, S., Pruden, B. & Rahimi, P., 1999. Molecular Weight and Specific Gravity Distributions for Athabasca and Cold Lake Bitumens and Their Saturate, Aromatic, Resin, and Asphaltene Fractions. *Ind. Eng. Chem. Res.*, 38(8), pp.3121–3130.

Petersen, J., Roberston, R., Branthaver, J., Harnsberger, P., Duvall, J., Kim, S., et. al., 1994. *Binder Characterization and Evaluation, Volume 4: Test Methods*, Washington, DC: National Research Council.

Pritz, L., 1999. Verification of Local Kramers-Kronig relations for Complex Modulus by Means of Fractional Derivative Model. *J. Sound and Vibration,* 228 (5) 1145-1165.

Putz, A. & Burghelea, T., 2009 "The solid-liquid transition in a yield stress shear thinning physical gel"., *Rheol Acta* 48, pp. 673-689

Qiu, J., van de Ven, M., Wu, S., Yu, J. & Molenar, A., 2011. Investigating self healing behaviour of pure bitumen using Dynamic Shear Rheometer. *Fuel*, 90, pp.2710–2720.

Ramachandran, V.S. & Beaudoin, J.J., 2000. *Handbook of analytical techniques in Concrete Science and Technology*, United States of America: Elsevier Science Ltd.

Ritchie, G.S., Roche, R.S. & Steedman, W., 1979. Pyrolysis of Athabasca tar sands: analysis of the condensible products from asphaltene. *Fuel*, 58(July), pp.523–530.

Rodrigues, P. & Batzle, M., 2013. Shear modulus of heavy oils: Measuring at Low Frequencies. In Houston, Texas: SEG.

Rojas, M.A., 2010. *Viscoelastic Properties of Heavy Oils*. Doctor of Philosophy. Houston, Texas, USA: University of Houston.

Sheu, E.Y. & Acevedo, S., 2001. Effect of Pressure and Temperature on Colloidal Structure of Furrial Crude Oil. *Energy Fuels*, 15(3), pp.702–707.

Da Silva, A., haraguchi, L., Notrispe, F., Loh, W. & Mohamed, R., 2001. Interfacial and colloidal behavior of asphaltenes obtained from Brazilian crude oils. *Journal of Petroleum Science and Engineering*, 32, pp.201–216.

Spencer, J.W., 1979. Bulk and Shear Attenuation in Berea Sandstone: The Effects of Pore Fluids. *J. Geophysical Research*, 84(B13), pp.7521–7523.

Sumita, I. & Manga, M., 2008. Suspension rheology under oscillatory shear and its geophysical implications. *Earth and Planetary Science Letters*, 269, pp.468–477.

Tendel, R., LaBrecque, D., Schutt, H., McCormick, D., Godfrey, R., Rivero, J., et al., 2011. Reservoir monitoring in oil sands: Developing a permanent cross-well system. In San Antonio, Texas: SEG.

Twardos, M. & Dennin, M., 2003. Comparison of Steady-State Shear Viscosity and Complex Shear Modulus in Langmuir Monolayers. *Langmuir*, 19, pp.3542–3544.

Urbanovici, E., Popescu, C. & Segal, E., 1999. Improved Iterative Version of the Coats-Redfern Method to Evaluate Non-isothermal Kinetic Parameters. *J. Therm. Anal. Calorim.*, 58, pp.683–700.

Vasquez, D. & Mansoori, G.A., 2000. Identification and measurement of petroleum precipitates. *Journal of Petroleum Science and Engineering*, 26, pp.49–55.

Witten, T.A. & Pincus, P., 2004. *Structured fluids: polymers, colloids, surfactants*, Great Britain: Oxford.

Wolf, K., Vanorio, T. & Mavko, G., 2008. Measuring and monitoring heavy-oil reservoir properties. *The Leading Edge*, (September), pp.1138–1147.

Wu, W., Saidian, M. gaur, S. & Prasad, M., 2012. Errors and Repeatibiliy in VSARA Analysis of Heavy Oils. In SPE Heavy Oil Conference. Calgary, Canada: SPE.

Yoshimura, A. & Prud'homme, R.K., 1988. Wall Slip Corrections for Couette and Parallel Disk Viscometers. *J. Rheol.*, 32(1), pp.53–67.

Zhai, H., Bahia, H. & Erickson, S., 2000. Effect of Film Thickness on Rheological Behavior of Asphalt Binders. *Transportation Research Record*, 1728(Paper No. 00-1373), pp.7–14.

APPENDIX A. ADDITIONAL RHEOMETER RESULTS

In this appendix, I show additional rheometer results for the three samples tested which are described in appendix C. Among the results reported here are frequency sweeps and strains weeps. All results are at the testing temperature unless otherwise stated.

GP029-Asphalt Ridge

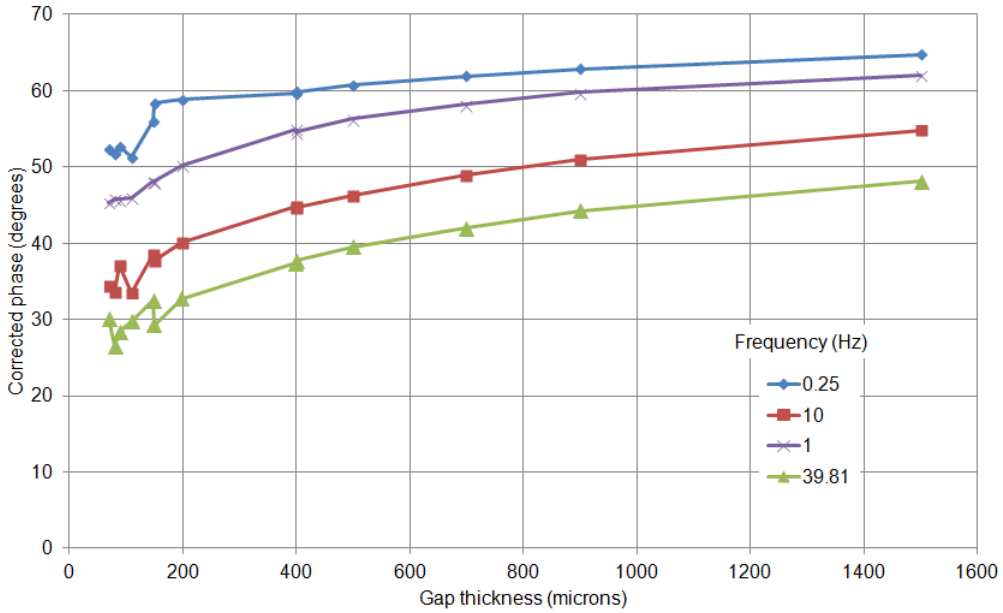

Figure A.1. Corrected phase versus gap for GP029-Asphalt Ridge sample. Phase decreases when reducing the gap and indicative of solidification of the sample.

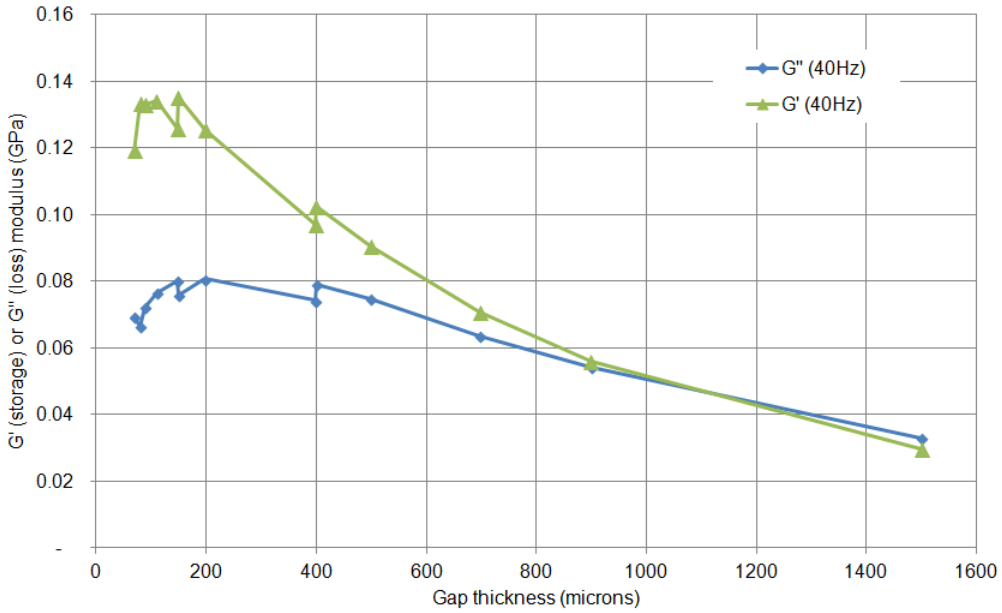

Figure A.2. Storage (G') and loss (G") modulus for the GP029-Asphalt Ridge sample at 40 Hz for varying gaps. At this frequency the sample behaves almost solid-like for all gaps until passing 1100 microns when the loss modulus is greater than the storage modulus.

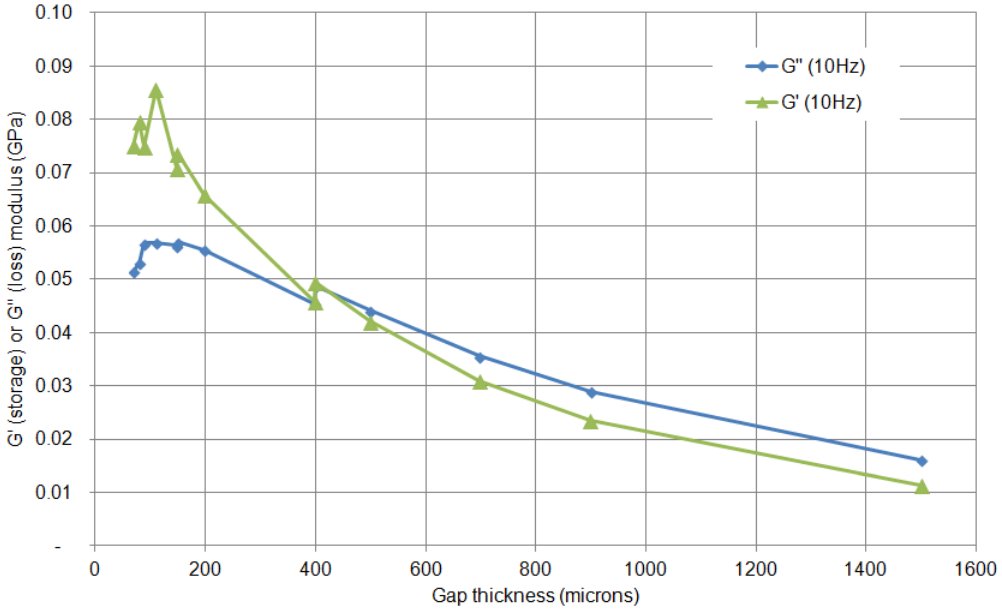

Figure A.3. Storage (G') and loss (G") modulus for the GP029-Asphalt Ridge sample at 10 Hz for varying gaps. Sample behaves solid-like at gaps values below 400 microns.

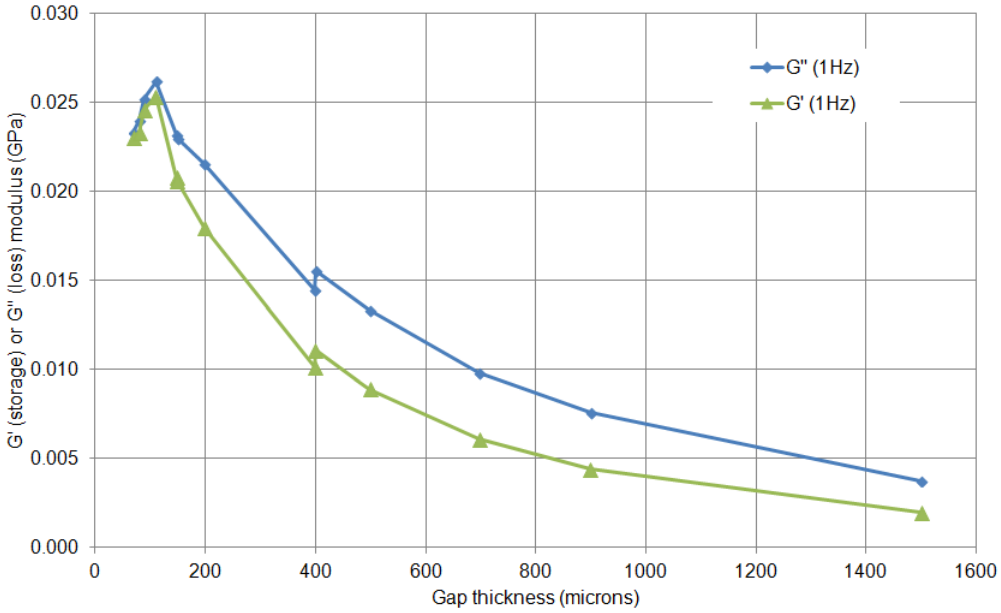

Figure A.4. Storage (G') and loss (G") modulus for the GP029-Asphalt Ridge sample at 1 Hz for varying gaps. Sample behaves liquid-like for all gaps values.

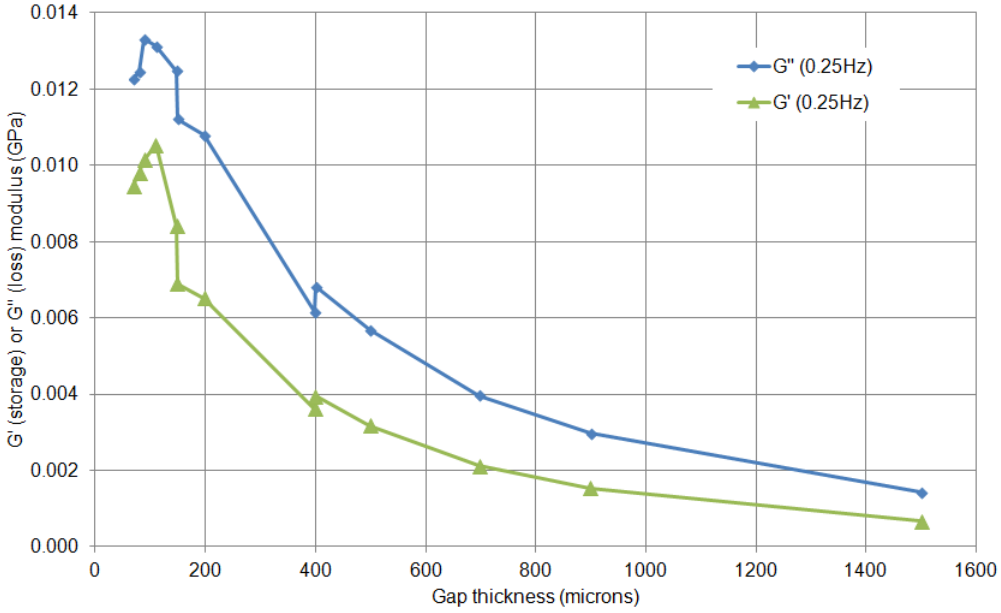

Figure A.5. Storage (G') and loss (G") modulus for the GP029-Asphalt Ridge sample at 0.25 Hz for varying gaps. Sample behaves liquid-like for all gaps values.

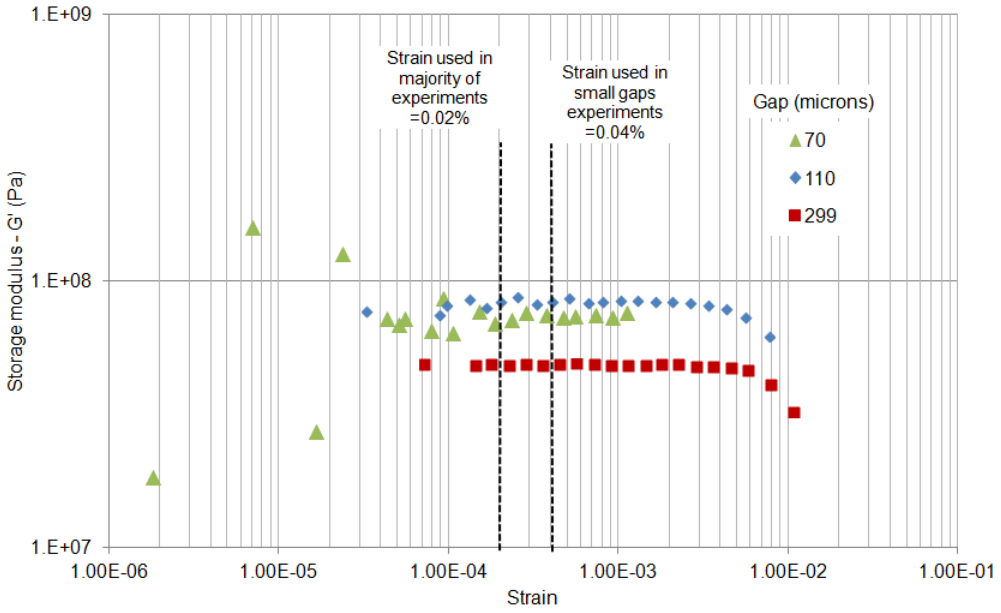

Figure A.6. Storage modulus (G') versus strain for sample GP029-Asphalt Ridge at 10 Hz and three different gaps. The figure shows the strain used during the experiments to ensure testing within the LVR. At large strains we can see the end of the LVR.

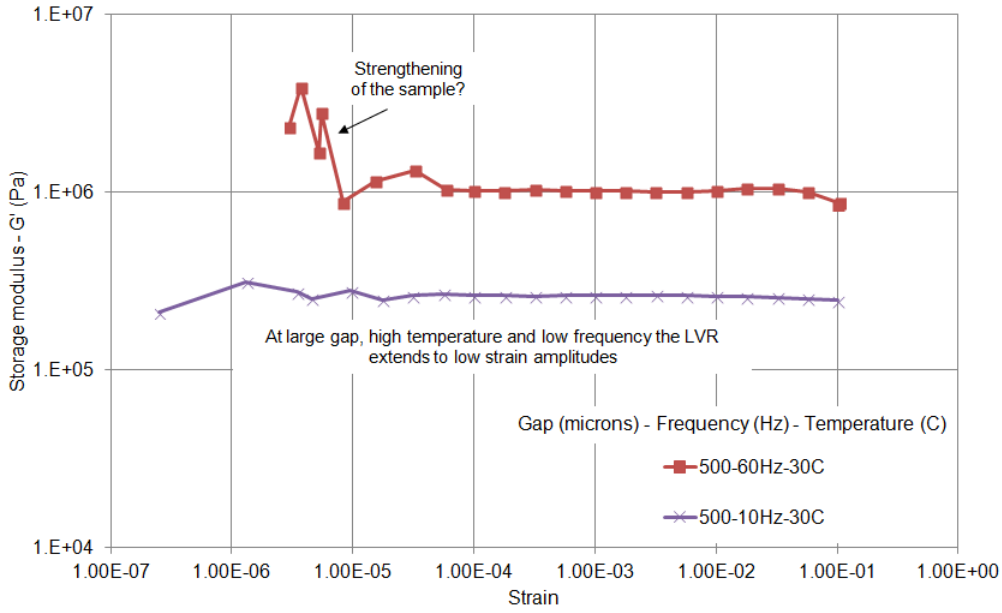

Figure A.7. Storage modulus (G') versus strain for sample GP029-Asphalt Ridge at 10 and 60 Hz, 30 degrees C and 500 microns gap. The figure shows how the LVR can extend to low strain amplitudes at higher temperatures. Also indicated with an arrow an increase of the G' at low gap values could be indicative of strengthening of the sample as presented in section 4.3.

GP010-Goleta: All GP010-Goleta tests were performed at 40C unless stated differently.

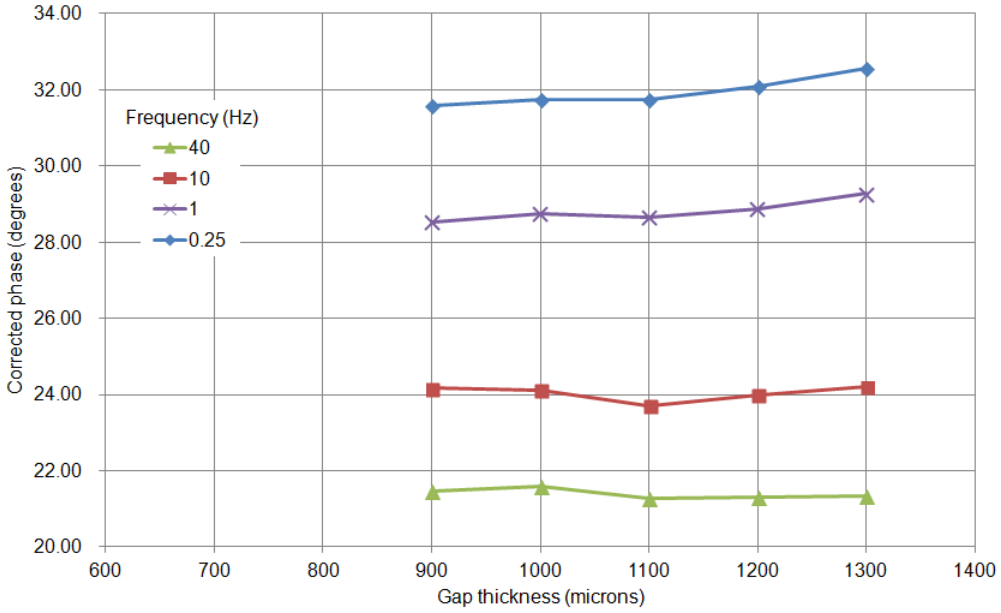

Figure A.8. Corrected phase versus gap thickness for the GP010-Goleta sample. Changes in phase for this sample were very subtle, but a reduction of phase (or solidification) can be seen when reducing gap, followed by an increase due to slip.

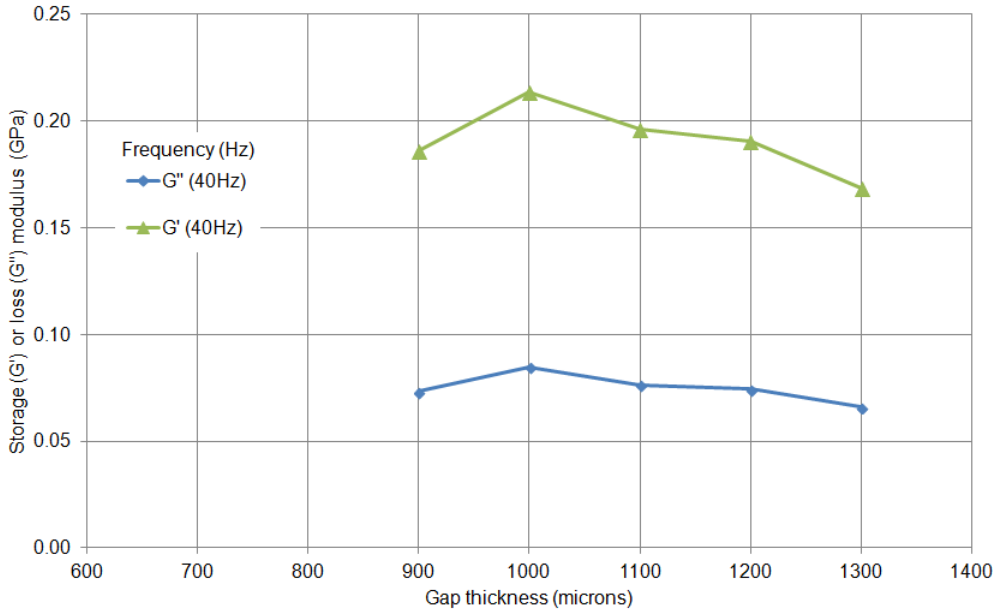

Figure A.9. Storage (G') and loss (G") modulus versus gap thickness for GP010-Goleta sample at 40 Hz. The sample behaves solid-like at all gap thicknesses tested.

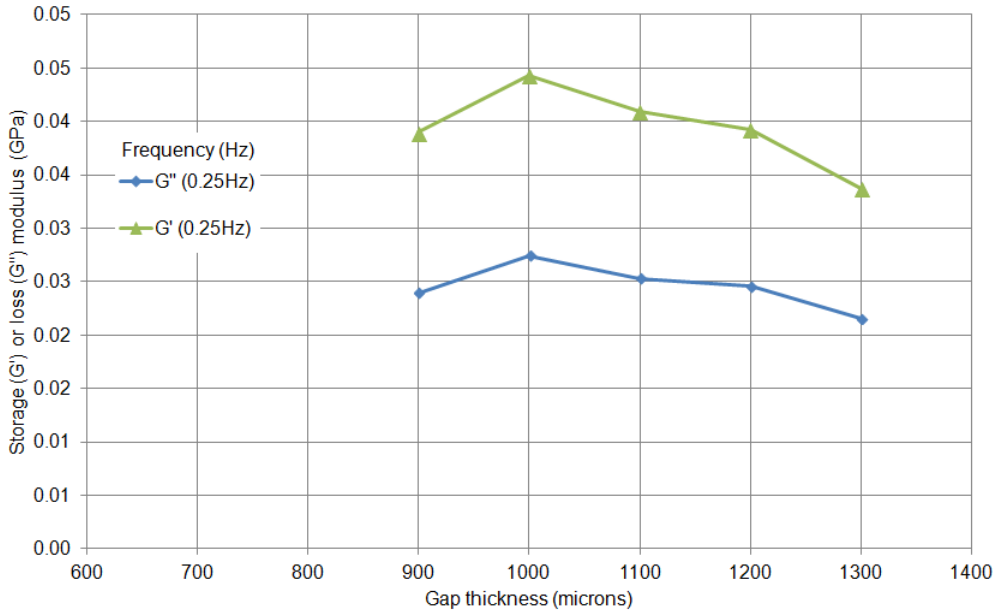

Figure A.10. Storage (G') and loss (G") modulus versus gap thickness for GP010-Goleta sample at 0.25 Hz. The sample behaves solid-like at all gap thicknesses tested even at low frequencies.

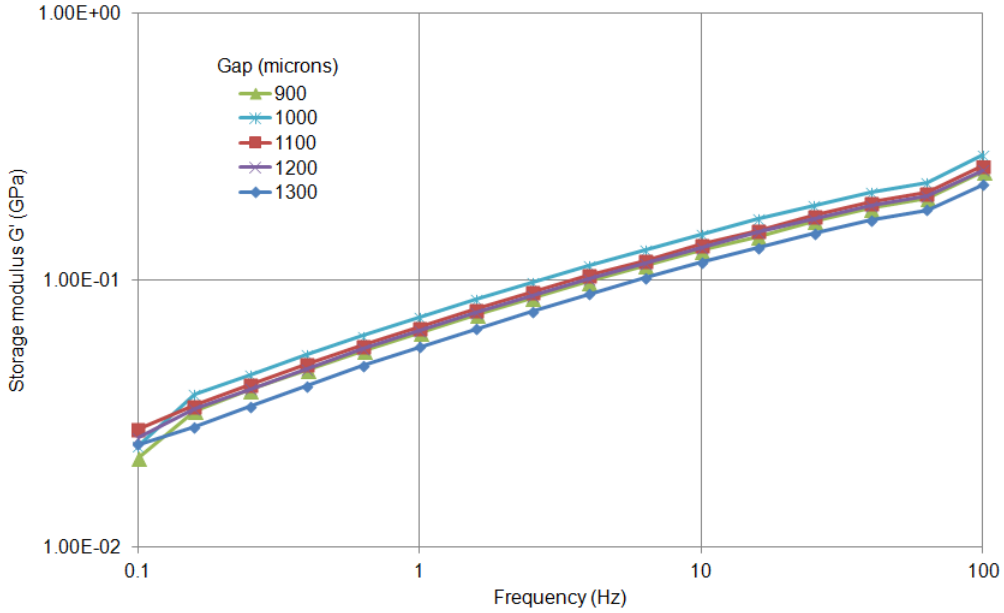

Figure A.11. Storage modulus (G') versus frequency for five gap thicknesses for GP010-Goleta sample, no slip effects are evident in this sample at high frequencies.

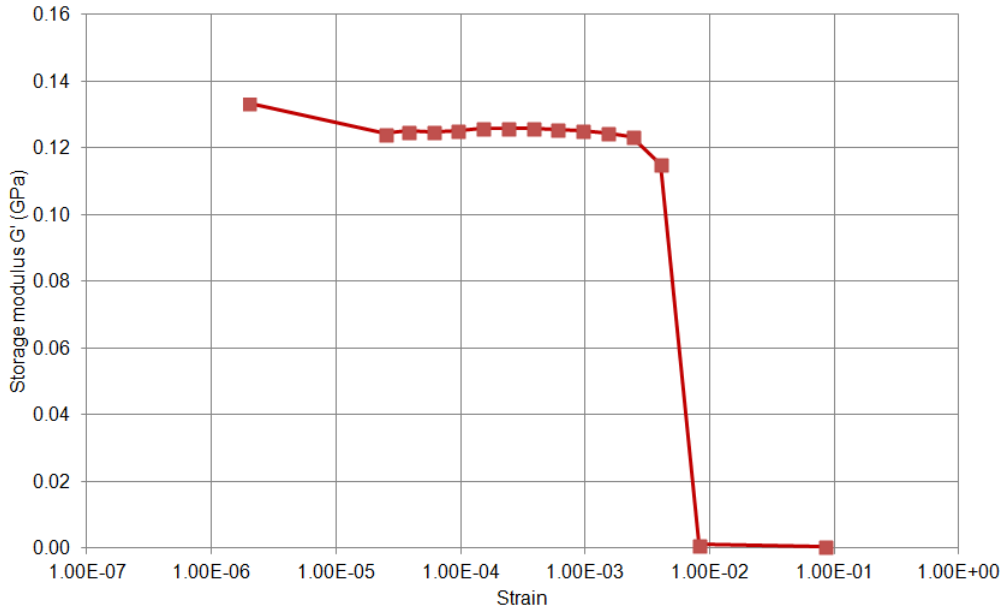

Figure A.12. Storage modulus (G') versus strain at 10 Hz and 1200 microns gap for GP010-Goleta sample showing the LVR and the sharp reduction in modulus when reaching the critical strain. Tests were performed at 2.10^{-4} strain amplitude.

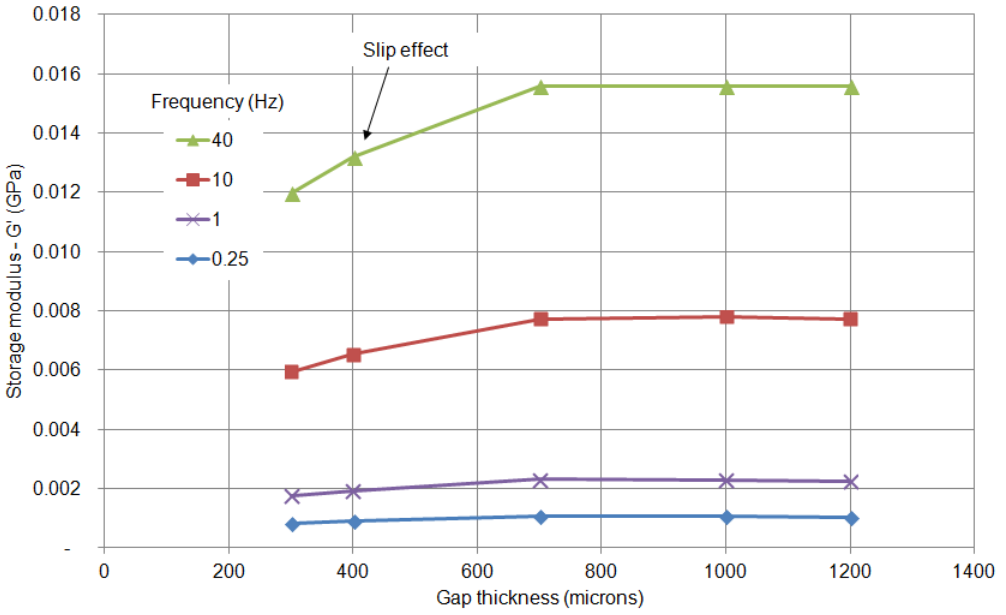

Figure A.13. Storage modulus (G') versus gap thickness at four frequencies and 70 C for GP010-Goleta sample. At higher temperatures the sample does not show any increase of modulus with gap on the contrary the effects of slip appear directly after a constant value.

GP007-Uvalde: All GP007-Uvalde tests were performed at 30C unless stated differently.

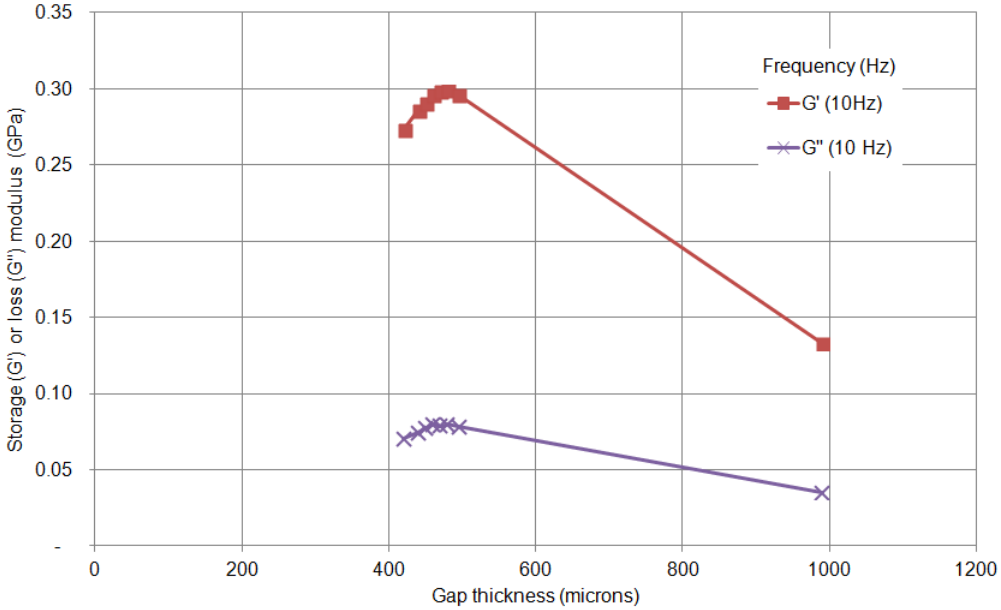

Figure A.14. Storage (G') and loss (G") modulus versus gap thickness for GP007-Uvalde at 10 Hz. The sample behave solid-like at all gap thicknesses.

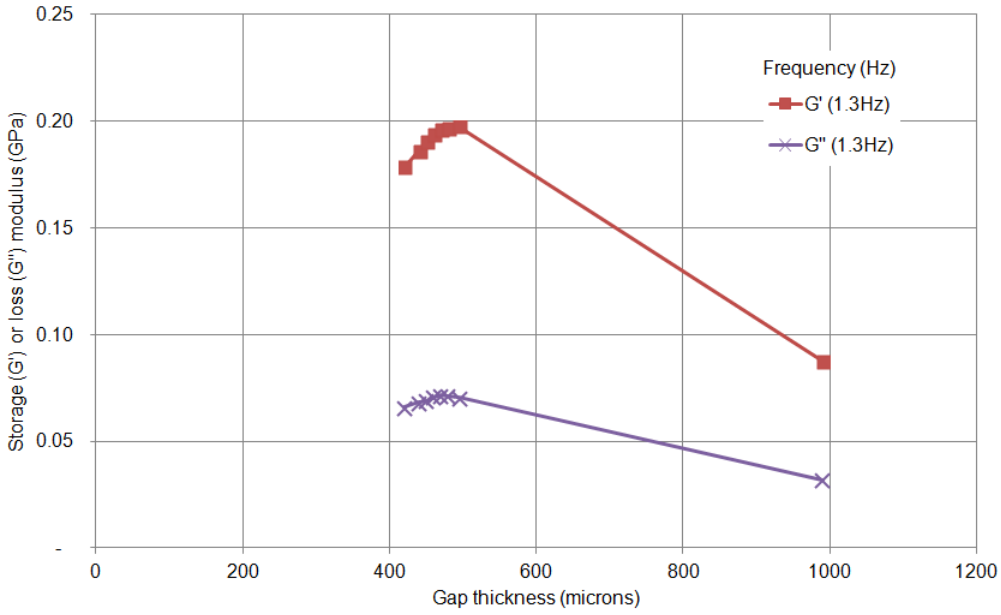

Figure A.15. Storage (G') and loss (G") modulus versus gap thickness for GP007-Uvalde. The sample behaves solid-like at all gap thicknesses tested.

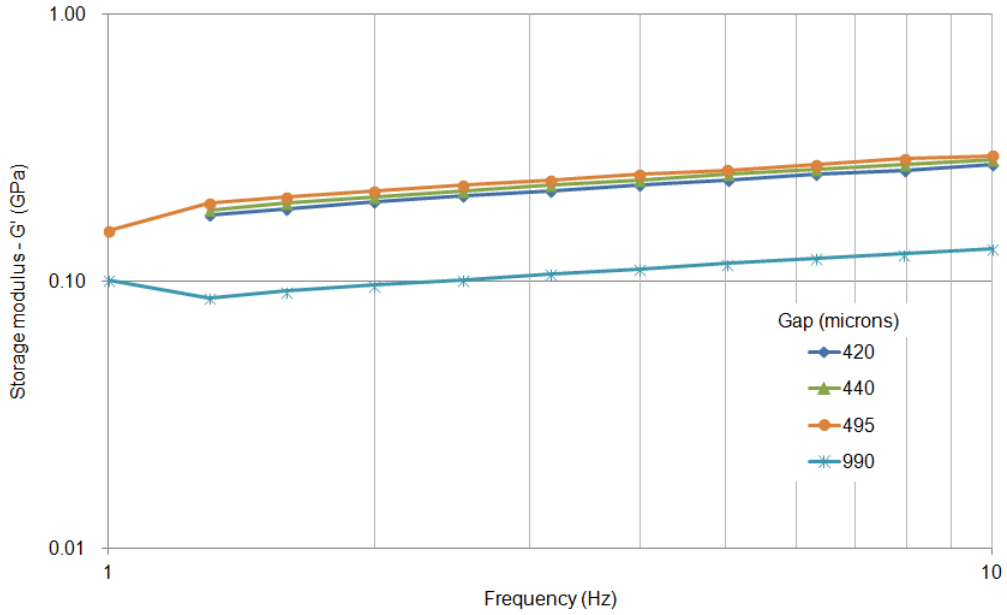

Figure A.16. Storage modulus (G') versus frequency for sample GP007-Uvalde at four gap thicknesses. No effects of slip are evident in this sample at high frequencies (sample was tested up to 10 Hz only)

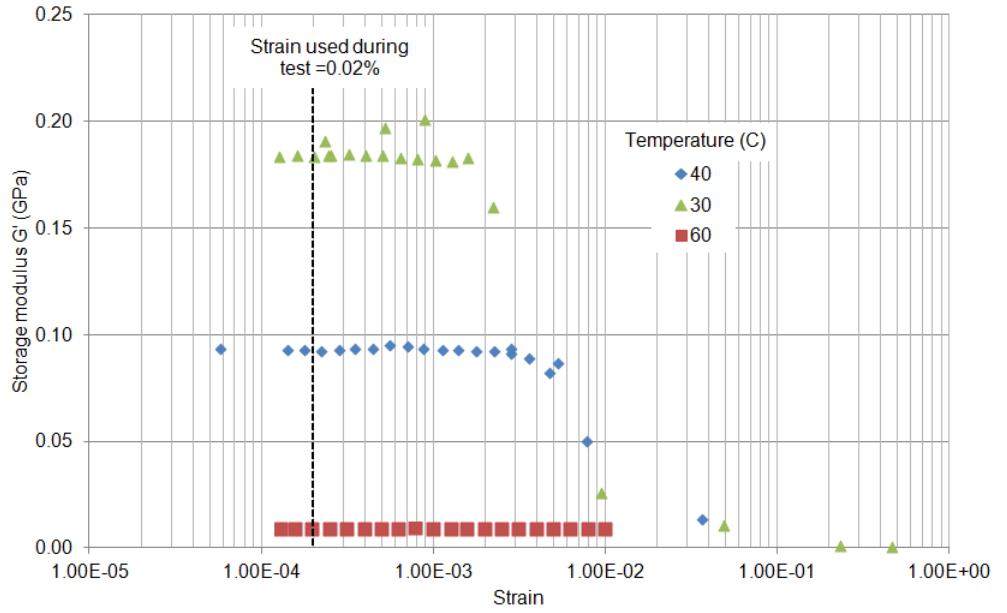

Figure A.17. Storage modulus (G') versus strain for sample GP007-Uvalde at 1Hz and three different temperatures. As expected, the critical strain is reached at lower values of strain when reducing the temperature.

APPENDIX B. ADDITIONAL ULTRASONIC AND TENSION/COMPRESSION RESULTS FOR SAMPLE GP029-ASPHALT RIDGE

Ultrasonic Measurements: Figure B.1 and Figure B.2 show the ultrasonic P-wave and S-wave results for the GP029-Aspahlt Ridge sample. A good linear correlation is obtained versus temperature with an error of less than 2 percent. Values from these correlations were used to calculate the shear modulus at -6.5C used in figures of the results chapter.

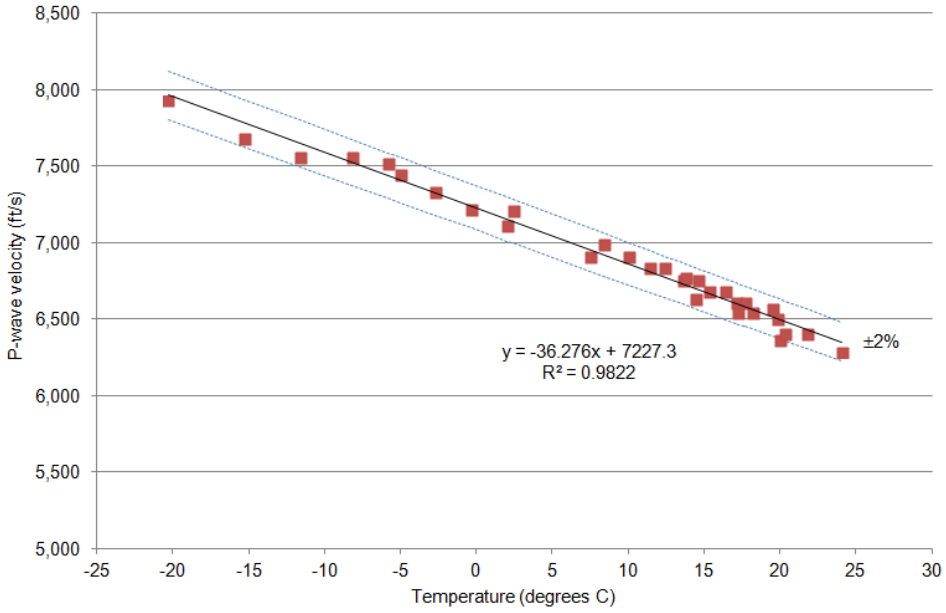

Figure B.1. Ultrasonic P-waves velocities at a temperature range between -20 and 25 degrees C. Test were conducted in three different days with two different samples with an error of less than 2 percent.

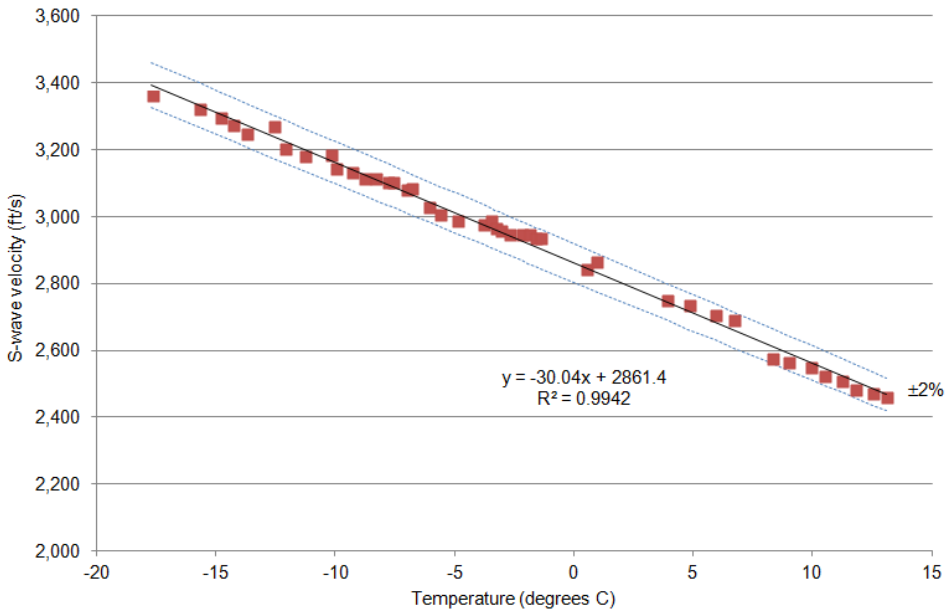

Figure B.2. Ultrasonic S-waves velocities at a temperature range between -18 and 14 degrees C. Tests were conducted in two different days with two different samples with an error of less than 2 percent.

Tension Compression (outside gages-1" sample diameter): The following results are for the sample with 1" diameter and outside gages, corresponding to Figure 4.28 and Figure 4.30. The next figure shows the strain values for the different gages.

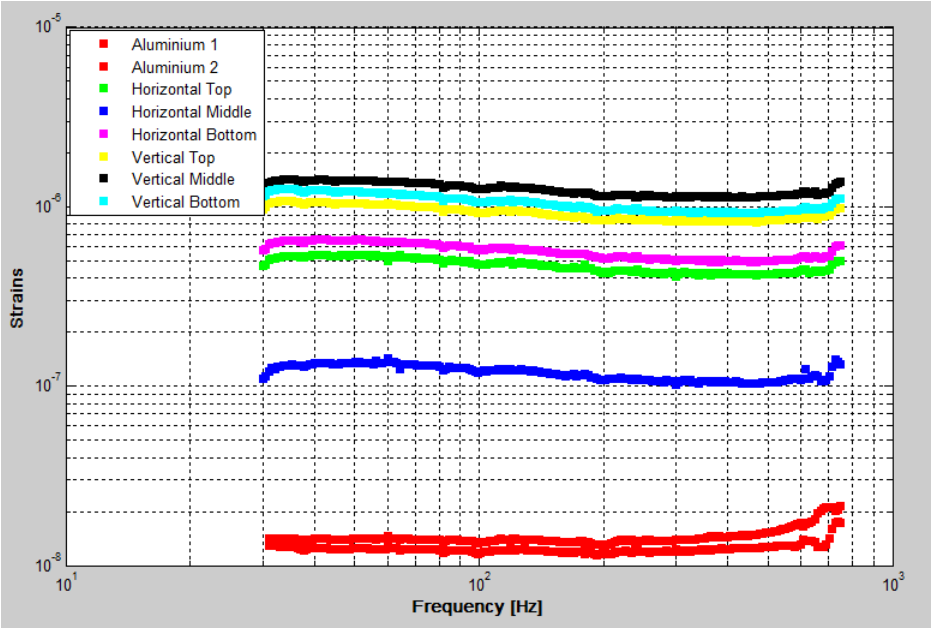

Figure B.3. Strain amplitudes for eight gages. Two semi-conductor gages in the aluminum standard, three vertical gages and three horizontal gages placed at the top, middle and bottom of the sample. Bottom corresponds to the location of the shaker.

Phase lag measurements are shown in the next figures (B.4, B.5 and B.6), even though phase measurements have significant noise, it can be seen that values are below 20 degrees which indicate a solid-like behavior. Noise peaks are more pronounced around the frequencies multiple of 60 Hz (60, 120, etc), with a pronounce peak at the resonance frequency of the equipment round 800 Hz.

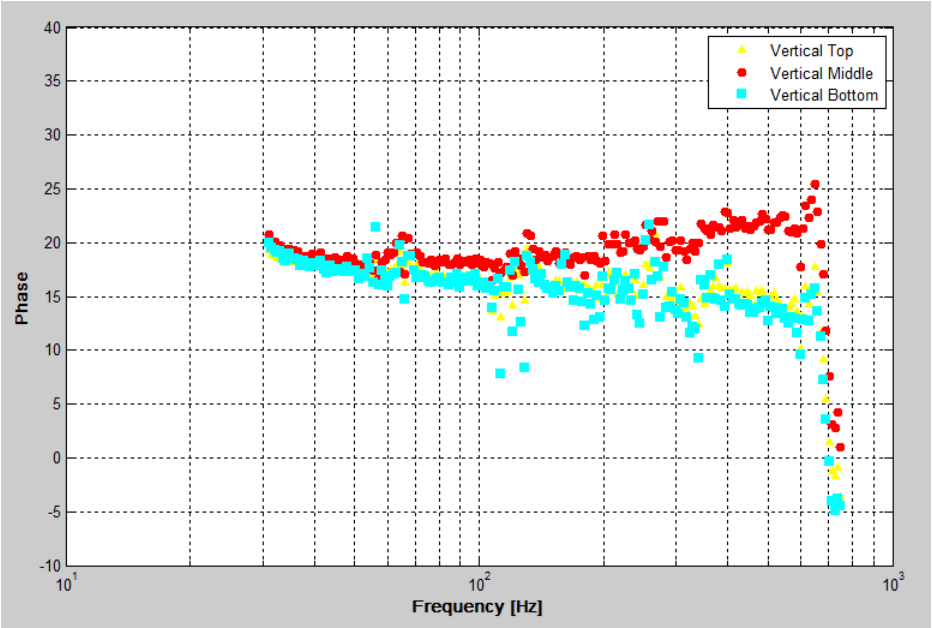

Figure B.4. Phase measurements for the three vertical gages (top, middle and bottom), with respect to the aluminum standard of the 1"diameter sample with outside gages. Phase values are in the range from 15 to 20 degrees corresponding to a solid-like behavior of the sample.

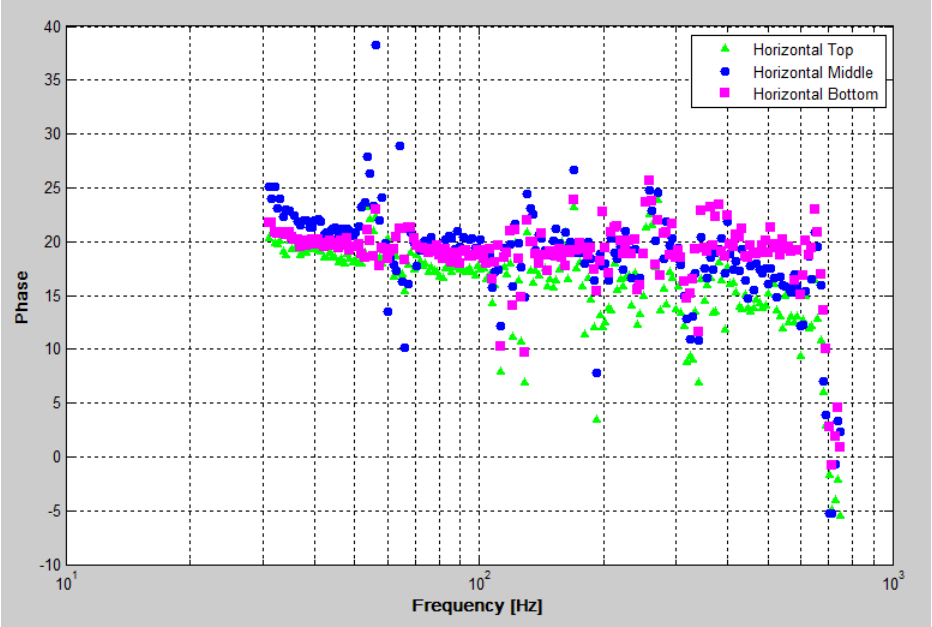

Figure B.5. Phase measurements for the three horizontal gages for the 1" diameter sample with outside gages (top, middle and bottom), with respect to the aluminum standard.

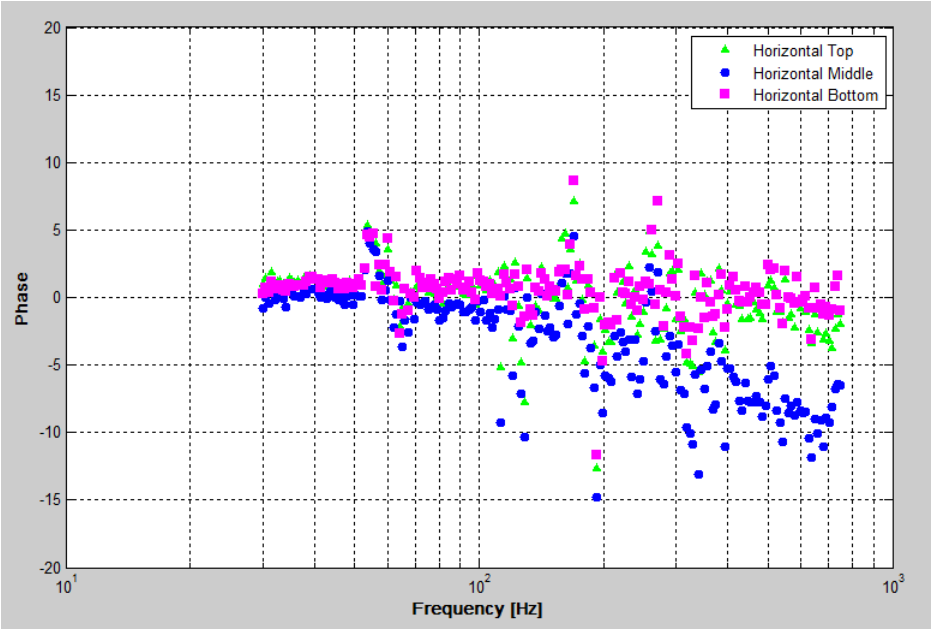

Figure B.6. Phase measurements for the three horizontal gages (top, middle and bottom), with respect to the corresponding vertical gages (Poisson's attenuation). The top and bottom gages show a small phase lag with respect to the verticals (close to 0 degrees), while the middle gage diverges from the zero phase lag at high frequencies. When comparing to figures B.5. and B.6. deviation is due to the behavior of the vertical gage.

Figure B.7 shows the Young's modulus for the three pair of gages in the sample (top, middle and bottom). The average of the three gages is the value used in the results section. Averaging the three gages helps to eliminate the effects of the sample geometry.

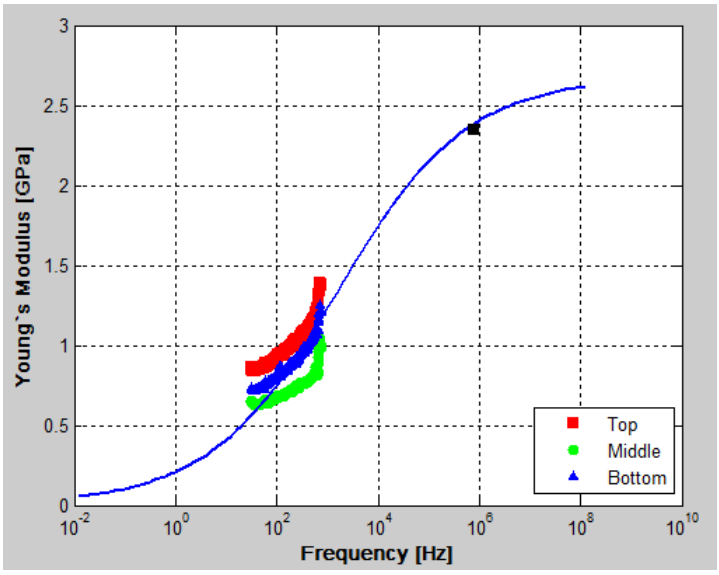

Figure B.7. Real part of the Young's modulus for the three gages (top, middle and bottom) for the 1" diameter sample with outside gages compared to ultrasonic results. Cole-Cole dispersion model fit is shown as reference.

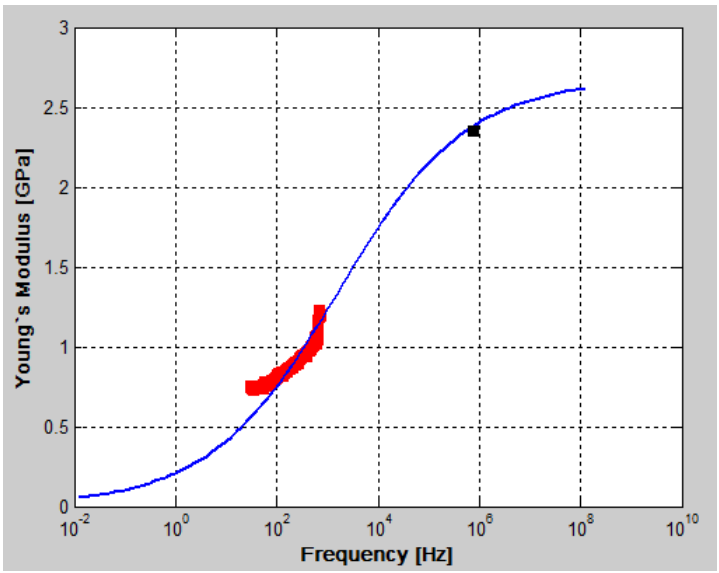

Figure B.8. Average of the real part of the Young's modulus from Figure B.7. compared to ultrasonic results. Cole-Cole dispersion model fit is shown as reference

Tension/Compression (inside gages-2" sample diameter): The following results are for the sample with 2" diameter and inside gages, corresponding to Figure 4.29. The following figure shows results of three combined runs with overlapping frequencies.

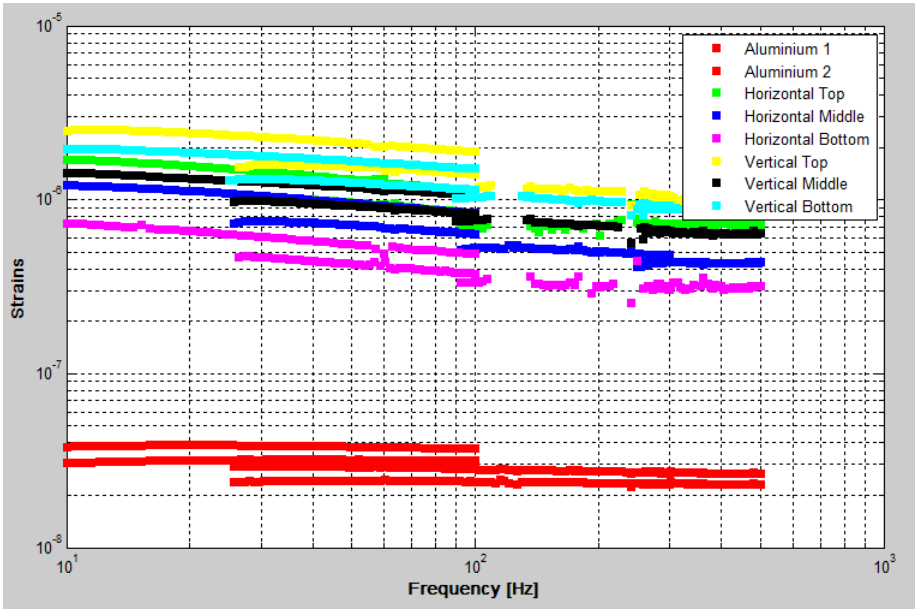

Figure B.9. Strain amplitudes for eight gages, two semi-conductor gages in the aluminum standards, three vertical and three horizontal located at the top, middle and bottom of the sample. Bottom corresponds to the location of the shaker.

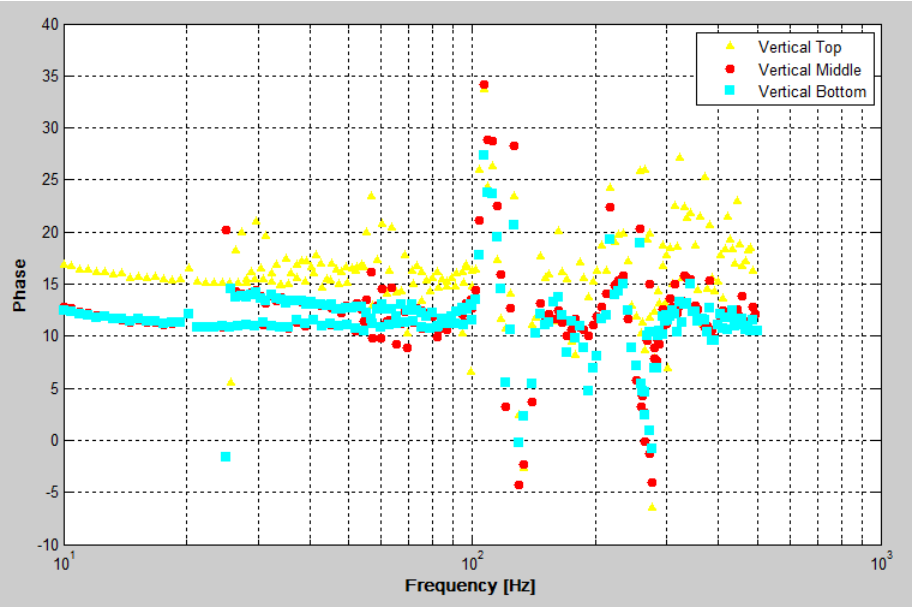

Figure B.10. Phase measurements for the three vertical gages (top, middle and bottom), with respect to the aluminum standard of the 2"diameter sample with inside gages. Phase values are in the range of 10 to 15 degrees corresponding to a solid-like behavior of the sample.

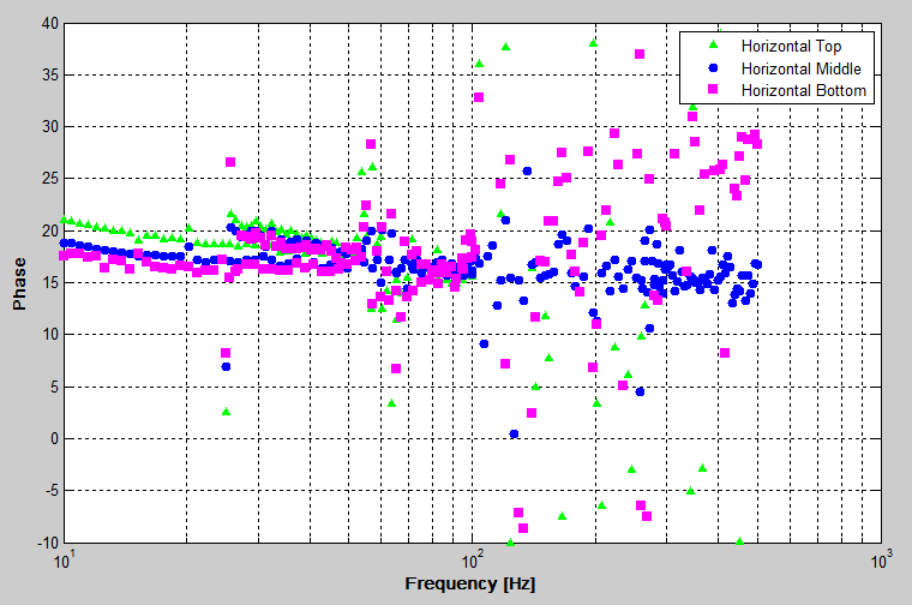

Figure B.11. Phase measurements for the three horizontal gages for the 1" diameter sample with outside gages (top, middle and bottom), with respect to the aluminum standard. Bottom gages had large noise for frequencies above 100 Hz.

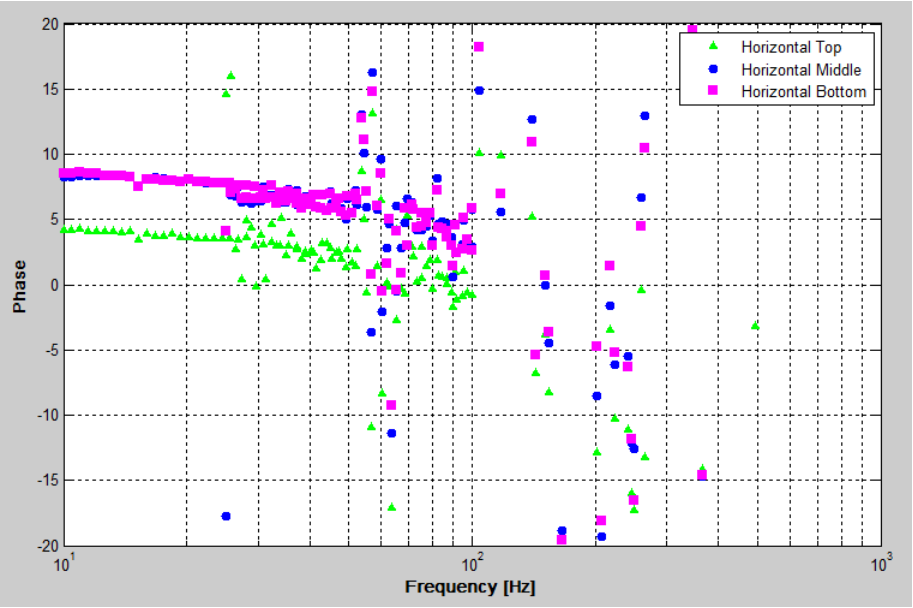

Figure B.12. Phase measurements for the three horizontal gages (top, middle and bottom), with respect to the corresponding vertical gages (Poisson's attenuation). Phase lags are in the range of 5 to 10 degrees, with significant noise above 100 Hz.

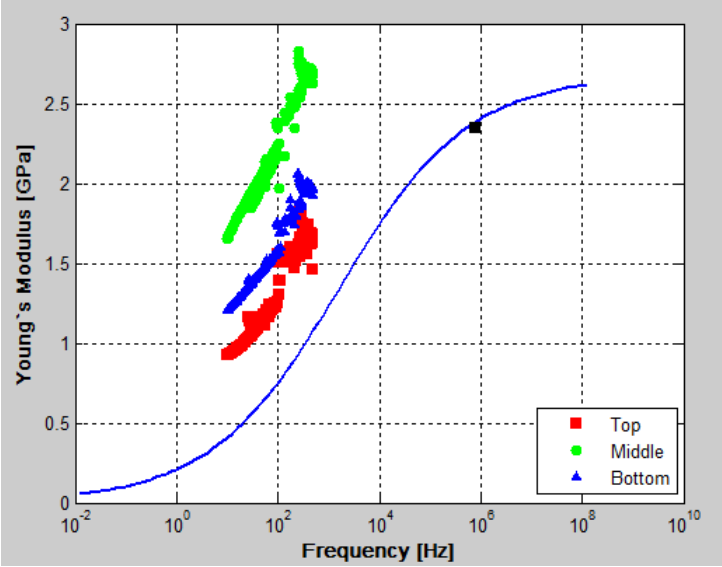

Figure B.13. Real part of the Young's modulus for the three gages (top, middle and bottom) from the 2" sample with inside gages compared to ultrasonic results. Cole-Cole dispersion model fit used in Figure B.7 and Figure B.8. is shown as reference.

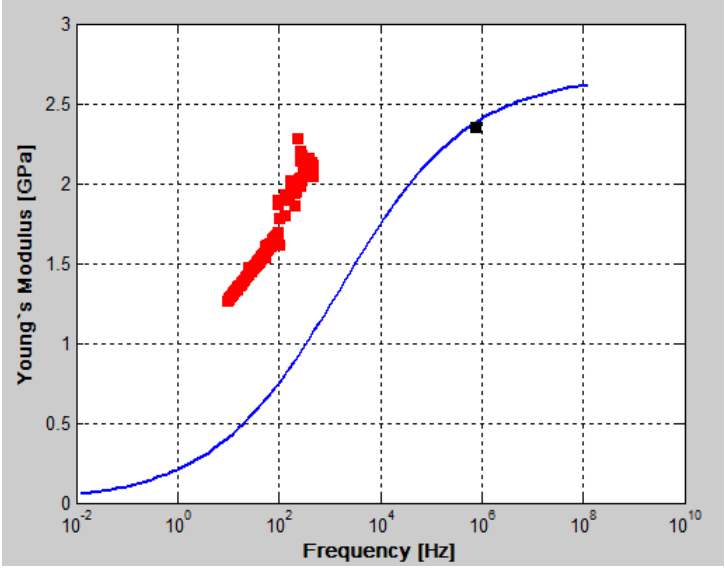

Figure B.14. Average of the real part of the Young's modulus from Figure B.13 compared to ultrasonic results. Cole-Cole dispersion model fit used in Figure B.7 and Figure B.8. is shown as reference.

APPENDIX C. BACKGROUND INFORMATION FOR HEAVY OILS TESTED IN THIS WORK

The three samples I tested in my research were GP007-Uvalde, GP010-Goleta and GP029-Asphalt Ridge. Figure C.1. show the location of asphalt bearing rocks in the Western United States (Hail Jr. 1957) and the location of the three tested samples are highlighted in red. The three samples were collected from the outcrops shown in the map and the heavy oil was extracted with toluene. The toluene was then evaporated in the oven for few days, stirring occasional to ensure a complete evaporation.

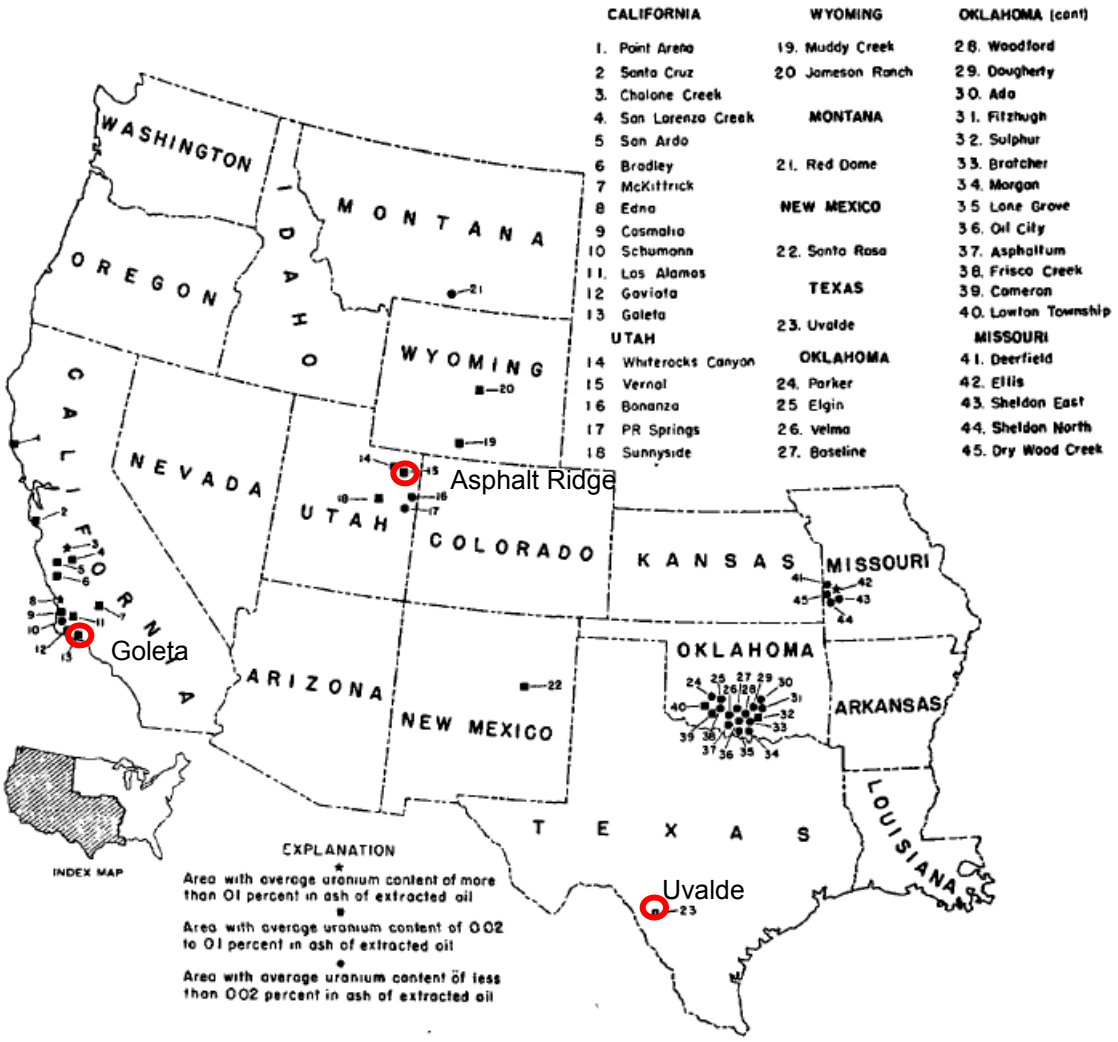

Figure C.1. Map of Western United States showing the location of asphalt-bearing rocks. Highlighted in red are the locations of the three samples tested in this research (Hail Jr. 1957).

GP007-Uvalde: The samples were collected at an outcrop in Texas and the rocks containing the heavy oil are limestones of the Late Cretaceous (Hail Jr. 1957).

GP010-Goleta: The sample was collected at Goleta Beach, Santa Barbara California. The rocks containing the heavy oil are siltstones of the Monterey shale formation of Miocene age (Hail Jr. 1957). The presence of heavy oil (tar) in the Goleta Beach area is due to a natural tar seep which is said to be the second largest in the world, expulsing approximate 150 barrels of oil per day (Costales n.d.).

GP029-Asphalt Ridge: The sample was collected at an outcrop in Utah and the reservoir rock is composed primarily of sandstone. It is believed the oil is sourced from the rich organic lacustrine sediment of the Green River formation. Figure C.2. show a detailed map around the location of the Asphalt Ridge outcrop in Utah.

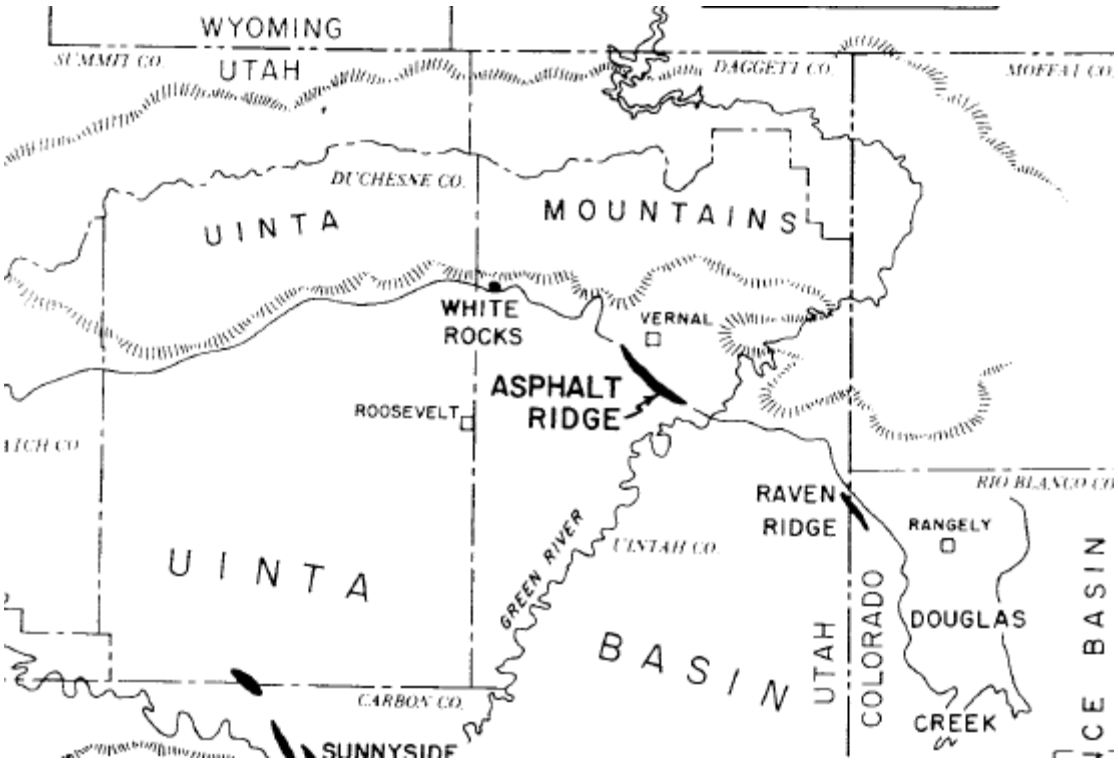

Figure C.2. Detail map around the area of the Asphalt Ridge outcrop location in Utah (Kayser 1966).

Figure C.3. compares the SARA composition of the three sample in a spider graph. GP010-Goleta and GP007-Uvalde have a very similar composition with a high amount of asphaltenes, while the GP029-Asphalt Ridge sample has a lower content of asphaltenes but a high content of resins and maltenes

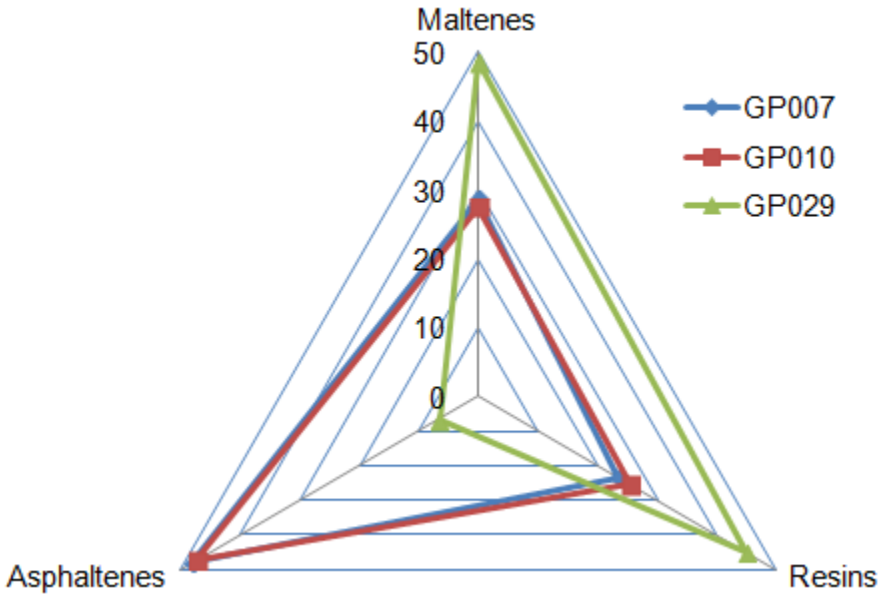

Figure C.3. Spider graph showing the SARA composition of the three samples tested.

APPENDIX D. DENSITY ANALYSIS (API GRAVITY)

The measurement of density is done using the pycnometer which is a standard vessel of fix volume and a calibrated microscale; and the API gravity is calculated using equation 2.7. Below is the list of steps to perform the measurement:

1. Weigh the empty pycnometer with cap.
2. Fill the pycnometer with distilled water and weigh again.
3. Empty the pycnometer, flush with acetone and dry with pressured air.
4. Add the heavy oil sample with care to avoid staining the vessel's neck. It is recommended to add at least 10 percent of the total weigh in heavy oil. This means that if we are using a 10 ml pycnometer, it is recommended to use at least 1 g of heavy oil sample. If the heavy oil sample is solid, the sample can be crushed prior to put t in the vessel. If the sample is crushed it is important to put it in the oven for enough time to melt the sample again and eliminate any air trapped in the sample.
5. Weigh the pycnometer with the heavy oil but make sure to wait until the pycnometer and sample are back to room temperature.
6. Fill the pycnometer with water and weigh again. NOTE: make sure there are not bubbles.
7. Calculate the density of the oil as follows:
    a. The density of water should be read from standard tables at the temperature the measurements are being done
    b. Calculate the mass of water subtracting the total mass minus the mass of the pycnometer (#2 - #1).
    c. Using the density and the mass of water we can calculate the volume of water (#b / #a) (which is the volume of the pycnometer) . NOTE: The pycnometer has a nominal volume but it in most of them it says it is an approximate volume, therefore the actual volume has to be calculated.
    d. The mass of sample is also calculated subtracting the mass of the pycnometer (#5 - #1).
    e. In a similar way, calculate the mass of water "added" to the pycnometer when the oil sample is inside (#6 - #5).
    f. The volume of "added" water can be calculated with the mass of added water and the density of water (#e / #a).
    g. The volume of sample is calculated as the volume of the pycnometer minus the volume of "added" water (#c - #f).
    h. With the mass of sample and the volume of the sample we can then calculate the density of the sample (#d / #g).
8. Repeat the above procedure at least three times and calculate the standard deviation of the measurement.

APPENDIX E. WATER CONTENT ANALYSIS

Water content measurements were done using the Karl-Fischer titration method. Following is the procedure using a METTLER TOLEDO V20 volumetric KF titrator:

1) Turn equipment on at the front panel
2) Use the “manual” option to “stir”, “pump” or “drain” the liquids at the testing vessel.
3) Use the “pump” option to fill around 80 ml of Methanol anhydrous.
4) Go to methods and select a preset method to do the water estimation.
5) It will titrate the methanol to eliminate any water that was absorbed by the equipment while not in use.
6) The equipment has to read a level below 25 µg/min (drift). The equipment will not allow the user to test a sample until it reaches this level. If the system over titrates, the user has to wait until it reaches the correct level.
7) While the equipment reaches the reference level of zero water the user can prepare the sample to test:
8) Using the microscale, weigh a small vial and cap
9) Add approximate 0.5 g of sample. Note: The amount of sample to add will depend on the amount of water in the sample. The system needs a minimum of 10 mg of water to give good results. If the user has no previous indications of how much water the sample may have, it is better to start with a small amount of sample and adjust for the second test.
10) Add toluene and weigh to estimate the amount of toluene added. Close the cap to ensure no toluene is evaporated.
11) Stir until all the oil is dissolved in the toluene.
12) Calculate the concentration of the solution.
13) After the equipment reached the drift level, press the start button and add the sample to the vessel.
14) Weigh the vial and cap with the leftover sample and calculate how much sample remained in the vial after adding the solution to the testing vessel.
15) Insert the amount of sample in the equipment as it will automatically calculate the water content.
16) Repeat the above procedure at least three times and calculate the standard deviation of the measurement.

APPENDIX F. PROPERTIES OF TESTING MATERIALS

In the tension/compression measurements of soft samples it is of great importance that the materials used to build or contain the sample has a lower strength than the sample itself at the testing conditions. Some of the materials used for the sample preparation were different types of epoxies and the jacket and gages support material. The samples had a shear modulus in the range of 0.25 to 1 GPa, for soft samples with Poisson's ratio close to 0.5, the range of Young's modulus would be 0.75 to 3 GPa. In table F.1, is a list of the materials used for soft sample preparation together with some strength properties reported by the different providers. Even though all the values are below the properties of the samples tested, care needs to be taken when testing at higher temperatures or lower frequencies when the modulus of the sample is reduced.

Table F.1. List of materials used for soft sample preparation and reference properties

Material	Used for	Property	Value
Kapton® film	Jacketing	Tensile Strength	110 - 165 MPa
5 minute® Epoxy	To attach jacket to aluminum standards, to cover gages, etc.	Adhesive Tensile Shear	13 MPa
Easyepoxy® K-20	To attach and cover gages	Flexural strength	41 MPa
		Compressive strength	69 MPa
Flexible epoxy (Resinlab)	To cover gages	Tensile modulus	14 MPa
		Compressive modulus	34 MPa
		Lap shear strength	7 MPa

APPENDIX G. PAPERS FOR PUBLICATION

Published:

- Rodrigues, P. and Batzle, M. (2013) Shear modulus of heavy oils: Measuring at low frequencies. SEG Technical Program Expanded Abstracts 2013: pp. 2647-2652. doi: 10.1190/segam2013-0250.1

In preparation for publication (not submitted yet at the time of thesis upload):

- Rodrigues, P and Batzle, M. "Shear Modulus of Heavy Oils: Liquid to Solid Transition due to Confinement in Rheometer Measurements". *Journal: FUEL*
- Rodrigues, P and Batzle, M. "Shear Modulus of Heavy Oils, Rheometer vs. Tension/Compression Techniques: Solid to Liquid Transition due to Strain Amplitude Effects". *Journal: GEOPHYSICS.*
- Rodrigues, P and Batzle, M. "Programmed Pyrolysis versus SARA analysis in Heavy Oils". *Journal: JCPT*